5-2014

Causes and Countermeasures for Nappe Oscillation: An Experimental Approach

Aaron Allan Anderson
Utah State University

CAUSES AND COUNTERMEASURES FOR NAPPE OSCILLATION: AN EXPERIMENTAL APPROACH

by

Aaron Allan Anderson

A thesis submitted in partial fulfillment
of the requirements for the degree

of

MASTER OF SCIENCE

in

Civil and Environmental Engineering

Approved:

_____	_____
Blake P. Tullis Major Professor	Marvin W. Halling Committee Member
_____	_____
Brian M. Crookston Committee Member	Mark R. McLellan Vice President for Research and Dean of the School of Graduate Studies

UTAH STATE UNIVERSITY
Logan, Utah

2014

ABSTRACT

Causes and Countermeasures for Nappe Oscillation:

An Experimental Approach

by

Aaron A. Anderson, Master of Science

Utah State University, 2014

Major Professor: Dr. Blake P. Tullis
Department: Civil Engineering

Weirs are commonly used as spillways to release flows from a reservoir. The free-falling jet on the downstream side of the weir is called the nappe. Under certain hydraulic conditions, determined mainly by the size, design, and construction of the weir, nappe oscillation, otherwise known as nappe vibration, can occur. Characteristics of this dynamic behavior include excessive acoustic energy manifested as sound pressure waves and low-frequency noise accompanied by horizontal waves or banding on the nappe. Mitigation of this process may be required, especially if the weir operates in close proximity to occupied structures. Instability of water jets moving through air has been a topic of study for over a century, although studies specific to curvilinear weir nappe flow are less common. The objective of this research is to further the understanding related to the mechanisms that cause nappe vibration, document the occurrence conditions, and investigate mitigation techniques.

Research was conducted at the Utah Water Research Laboratory (UWRL) using three physical models:

- A 6 ft wide x 3.5 ft tall weir with a quarter round crest (model #1)
- A 15.4 ft wide x 11 ft tall weir with a broad crest (model #2)
- A 16 ft wide x 12 ft tall weir with a quarter round crest (model #3)

Testing included confined and unconfined nappe conditions (open air cavity behind the nappe vs. closed air cavity) for model #1 and model #3. Vibration frequencies were recorded and analyzed using an accelerometer and microphone. Comparisons were made between the three models of different scale. Testing included modifications to the weir crest and the weir apron to study the effect on the behavior of the nappe.

The results of this study are presented, including a review of previous literature and theories. The mechanisms that sustain and amplify the nappe vibration phenomenon varied at the different size-scales, while evidence exists that the root cause of initial instability leading to self-induced vibration can be traced to the same source. The results of this study should be of practical use to engineers, researchers, and those concerned with dam safety.

(151 pages)

PUBLIC ABSTRACT

Causes and Countermeasures for Nappe Oscillation:

An Experimental Approach

by

Aaron A. Anderson, Master of Science

Utah State University, 2014

Major Professor: Dr. Blake P. Tullis
Department: Civil Engineering

Weirs are commonly used as spillways to release flows from a reservoir. The free-falling jet on the downstream side of the weir is called the nappe. Under certain hydraulic conditions, determined mainly by the size, design, and construction of the weir, nappe oscillation, otherwise known as nappe vibration, can occur. Characteristics of this dynamic behavior include excessive acoustic energy manifested as sound pressure waves and low-frequency noise accompanied by horizontal waves or banding on the nappe. Mitigation of this process may be required, especially if the weir operates in close proximity to occupied structures. Instability of water jets moving through air has been a topic of study for over a century, although studies specific to curvilinear weir nappe flow are less common. The objective of this research is to further the understanding related to the mechanisms that cause nappe vibration, document the occurrence conditions, and investigate mitigation techniques.

Research was conducted at the Utah Water Research Laboratory (UWRL) using three physical models:

- A 6 ft wide x 3.5 ft tall weir with a quarter round crest (model #1)
- A 15.4 ft wide x 11 ft tall weir with a broad crest (model #2)
- A 16 ft wide x 12 ft tall weir with a quarter round crest (model #3)

Testing included confined and unconfined nappe conditions (open air cavity behind the nappe vs. closed air cavity) for model #1 and model #3. Vibration frequencies were recorded and analyzed using an accelerometer and microphone. Comparisons were made between the three models of different scale. Testing included modifications to the weir crest and the weir apron to study the effect on the behavior of the nappe.

The results of this study are presented, including a review of previous literature and theories. The mechanisms that sustain and amplify the nappe vibration phenomenon varied at the different size-scales, while evidence exists that the root cause of initial instability leading to self-induced vibration can be traced to the same source. The results of this study should be of practical use to engineers, researchers, and those concerned with dam safety.

ACKNOWLEDGMENTS

I have many people to thank for making this research possible. First, I must thank my advisor and mentor, Dr. Blake Tullis. His support and patience throughout this research were pivotal. Along with Dr. Tullis, I thank my advisors, Marvin Halling and Brian Crookston, for their advice and expertise. I also would like to thank my student peers, Tyler Seamons, Mitch Dabling, and Rhen Thurgood, for their aid in many aspects of this project.

I would like to thank Zac Sharp and the entire hydraulics lab crew for their assistance in building and running the many models that were utilized for this research. Finally, I would like to thank my beautiful wife, Jessica, for her constant support and encouragement throughout this challenging period of research. My family and friends were with me every step of the way.

Aaron A. Anderson

CONTENTS

Page

LIST OF TABLES

LIST OF FIGURES

CHAPTER I

INTRODUCTION

Weirs are commonly used in conjunction with dam structures as a means of passing flow through a reservoir. The free-falling jet of water on the downstream side of the weir is called the nappe. The phenomenon of nappe oscillation can occur under certain hydraulic conditions (see Fig. 1)

Fig. 1. Visible waves due to nappe oscillation

Oscillating nappes, which will be interchangeably referred to as wavy or vibrating nappes in this report, have been known to create excessive acoustic energy (noise and sound pressure) in prototype and model weir structures. For prototype structures, the noise and vibration created by this process can be heard and felt up to several hundred yards away from the structure (Schwartz, 1966). Oscillation of a falling liquid curtain has been

the topic of study for over a century, although studies specific to weir nappe flow are less common.

Nappe vibration can be attributed to three different factors: Instability of the nappe itself, fluctuation of air pressure behind the nappe, and the structure acting as a vibrating system (Sato et al., 2007). One major focus of research regarding nappe vibration has been to develop a better understanding of countermeasures, such as in the case of the Avon Dam Spillway (Metropolitan, 1980). The objective of this research is to further clarify the physical mechanism underlying nappe vibration, focusing mainly on conditions at the weir crest, the confined air pocket behind the nappe, and the point of impact on the apron. In addition, this research will focus of the effectiveness of a variety countermeasures for attenuating and terminating nappe vibration at different size-scales.

CHAPTER II

LITERATURE REVIEW

Physical Vibration Mechanism

Nappe vibration has been investigated by numerous researchers over the past century. The most common theory behind the mechanism is based on the Kelvin-Helmholtz instability, which is driven by shear forces occurring at the interface between two fluids with different velocities (von Helmholtz, 1868); the current study features a liquid jet (water) passing through a gas (air) medium. Later studies by Lord Rayleigh (1878) developed numerical expressions for the instability of water jetting into an air medium as well as into a water medium. Rayleigh's study is related to nappe instability, and laid the groundwork for further study.

Squire (1953) investigated the numerical solutions to the wave characteristics of a thin water sheet with constant thickness moving through air, in which the Weber number, which is the ratio of inertial to surface tension forces, is a factor in determining the wavelength of transverse waves that form and lead to sheet breakup. Such sheet breakup due to wave formation has been observed by several authors, including the author of this report. De Luca and Costa (1997) further studied the instability of a falling liquid sheet, formulating equations representing the spatial development of waves, while incorporating the curvature due to the influence of gravity. They state that the location of sheet breakup occurs at the location where the Weber number is equal to the dimensionless sheet thickness. Studies by Squire and De Luca and Costa shed light on what occurs at the

location of nappe breakup (a location of two-phase flow), but do not explain the entire nappe oscillation phenomenon.

Schwartz (1966) discussed theories behind the nappe vibration mechanism occurring on weirs, including the possible effects of edge tones, as well as the possible link between nappe oscillations and weir crest boundary layer conditions. Casperson (1991) studied nappe oscillations occurring on fountains in New Zealand (weir flow conditions), deriving equations to model the position of the nappe during oscillation, and attributed the cause of instability to the Helmholtz effect. In a later study, Casperson (1994) reported on stability criteria of nappe oscillation, determining general conditions under which weir nappe oscillations will occur. Casperson (1995) then reported on the occurrence of nappe oscillations on a circular weir, demonstrating that the process is not limited to linear weirs.

Along with the driving force of the Helmholtz instability, it is understood that having an enclosed air cavity behind the nappe, whether it be a vertical falling sheet or curvilinear weir nappe flow, can serve as a mode of nappe vibration amplification. Changes in pressure behind the nappe, the origins of which are not completely understood, can occur as the water jet falls, promoting an oscillatory variation of positive and negative pressures in the air cavity. These pressure pulses "push" and "pull" the nappe, providing a vibration feedback loop (Naudascher and Rockwell, 1994). Naudascher (1974) presents an extensive amount of research on the topic of flow induced vibrations, including the vibration mechanism of free falling nappes over a weir or gate. While it is believed that the cause revolves around the interaction between the falling nappe and the enclosed air pocket behind the nappe, logic would argue that the instability must *originate* at some specific

location or have a specific source. The origin of the instability is unclear, but Naudascher points out that, although not the definite cause, instability due to flow separation as the water leaves the weir crest could intensify vibration. This theory is supported by studies from Chanson (1996), where attention is drawn to the pressure distribution of water flowing over a curved surface, with negative pressures forming at the boundary layer. Under such conditions, the weir nappe would experience a sudden pressure discontinuity as the negative pressure boundary layer is suddenly introduced to atmospheric pressure (or the ambient pressure of the air cavity behind the nappe) as the weir enters free falling conditions.

Schmid and Henningson (2002) investigated a falling vertical water sheet with an enclosed air cavity behind the nappe. Comparing mathematically predicted behavior of the sheet and experimental results demonstrated a fairly accurate correlation. Sato et al. (2007) determined that, in the case of vibration of a vertical water sheet with an enclosed space behind the nappe, the frequency of vibration in the water sheet matches the frequency of pressure variations of the enclosed air space. They also discovered that, in the case of a vertically falling sheet, a baffle wall projected horizontally from the back confining wall near the bottom of the falling water curtain impeded the feedback mechanism and suppressed the vibration. Kolkman (1972) explored a vertical falling water sheet with and without a confined air pocket. He observed that changing the shape of the slit which produced the sheet had no effect on the vibrations, but that increasing the initial velocity of the water sheet "eases the vibration."

Kyotoh (2002) conducted an extensive study on nappe instability, examining conditions of a weir under different flow conditions, including the conditions with and without a confined air cavity behind the nappe. He made the conclusion that the factors affecting nappe vibration are: The propagation of pressure fluctuations under the influence of confined air, the shear wave instability of air flow induced by the falling water, and surface tension effects on the water sheet (Kyotoh, 2002). Each factor can be predominant depending on the conditions of the falling water sheet. Binnie (1971) investigated a vertically falling water sheet in a vacuum chamber, and reported no nappe vibrations, suggesting that the presence of a second fluid (i.e. air) surrounding the water jet is necessary to induce the vibration. Binnie noted that the vibration is sensitive to the depth of the tail water plunge pool, and also reported seeing instances of nappe vibration for fully vented nappes.

Vibration Attenuation/Remediation

In addition to literature regarding the nappe vibration mechanism, several studies have focused on nappe vibration mitigation. Nappe vibration countermeasure experience at Avon Dam (Metropolitan, 1980) determined the level of effectiveness of certain countermeasures for a labyrinth weir experiencing nappe vibration. The addition of nappe splitters located on the crest proved to be effective in suppressing the vibration. Stones glued to the crest to increase the roughness also proved to be a promising countermeasure. Another weir crest modification that was evaluated was the addition of a bulbous nose to the downstream side of the crest, causing the nappe to cling to the downstream crest profile over a wider range of discharges. Although this method was successful in stopping the

vibration, it is most likely not a cost-effective alternative for remediation. The final remediation technique involved sections of angle iron serving as roughness elements attached to the weir crest, which were observed to be relatively effective but difficult to install. In a model study conducted by the United States Bureau of Reclamation (Falvey, 1980), roughening of an ogee crest weir with paint droplets terminated vibration.

The United States Bureau of Reclamation (1964) conducted a similar trial at Black Canyon Dam, but nappe splitters were placed horizontally on the downstream side of the weir and supported with ropes. By placing a splitter at 1/3rd the total weir length from the side abutment, two sections of weir flow were created. The shorter section with a length equal to 1/3rd the total length ceased to vibrate, while the larger section equal to 2/3rd the total weir length continued to vibrate. However, placing the splitter in the center of the weir, creating two equal sections of length equal to ½ the total width, eliminated the vibration waves in both sections. Aside from nappe splitting, attempts to vent Black Canyon Dam were unsuccessful in disrupting the vibration mechanism.

Sumi (1990) investigated the three-dimensional aspects of nappe oscillation with aerated and non-aerated conditions. In the study, the effects of weir width, fall height, and nappe splitting were investigated. Effectiveness of splitters was determined by the noise level produced by vibrations. Knisely (1994) experimented with the addition of rubber flaps suspended on the downstream side of the weir crest. As flow passes over the spillway, the flexible rubber flaps were drawn up to the underside of the nappe, and in several cases, this method proved to be effective. But, Knisely reports, "For a given gate, there is no way to predict analytically the *definite occurrence* of nappe oscillations, the range of water

depths and fall heights over which oscillations *will definitely occur* , the *exact* frequency of oscillation (a *set* of possible frequencies can be predicted), the amplitude of pressure fluctuations or the most effective spacing for spoilers (splitters)."

While extensive research has been conducted on nappe vibration, some aspects still remain unclear, such as the source of initial instability in the nappe. Additional needed research regarding nappe vibration countermeasures would lead to a better understanding of how and why a particular remediation does or doesn't work. The goal of this research is to further understand the causes of nappe vibration at different model scales and to develop a greater knowledge concerning the countermeasures to this troublesome dynamic process.

The objectives of the research project are:

- Further investigate the process of nappe oscillation, attempting to distinguish between the source of initial instability and the sources of wave amplification
- Determine the effectiveness of different nappe oscillation countermeasures
- Compare results from three models of different scale

These areas of research will help better understand the mechanism of nappe vibration, supporting and expounding upon what has already been discovered about this fascinating yet troublesome dynamic process.

CHAPTER III

EXPERIMENTAL PROCEDURE

Testing Facilities

Model #1

All testing for this research was carried out at the Utah Water Research Laboratory (UWRL) in Logan, Utah. Model #1 utilized a 6 foot x 4 foot x 30 foot flume (see Fig. 2).

Fig. 2. Model #1 flume

Water is supplied to the flume by a higher elevation reservoir. Depending on the required flow rate, water is supplied to the flume through a 6 inch or 12 inch steel pipe which feed into a larger 24 inch pipe connected to the upstream side of the flume, all of which are controlled by butterfly valves (see Fig. 3).

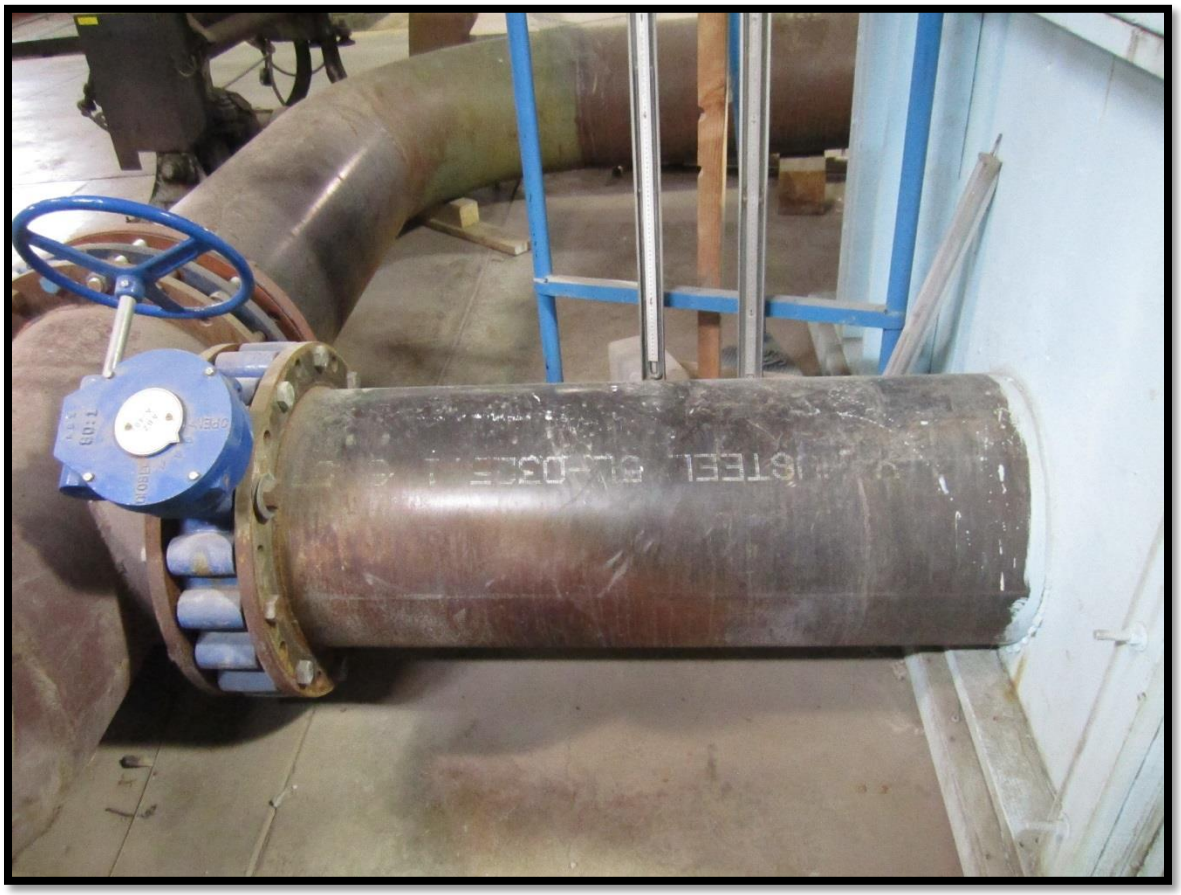

Fig. 3. Water supply pipe for model #1 flume

A baffle wall is located 3 feet from the flume inlet to provide flow straightening. Discharge into the flume is measured using a venturi flow meter, a pressure transmitter, volt meter, power source, and a transmitter communication device. The upstream flow depth was measured using a precision point gauge installed upstream of the weir and

referenced to the crest elevation. To measure the flow vibration intensity, an accelerometer was attached to the acrylic flume sidewall, which recorded acceleration in m/s^2 vs. time (see Fig. 4). Frequency of vibrations are presented in Hertz (Hz). In addition to the accelerometer, an effective method of detecting vibration was by simply being present and listening.

To produce a free falling nappe, a 6 foot wide x 3 ½ foot tall wooden weir was installed in the flume (see Fig. 5). The flume is constructed out of marine grade painted plywood with internal steel reinforcement. Due to large hydrostatic pressures on the upstream side of the weir, two steel cables with turnbuckles were connected from center of the upstream weir face to the sidewalls of the flume to restrain the weir from flexing or shifting downstream.

The 1 ½ inch quarter round crest for the weir was machined out of high-density polyethylene (HDPE) and fastened to the weir top with screws. The 8 foot x 4 foot flume featured acrylic sidewalls at the weir location to facilitate visual observation. The weir nappe was confined by the side walls of the flume (i.e. suppressed weir flow), preventing the free passage of air to and from the area behind the nappe and the surrounding atmosphere.

Water was discharged from the flume into a trench which was routed back into Logan River. The model was sealed from leaks using NP1 polyurethane sealant. A high definition video camera with high frame rate capability was used to document the model testing in real time and slow motion. Slow motion video helped to view the characteristics

of the oscillating nappe that were otherwise difficult or outright impossible to see in real time.

Due to issues with repeatability on model #1, one consistent flow rate (0.433 ft^2/s) was chosen for testing the different modifications to the model. This flow rate, and all other flow rates tested in each model, are given in terms of unit discharge, which is determined by dividing the units of flow, length^3/time, by the length of the weir, resulting in units of length^2/time. Unit discharge provides a more tangible and relatable system of units, especially when applying the results of this report to future research.

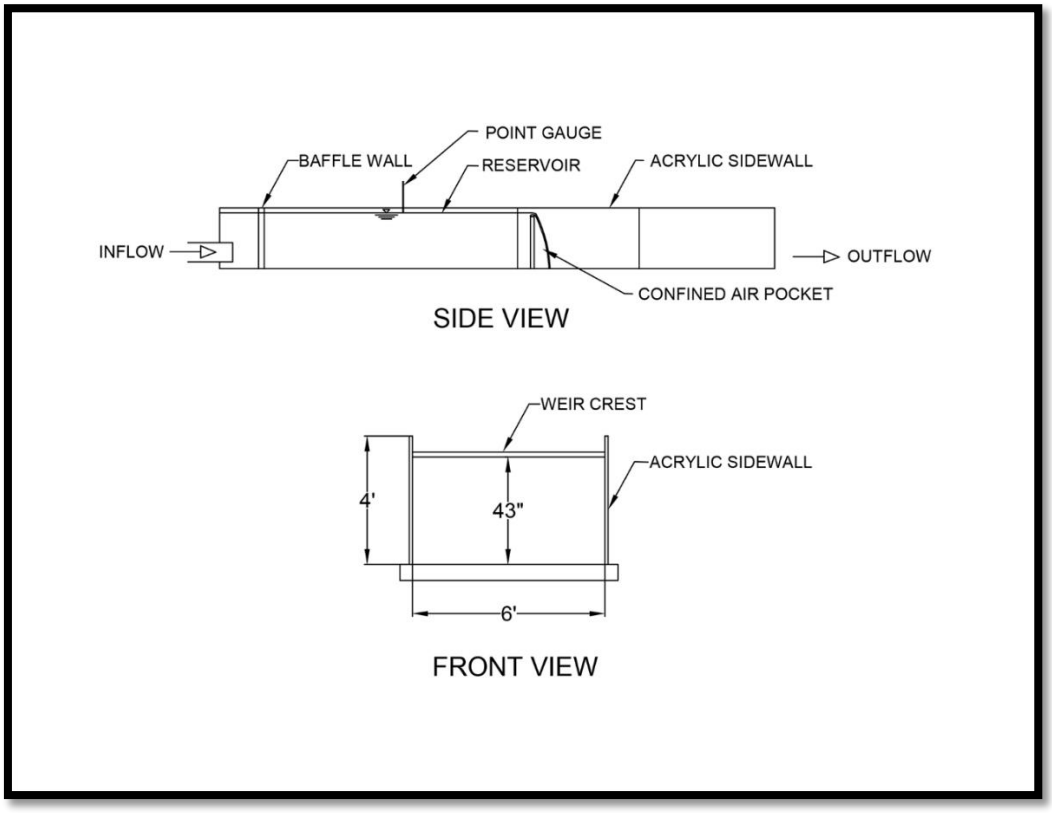

Fig. 4. Model #1 configuration

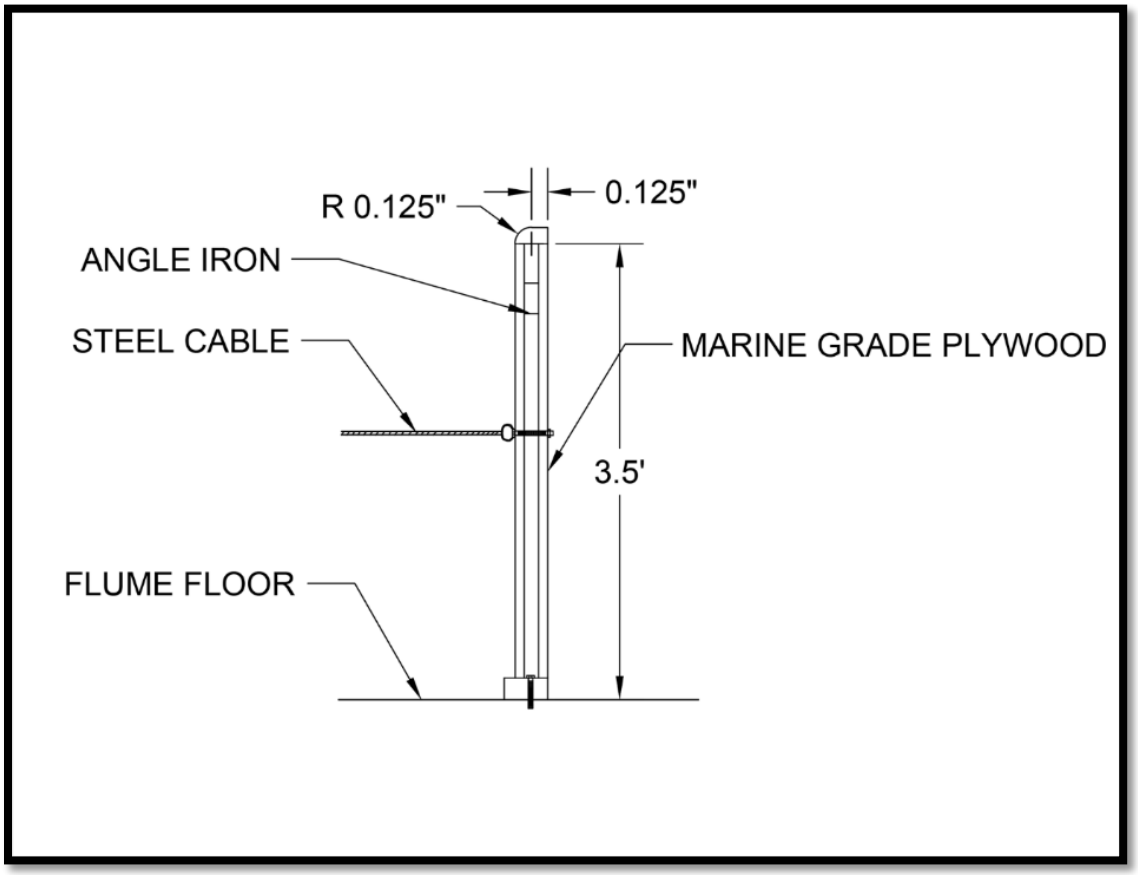

Fig. 5. Model #1 weir design

Model #2

Model #2 utilized a 27 foot x 27 foot x 5 foot suspended head box constructed from wood and supported with steel box beams (see Fig. 6). Water was supplied to the head box using a recirculating water distribution system. Two centrifugal pumps lift water through a 12 inch pipe which fills the head box. Water entering the box flowed through diffuser pipes and a baffle wall to reduce turbulence, which was important to maintain a tranquil water surface within the box reservoir with minimal surface waves that could affect the behavior of the nappe.

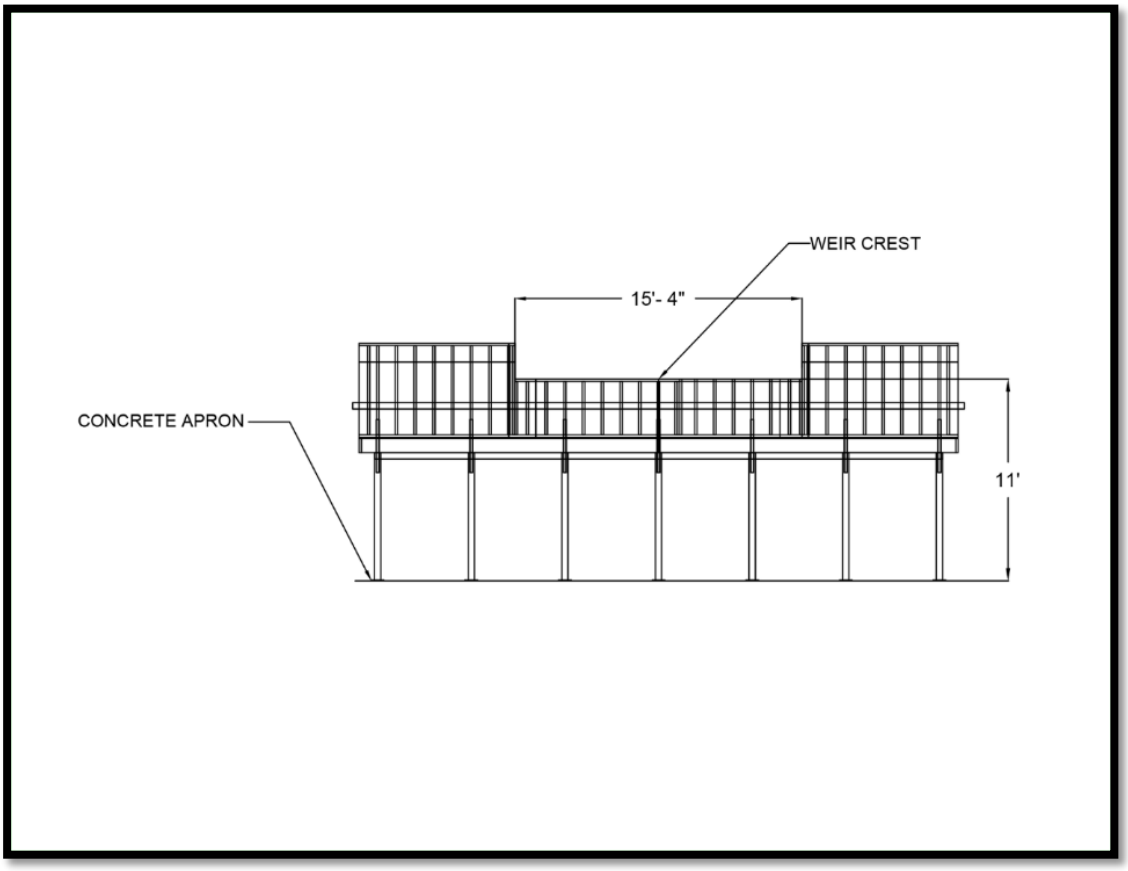

Fig. 6. Model #2 head box and weir location

To create a contracted weir flow condition, the head box wall was notched and a 15’ 4” wide x 12” deep broad weir crest was installed at the base of the notch using sections of durable plywood and 2 x 4 supports (see Fig. 7). The box iron beam installed around the entire perimeter of the box was used as support for the underside of the weir, providing a stable base on which the weir could be leveled. A channel made of sandbags was organized on the lab floor in order to direct water from the weir back into the sump where it could be recirculated back into the elevated box. In order to maintain consistency, all lab doors were kept closed during testing to prevent outside air currents from entering the model area and potentially affecting the falling nappe.

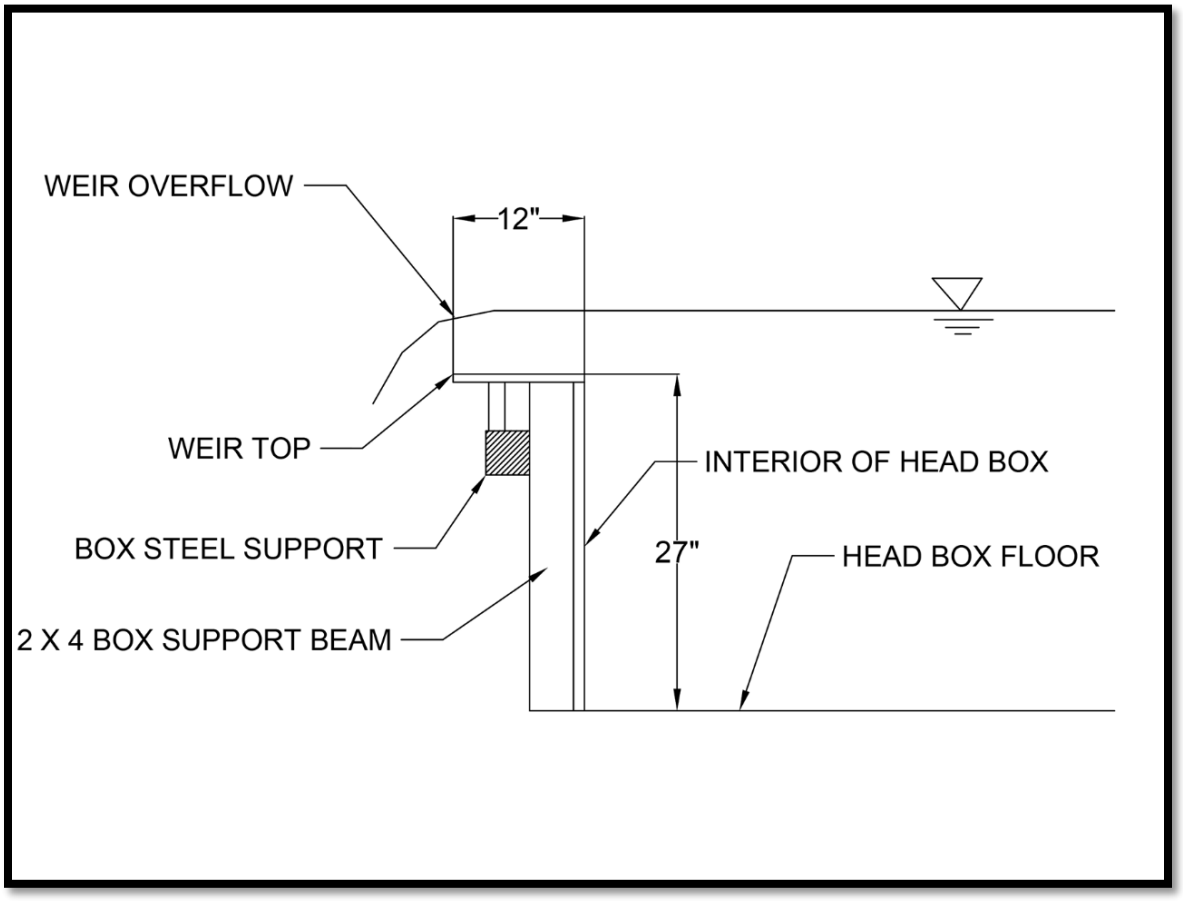

Fig. 7. Model #2a weir setup

It is understood that roughness on a weir crest is effective at attenuating nappe vibration, so the wooden sheets forming the broad crest were covered with a smooth thin tin sheeting. However, vibration still did not occur even with the added element of smoothness. The next modification, which succeeded in producing waves in the nappe, was the addition of rounded fillet on the upstream side of the crest (see Fig. 8). This rounded section on the upstream side of the weir reduced the turbulence in the flow caused by flow separation around the 90° upstream edge of model #2a. The model #2b weir configuration was used for testing for model #2 rather than model #2a.

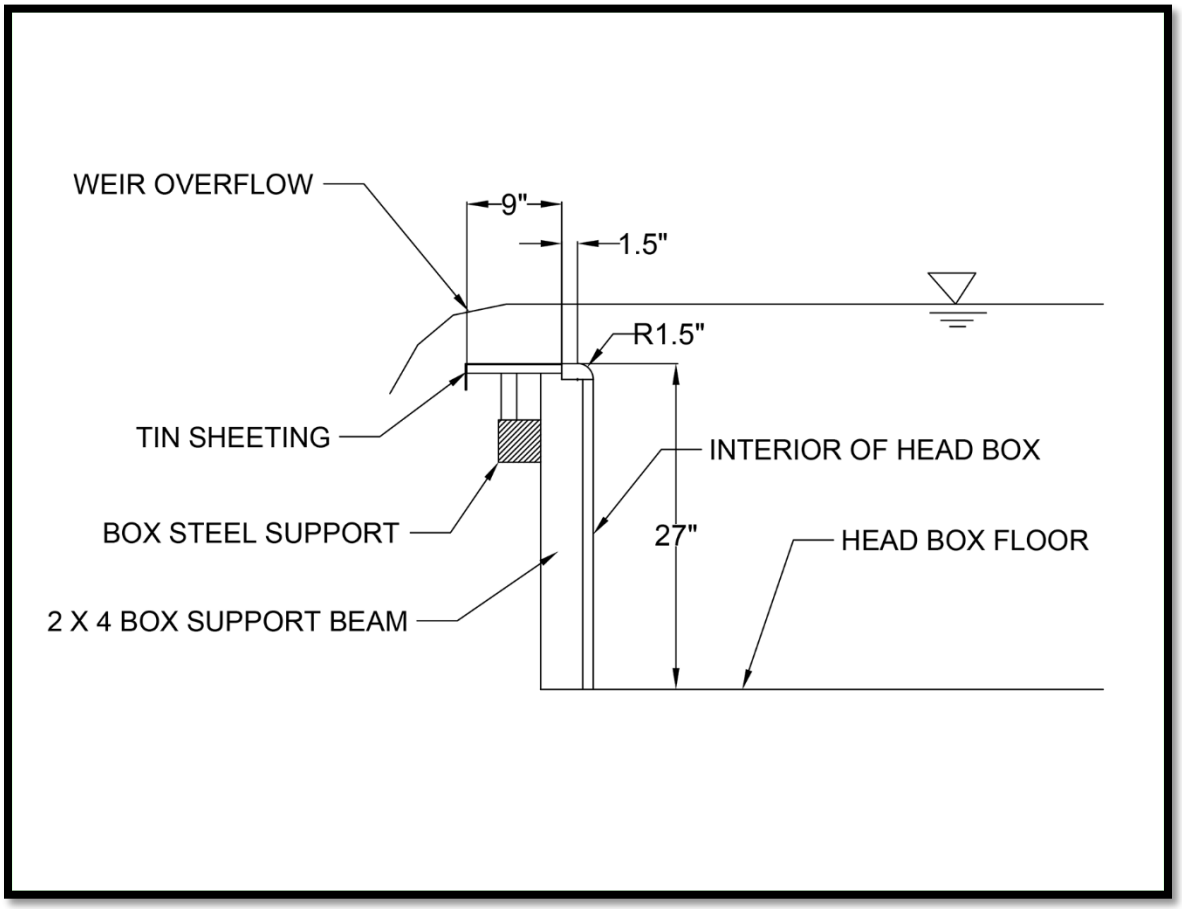

Fig. 8. Model #2b weir setup

Water discharged over the weir crest fell 11 feet onto the concrete laboratory floor before being routed back into the sump reservoir. Flow rates were measured using a magnetic flow meter located in the inlet pipeline. A range of five flow rates were tested on model #2, beginning with 0.22 ft^2/s and increasing to 0.47 ft^2/s at increments of 0.06 ft^2/s. Vibration frequency was measured using a microphone with audio editing software. The high definition camera was used to document testing, which was capable of high frame rate video which could be viewed in slow motion.

Model #3

Model #3 utilizes the same head box described for model #2, but the weir notch is located on a different side of the box (see Fig. 9). The width of the weir in model #3 is 15’ 11”, with a fall height from weir to apron of 11’ 11”. This weir is located above the pump sump, allowing the nappe to impact the protective metal grating (3 inch x 1 inch rectangular gaps) above the sump before landing in the pool below (see Fig. 10). Tests with a solid impact surface were also created by placing a long 2 inch x 12 inch wooden plank on the grate at the nappe impact location.

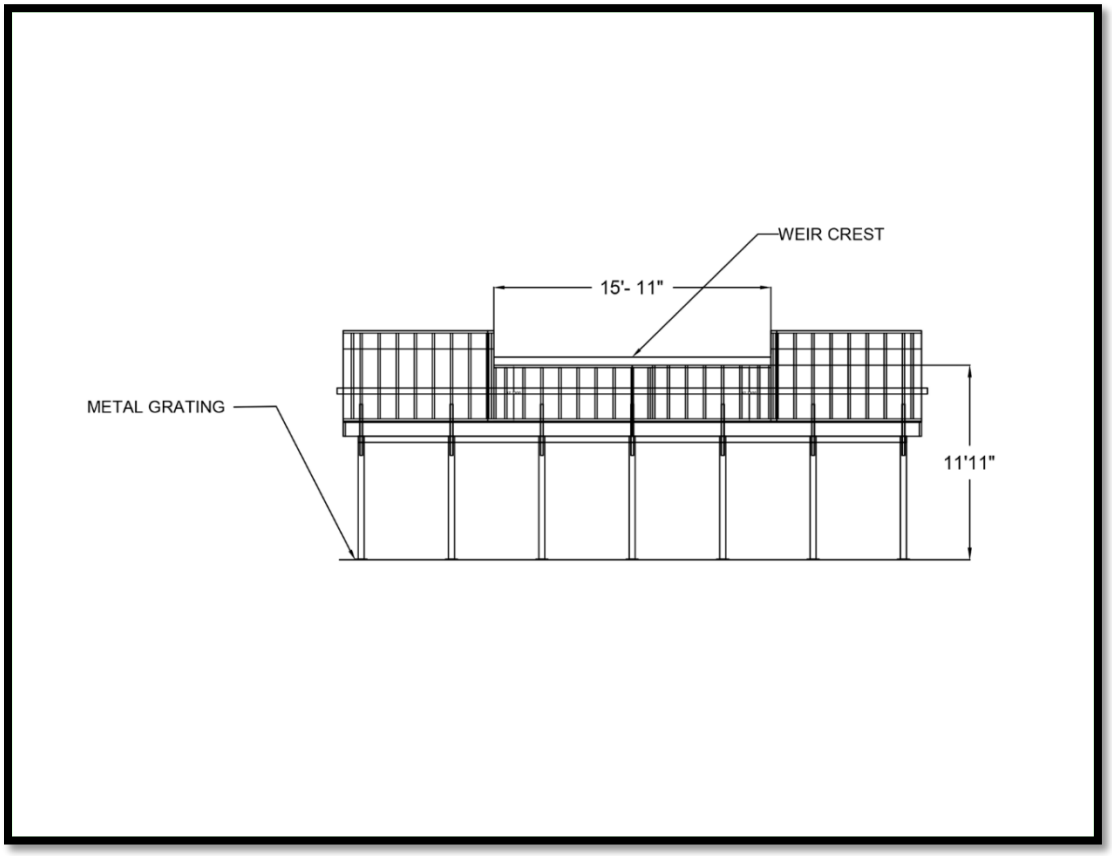

Fig. 9. Model #3 head box

Fig. 10. Model #3 nappe impact grate

The quarter round weir crest was constructed by combining two separate sections (see Fig. 11). The flat portion of the weir was built out of two 8 foot long x 6 foot wide x ¾ inch thick sheets of HDPE. The rounded portion on the upstream side of the weir was made by cutting a 12 inch diameter PVC pipe length-wise to create ¼ circle sections with an approximate 6 inch radius. The rounded portion was supported with PVC ribs placed on the underside of the quarter round sections to maintain its shape. The flat crest portion and rounded crest portion were placed on a level plywood base which was fastened to the elevated box with metal brackets, and the flat portion was supported by 2 inch x 4 inch

wooden studs. The joint between the sections was sealed with NP1 polyurethane sealant and covered with vinyl mat tape to smoothen the transition.

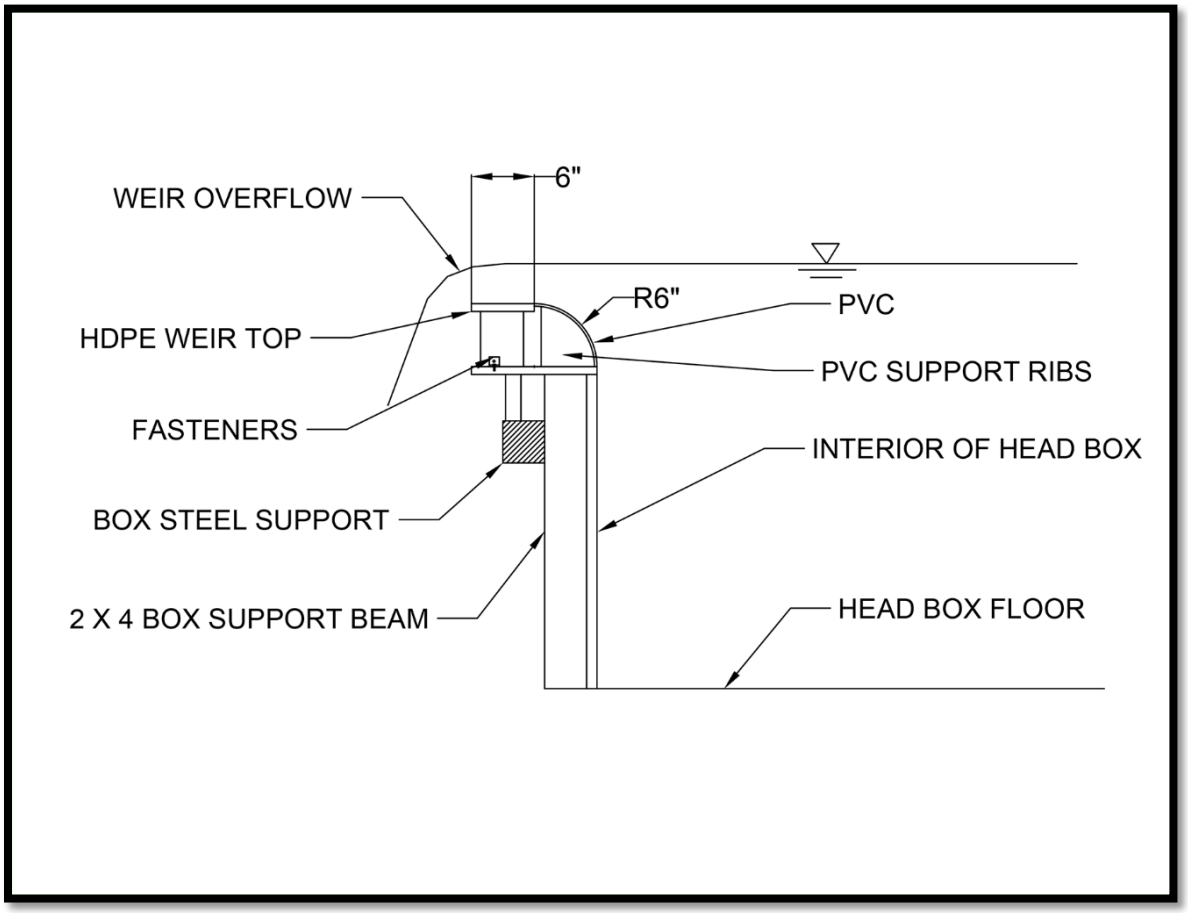

Fig. 11. Model #3 weir construction

To investigate confined nappe conditions on model #3 (enclosed air pocket behind the nappe), side and back walls were constructed from particle board. In addition, sheets of particle board where placed on the grating to prevent the passage of air (see Fig. 12). The total head upstream of the weir was measured using a stilling well and high accuracy point gauge (see Fig. 13). The occurrence of vibrations in the nappe or lack thereof were

documented using a high definition video camera with slow motion capture capabilities. The frequency and amplitude of vibrations were measured using a microphone with audio recording software for the unconfined nappe (without sidewalls and back wall in place), while the vibration frequency for the confined nappe (with sidewalls and back wall in place) was measured using an accelerometer attached to the sidewall. Six flow rates were tested on model #3; the lowest discharge was 0.14 ft^2/s and the highest discharge was 0.42 ft^2/s, increasing from low to high by increments of 0.06 ft^2/s.

Fig. 12. Model #3 weir nappe air containment

Fig. 13 Model #3 reservoir head point gauge

Model Modifications

To understand the effects of the weir crest and apron conditions on nappe vibration, different physical modifications were used on the models. The modifications were intended to help better understand the source of the initial instability leading to nappe vibration as well as the factors involved in sustaining the oscillatory behavior. Modifications were made to the weir crest and, where possible, to the point of impact on the apron.

Model #1 Modifications

As previous research has stated, changes to the flow conditions at the crest of a weir have shown promise in the remediation of nappe vibration. One modification in particular that has practical application is the addition of roughness elements to the weir crest surface. Roughness elements for the crest on model #1 included:

- Expanded metal mesh cloth covering the entire weir crest (model #1b, see Fig.14)
- A thin-gauge hardware cloth with ½ inch square openings. The top wire of the hardware cloth was removed, leaving ½ inch vertical "prongs." The hardware cloth was attached to the vertical downstream face of the weir crest with the prongs extending into the nappe flow (model #1c, see Fig. 15).

Fig. 14. Model #1b expanded metal roughness

Fig. 15. Model #1c hardware cloth prongs

The following apron modifications were tested on model #1:

- 3 inch thick open-cell foam pad (model#1d, see Fig. 16)
- Impact plate oriented at different angles on the apron (model #1e-g, see Fig. 17)
- Increased tailwater depth (deeper plunge pool where the water strikes the apron downstream of the weir)

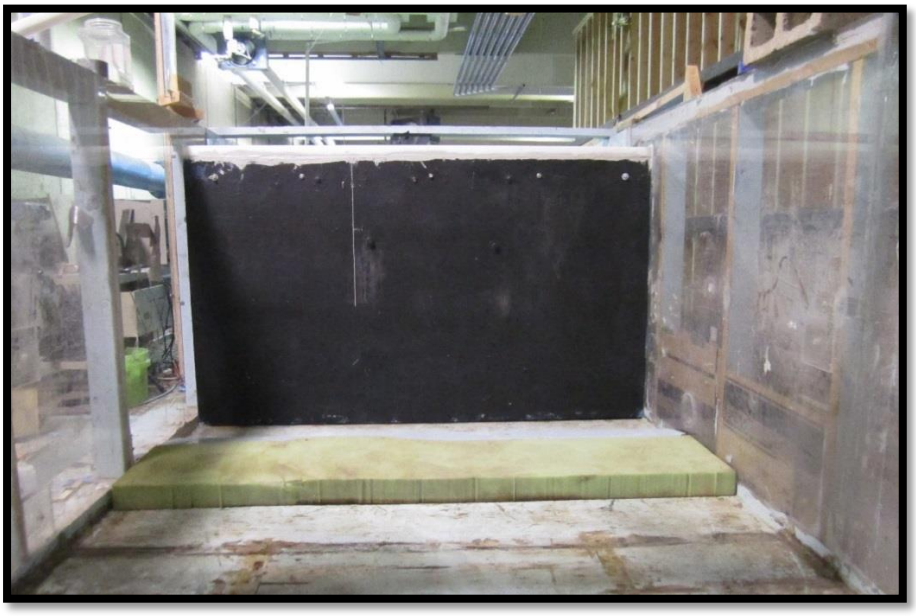

Fig. 16. Model #1d open-cell foam pad on the apron (flume floor)

Fig. 17. Model #1f wooden impact plate on the apron

The 6 foot long x 2 foot wide foam pad was secured to the flume apron with nails. The wooden plates were installed with 3 different orientations:

- 45° from horizontal, oriented toward the weir
- 45° from horizontal, oriented away from the weir
- 9° from horizontal, oriented toward the weir, so as to create an impact surface perpendicular to the nappe

A 1 ½ inch gap was left between the plate and the apron to allow water to drain from behind the nappe. Stop logs at the downstream end of the flume were used to increase the tailwater depth for model #1h.

In order to better understand the source of the initial instability which leads to nappe vibration, a combination of a crest and an apron modification was tested simultaneously. By pairing a crest modification observed to eliminate nappe vibration with an apron modification observed to amplify nappe vibration, study regarding the source of the instability (for model #1) could be performed.

Model #2 Modifications

To reduce the surface texture roughness of the plywood broad crest section of the weir (see Fig. 7), the crest was covered with thin gauge tin sheeting and secured on the upstream and downstream side with screws. Tests with this broad-crested weir configuration did not produce vibrations until the upstream side of the crest was retrofitted with a small radius (R=1 ½ inch) quarter round section made out of HDPE (see Fig. 18). To provide roughness elements to the crest (model #2c), expanded metal mesh cloth was

wrapped around and fastened to the top of the crest (see Fig. 19). To test the effectiveness of nappe splitters (model #2d), 2 inch wide by 8 inch tall sections of HDPE were clamped to the downstream side of the crest. Starting with one splitter located in the center of the crest, splitters were added one at a time and evenly spaced up to the maximum of three. Nappe splitters were tested without the expanded metal cloth on the weir crest configuration shown in Fig. 18. Due to the lack of a confined air cavity behind the nappe on model #2, the purpose of the nappe splitters is to divide the nappe into smaller, equally spaced sheets of water in order to observe the effect on the vibration of the nappe as a whole.

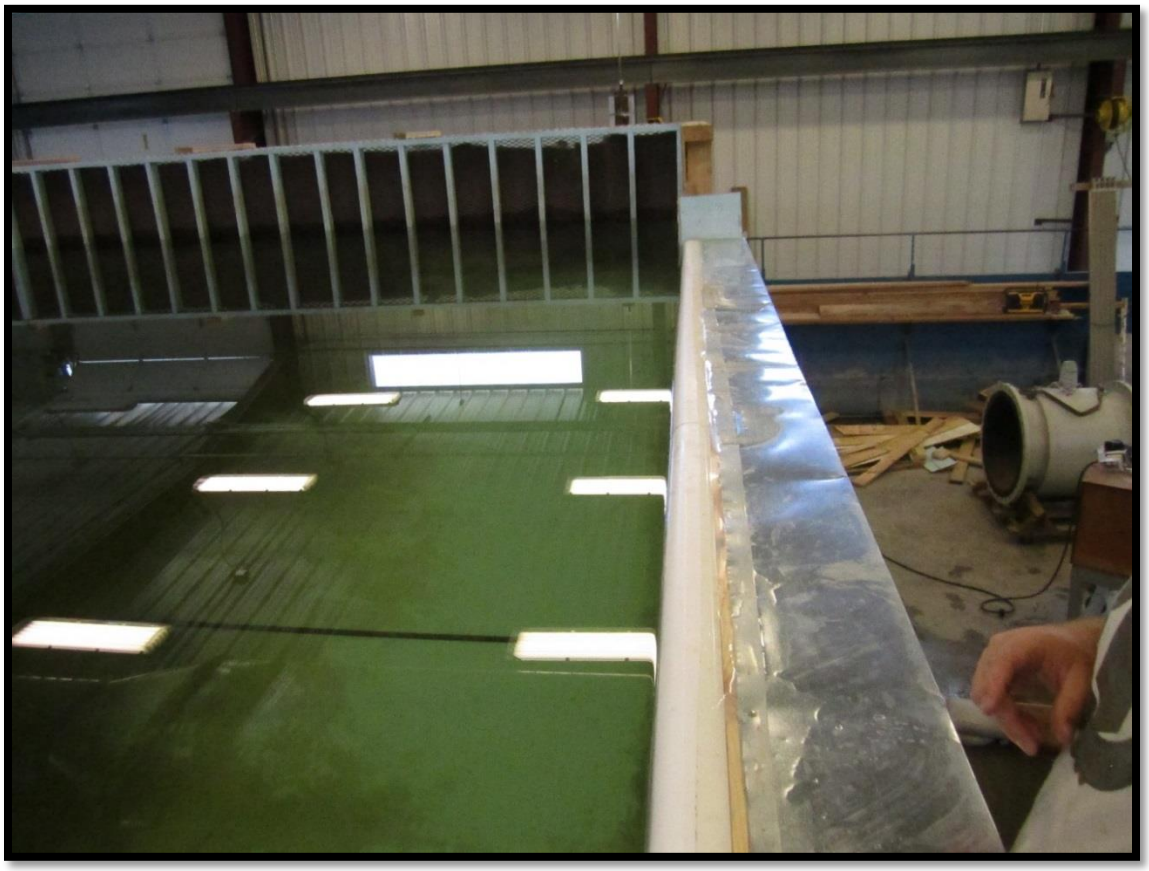

Fig. 18. Model #2b weir with rounded section upstream

Fig. 19. Model #2c expanded metal roughness

Model #3 Modifications

Rather than roughening the crest with expanded metal, roughness elements for model #3 are provided by gluing ¾" inch – 1 ¼ inch stones to the crest. For the first modification to model #3, deemed model #3b, the stones did not cover the entire crest, but were placed on the upstream rounded portion up to a point where the tops of the highest row of stones was at an elevation equal to the top of the crest (see Fig. 20 and Fig. 21).

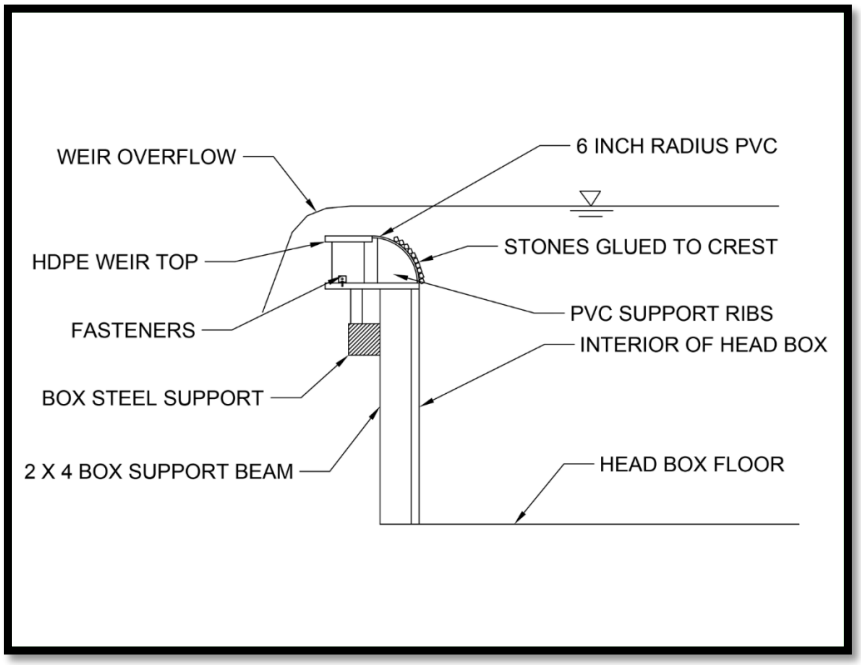

Fig. 20. Model #3b and #3d stone roughness modification

Fig. 21. Model #3b and #3d stone roughness

In order to investigate the effect of an enclosed air pocket behind the nappe (similar to that produced in model #1), sidewalls and a back wall were constructed out of plywood (see Fig 12). Model #3c was comprised of the non-modified crest (no roughness elements) and the confining walls (non-vented). Model #3d included the same partially roughened crest shown in Fig. 21, but with the confined air pocket behind the nappe. Model #3e utilized the same air pocket containment walls, but more ¾ inch- 1 ½ inch stones were added to cover the entire crest (see Fig. 22 and Fig. 23). Model #3f included the sidewalls and back walls for air containment, but the majority of the rocks were removed, leaving only one row of stones at the downstream edge of the crest (see Fig 24 and Fig. 25).

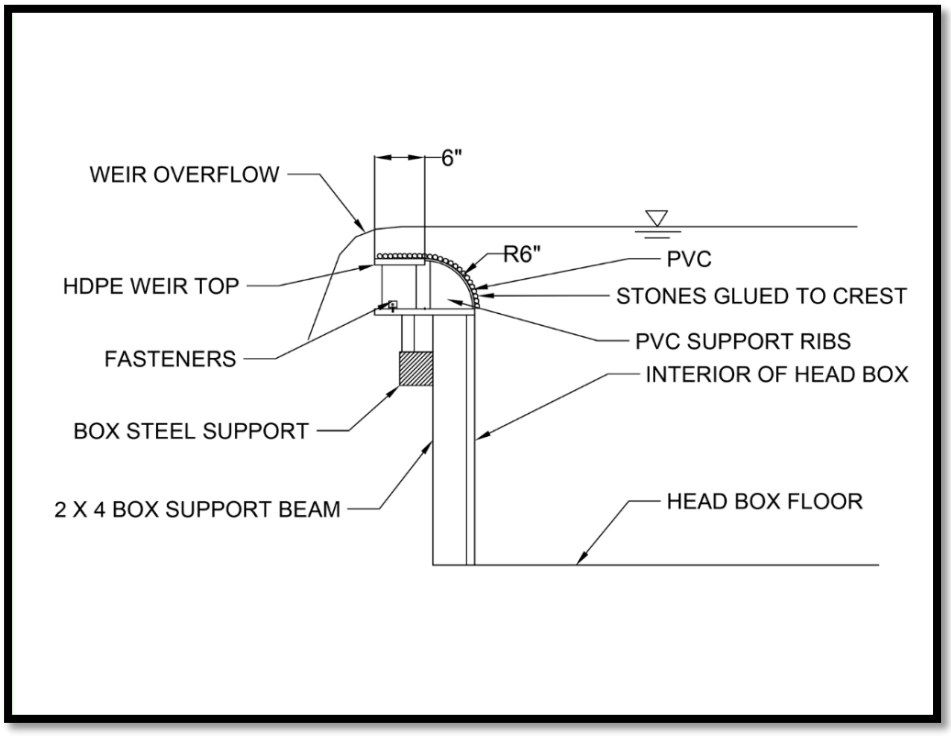

Fig. 22. Model #3e stone roughness modification

Fig. 23. Model #3e stone roughness

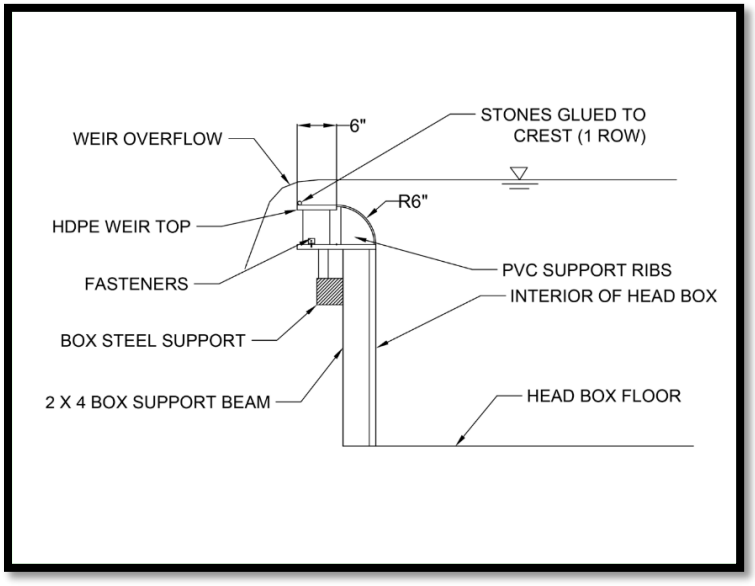

Fig. 24. Model #3f stone roughness modification

Fig. 25. Model #3f stone roughness

Model #3g-a, model #3g-b and model #3h involved modifications intended to be less intrusive and have less of an effect on the efficiency of the weir. For model #3g, ½ inch by ½ inch square notches were cut into the flat portion of the crest with an electric router starting at the downstream edge and continuing 4 ½ inches upstream (see Fig. 26 and Fig. 27). Model #3g-a had a 4 foot spacing between notches, and model #3g-b had 1 foot spacing between notches. The principle behind this modification was to either create enough turbulence in the flow due to the discontinuity in the weir crest to reduce or eliminate oscillations in the nappe, or to produce locally higher velocities of water moving through the notches which break through the nappe to effectively split and aerate the confined space behind the nappe.

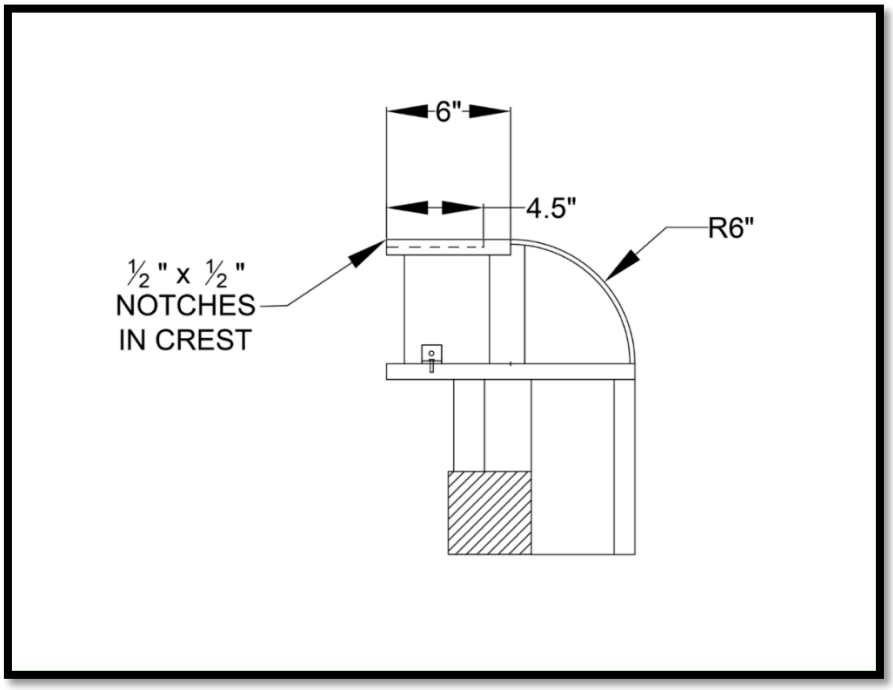

Fig. 26. Model #3g weir modification

Fig. 27. Model #3g crest notches

For model #3h, rather than having ½ inch x ½ inch notches cut into the crest at 1 foot spacing on center, ½ inch x ½ inch notches projecting upward into the flow from the crest were created by gluing 1 inch tall x ½ inch wide x 4 ½ inch long wooden sections into the preexisting ½ inch x ½ inch notches (see Fig. 28 and Fig. 29). The intent of this modification was to attempt to produce sufficient turbulence in the boundary layer of the flow over the weir crest to interfere with the vibrations in the nappe without requiring a continuous form of roughness across the entire length of the crest. Such a modification could be potentially cheaper to install and easier to maintain.

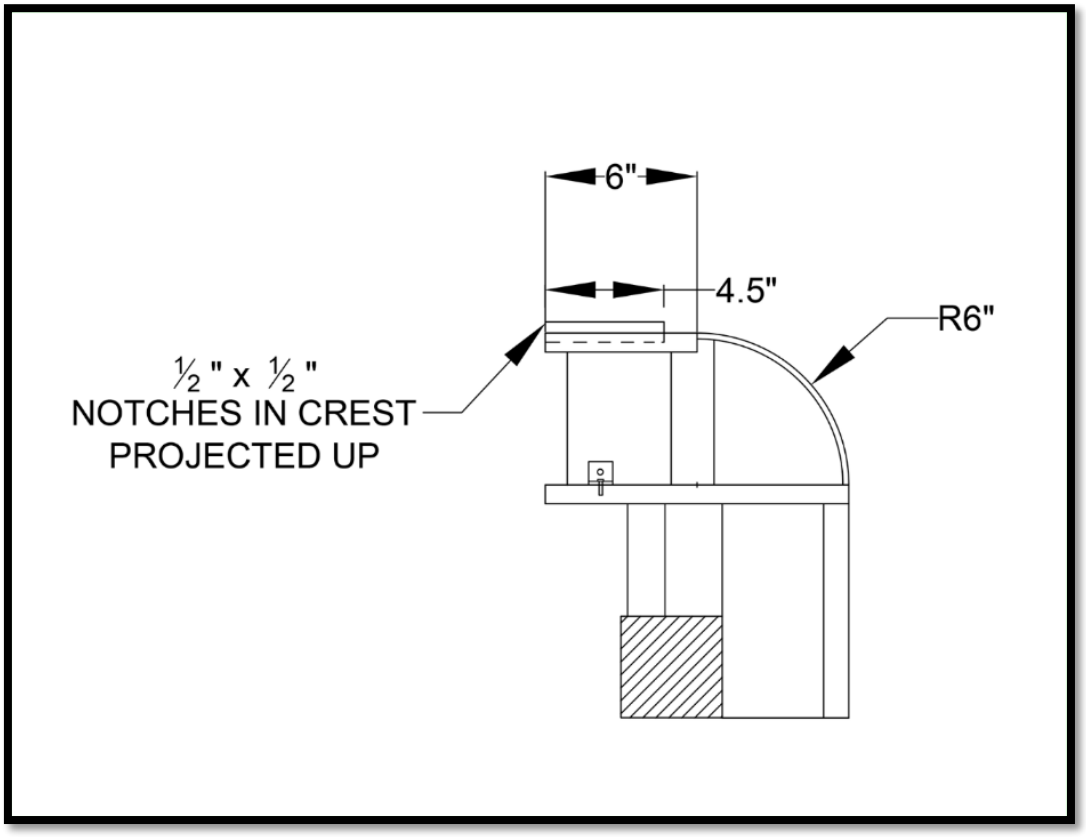

Fig. 28. Model #3h weir modification

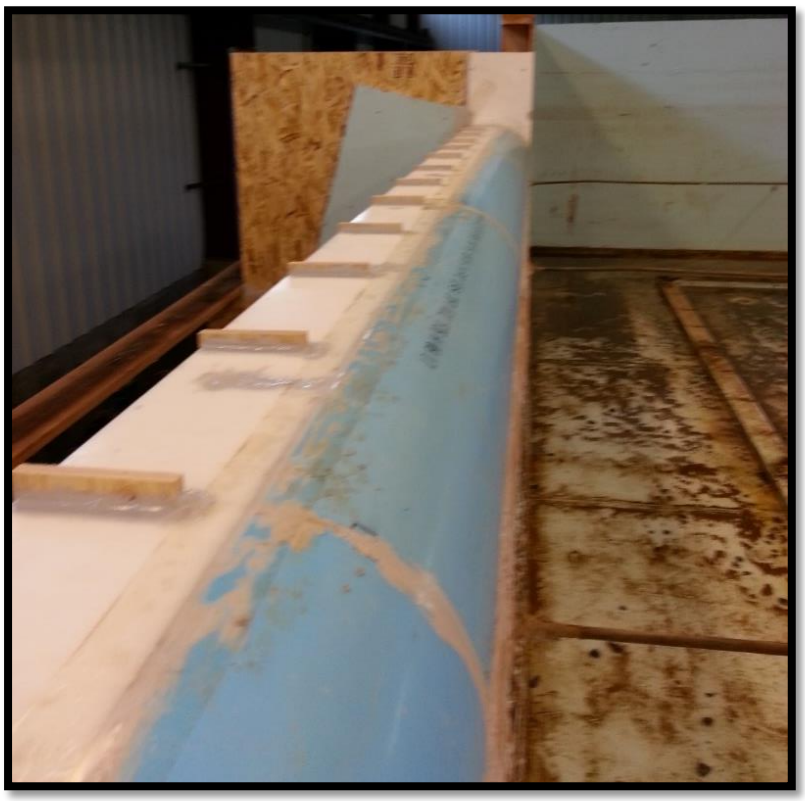

Fig. 29. Model #3h wood crest notches

CHAPTER IV

MODEL #1 RESULTS

General Observations

Before presenting the results of the tests performed on model #1, it is important to discuss some of the key preliminary observations that guided the testing method. The cause of the following observed behaviors of the vibration in model #1 is assumed to be mostly due to the dependence of the vibration on the enclosed air volume behind the nappe, which in itself is sensitive in nature. Another possible explanation for what was observed is the limited fall height of the nappe.

Nappe Vibration Sensitivity

The most common difficulty encountered while testing nappe vibration in model #1 is the overall sensitivity of the vibration, which often leads to non-repeatable results when a weir discharge condition is replicated. Substantial differences in the observed behavior of the nappe while discharging the same flow rate were seen not only on a day-to-day basis, but even on an hourly basis. Such sensitivity made the collection of reliable data for flow ranges under which nappe vibration occurs an almost impossible task. It was also observed that vibration occurred more prevalently on a weir crest that is slightly out of level from side to side.

Hysteresis

Hysteresis is an extraordinary phenomenon which causes the effects of a previous state to influence the current state. Nappe vibration in model #1 exhibited this behavior on

several occasions, and is a difficult aspect to quantify. Nappe vibration was, under certain discharges, observed to be highly dependent on the dynamic conditions leading up to a steady-state condition. For example, a certain flow condition could be established over the weir for which nappe vibration did not occur. If the flow condition was changed to a vibrating nappe condition and was then returned to the previous non-vibrating condition, the nappe would continue to vibrate in some cases. This hysteretic effect did not occur definitely, but introduced uncertainty when experimenting with variable discharges on model #1. The effects of hysteresis could play a role in nappe vibration occurrence on prototype spillways.

Vibration Induction

It is important to distinguish between self-induced nappe vibration and nappe vibration initiated by an external force. Testing on model #1 revealed the fact that, under certain flow rates, vibration could be initiated externally by agitating the nappe manually with a stick. For this research, the focus was self-induced vibration which does not require an exterior means of excitation such as that stated.

High Discharge vs Low Discharge

Distinct differences were observed between nappe vibration occurring at high and low discharges (see Fig. 30). Vibration occurring at higher discharges (~0.433 ft^2/s) was typically intense, displaying a high frequency and low amplitude, and was generally sustainable for a relatively long period of time. It was common to observe a periodic, pulsing oscillation of vibration intensity, generally on the order of 0.25-0.5 seconds. At

high discharges, the trajectory of the nappe when vibrating relative to the non-vibrating state suggests the development of sub-atmospheric pressures in the confined air space, manifested by the nappe being drawn in toward the air pocket. The time required for vibration to occur under high discharges was somewhat random; vibration would begin very quickly for some runs, while being delayed up to several minutes for others.

Lower discharges (approximately 0.16 ft^2/s and below) displayed different vibration characteristics. Rather than a sustained, high intensity vibration, low discharge conditions produced a distinct, cyclical vibration process involving high amplitude waves with a low frequency. As water discharged over the crest, the nappe would initially be stable (non-vibrating) with a constant trajectory, but the pressure in the air pocket behind the nappe would gradually increase as air entrained in the nappe was supplied to the enclosed air pocket, primarily occurring at the location where the nappe impacts the apron.

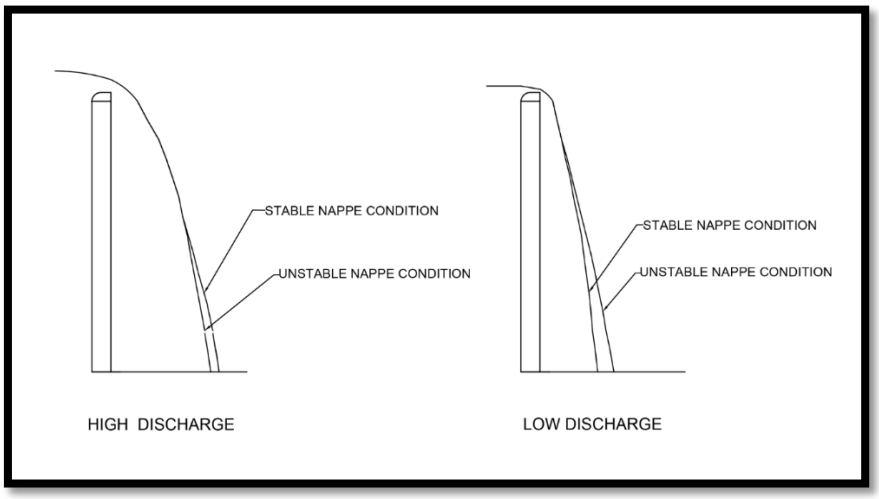

Fig. 30. High discharge vs. low discharge vibration characteristics

When the pressure differential became large enough (a process that took 2-3 minutes), the nappe would begin to oscillate, producing large, flapping waves most visible near the point of impact with the apron. The flapping nappe waves generally lasted 15-20 seconds, relieving the pressure behind the nappe. Once the nappe returned to stable conditions, the cycle repeated. Noise and sound pressure waves associated with this low discharge vibration mechanism were mild compared to the vibration observed at higher discharges.

Model #1 Results

Considering that the vibration observed for low discharges was milder in nature, the results presented in this report focus on the intense, higher frequency vibration associated with higher discharges. To avoid issues with hysteresis, a single target discharge was used to compare the different modifications to the crest or apron. The target discharge was 0.433 ft^2/s, and actual measured discharge ranged from 0.432 ft^2/s - 0.435 ft^2/s. The total driving head on the weir was 2.94 inches for the un-modified crest, while the expanded metal crest required 3.05 inches of head to pass the same flow. While this report does not specifically focus on weir efficiency, it is important to note that, for a given upstream head, roughness elements added to the weir crest do in fact decrease discharge over the weir.

Model #1a - Unmodified Quarter Round Crest

Nappe vibration for the un-modified, non-vented crest displayed a range of behaviors, even at the target flow rate, due to the effects discussed previously in this

chapter. The intensity of vibration was truly random; some runs would produce a strong, sustained vibration while others produced very little noticeable vibration. The data presented represents the most common and repeatable vibration frequency observed on model #1a while un-vented, which was somewhat mild in nature. Fig. 31 displays the commonly observed vibration intensity recorded by the accelerometer. The estimated frequency is 35 Hz, a value that comes from visually analyzing the accelerometer reading output.

Model #1a - Vented Nappe

To properly compare the effect of each modification tested in model #1, it was important to determine the level of vibration registered by the accelerometer for a "no nappe vibration" condition. By placing a small object, such as a stick, into the weir nappe and flume sidewall interfaces, the flow separated from the sidewall boundary and air was admitted into the space behind the nappe (vented nappe). Under most conditions (the exception of which will be discussed in a subsequent section), this simple technique eliminates visible and audible traces of vibration. However, there is still some vibration in the flume as a result of the nappe impacting on the apron. Fig. 32 displays the data recorded by the accelerometer for a nappe under vented conditions. The acoustic energy frequency for the vented nappe was much more inconsistent (both in frequency and amplitude), and the intensity of peak values decreased in comparison with the confined, non-vented condition of model #1a. While the graphs display what appear to be very minor differences, distinct differences were audibly and visibly detectable.

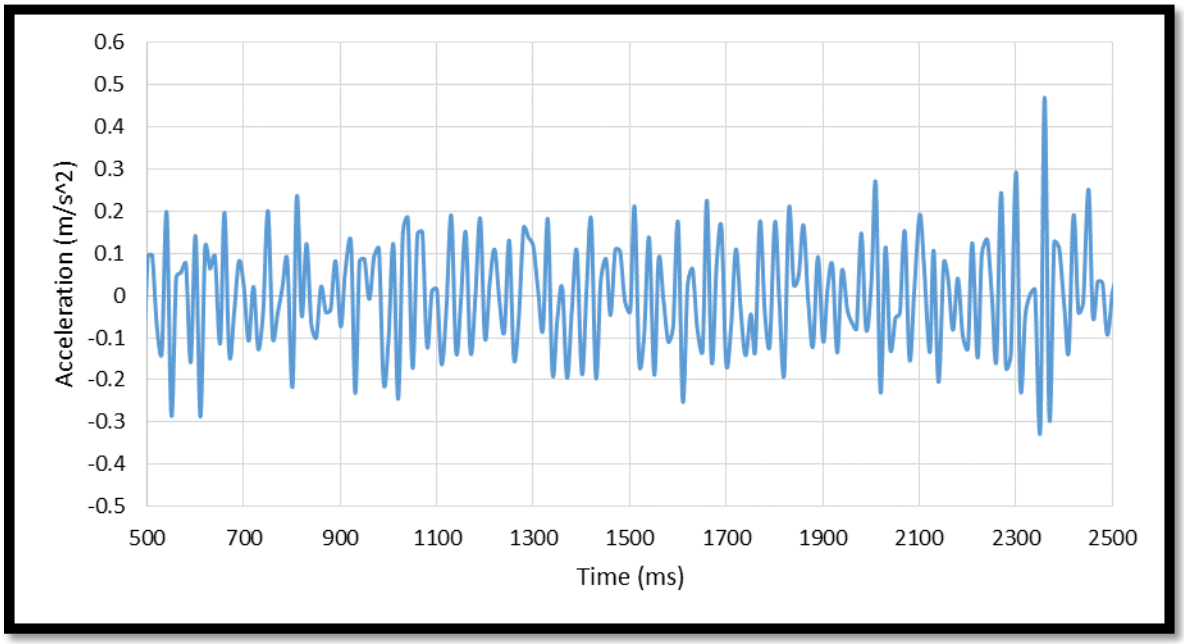

Fig. 31. Model #1a nappe vibration accelerometer data (35 Hz)

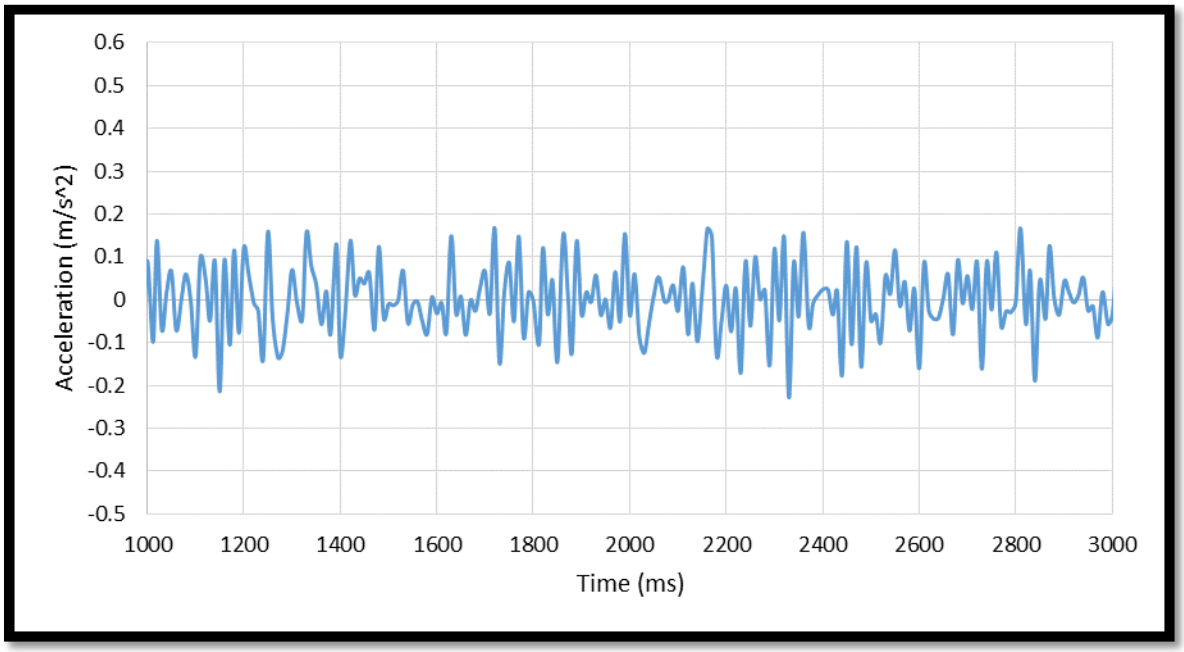

Fig. 32. – Model #1a nappe vibration accelerometer data with a vented nappe (non-vibrating nappe)

Model #1b - Expanded Metal on Weir Crest

Expanded metal attached to the weir crest successfully altered the vibration intensity, but did not eliminate its occurrence. As mentioned previously, nappe vibration at higher discharges in model #1a (non-vented nappe) was accompanied by sub-atmospheric pressures developing in the enclosed air pocket behind the nappe, manifested as the nappe was drawn in toward the spillway wall. This pressure differential was attributed to a negative net air transfer between the enclosed air volume behind the nappe and the surrounding atmosphere, caused by air being entrained into the falling sheet of water.

While the expanded metal on the crest did interfere with the vibration and caused turbulence at the boundary layer of the crest, it was also observed to increase the magnitude of the negative pressure in the air pocket (as indicated by changes in the nappe trajectory) in comparison with model #1a. As water flowed over the rough crest and entered free falling conditions, the turbulence provided a means of increasing air entrainment, pulling an increased volume of air from the enclosed air pocket, thus leading to a lower pressure behind the nappe relative to model #1a (see Fig. 33).

The decrease in pressure behind the nappe on model #1b lead to an unstable nappe condition. To the naked eye and ear, the expanded metal appeared to reduce the vibration of the nappe. However, accelerometer measurements provided evidence that the nappe was indeed actually vibrating. Fig. 34 displays the results of accelerometer measurements for the expanded metal crest modification (model #2b).

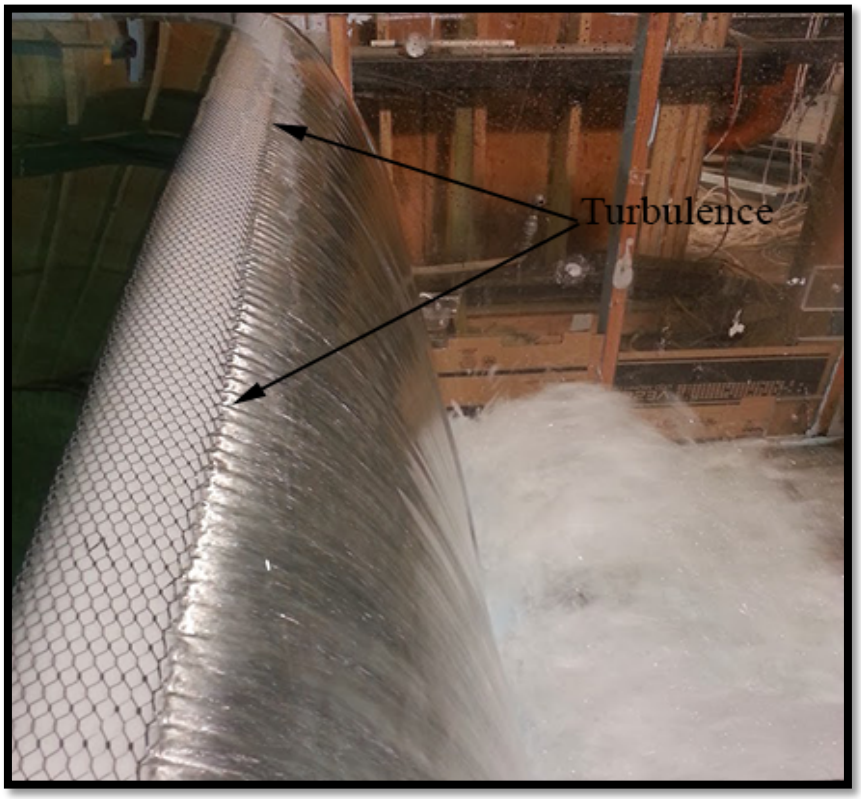

Fig. 33. Model #1b increased air entrainment due to roughness

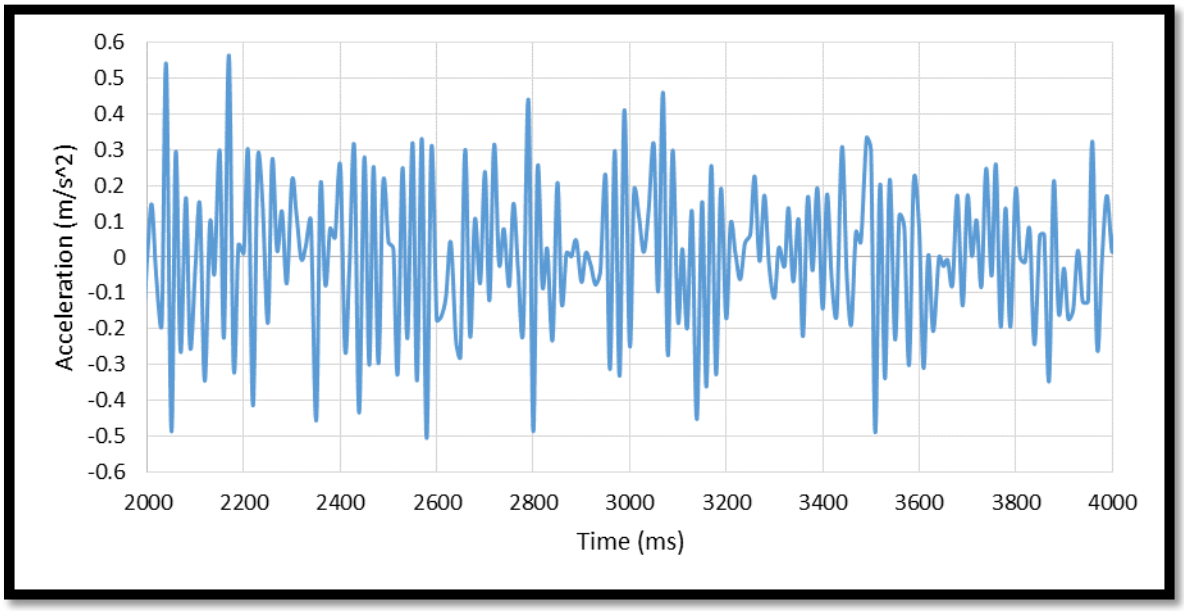

Fig. 34. Model #1b nappe vibration accelerometer data (variable frequency)

For model #1b, the addition of the expanded metal creates a vibration of variable intensity, with peak values exceeding those of the model #1a. It is important to note that the effect of the expanded metal on the crest differed greatly between model #1 and models #2 and #3, which is discussed in detail in subsequent chapters. Generally speaking, roughness elements have been observed to attenuate nappe vibration, but in this case, it appeared as if the increased pressure differential between the air pocket and the surrounding air caused by the expanded metal was the dominant driving force, outweighing the commonly observed attenuation property of roughness elements due to the introduction of turbulence at the boundary layer of the flow.

Model #1c -Hardware Cloth Prongs on Crest

Rather than wrapping the entire crest with a roughness element, this modification limited the flow disruption to the location where the discharge separated from the edge of the weir crest on the downstream side. The hardware cloth was clipped and fastened with screws on the downstream vertical face of the weir crest forming vertical prongs spaced ½ inch apart and ½ tall; the prongs did not extend up through to the free surface of the flow. This modification caused a significant reduction in measureable vibration in the model. The hardware cloth prongs provided the necessary turbulence in the flow to interfere with and reduce nappe vibration (see. Fig 35), while avoiding the instabilities associated with the large pressure differential between the atmospheric air surrounding the nappe and the enclosed air volume behind the nappe associated with the expanded metal cloth modification (model #1b).

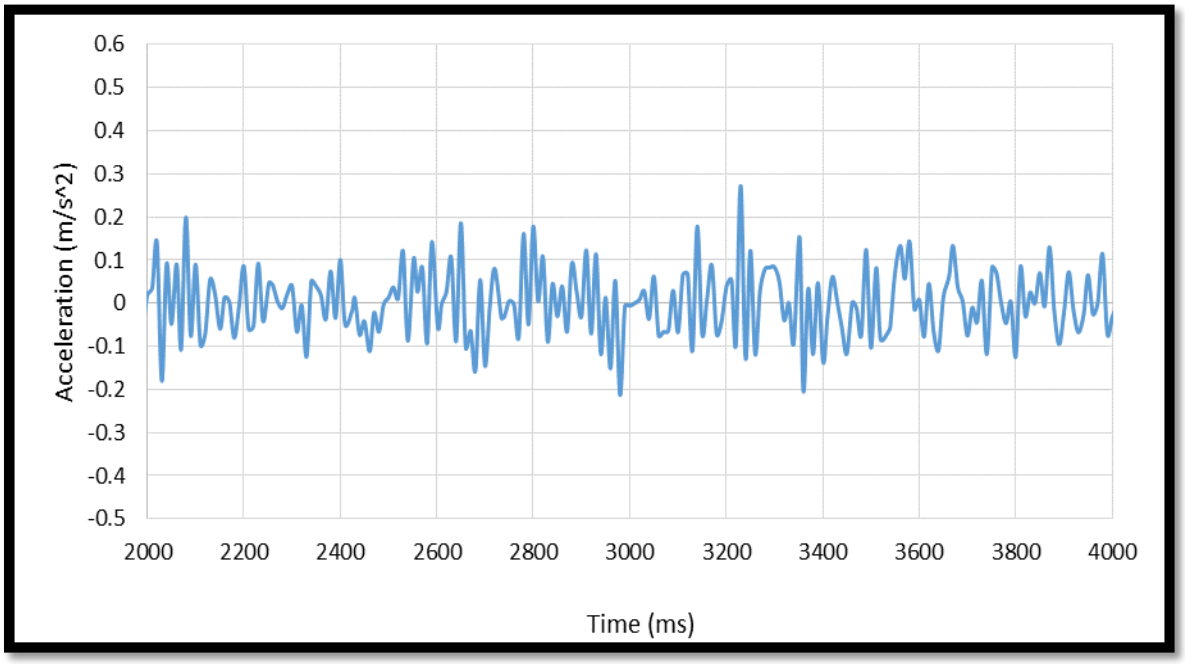

Fig. 35. Model #1c nappe vibration accelerometer data (non-vibrating nappe)

Model #1d - Foam Pad on Apron

As the nappe approached the downstream apron on model #1a runs, the amplitude of the vibration waves increased, likely due in part to the Helmholtz effect. As the wavy nappe impacted the apron, acoustic energy frequency appeared to coincide with the alternating positive and negative wave peaks hitting the apron. The majority of the sound generated by the vibrating nappe appeared to originate from the point of impact on the apron. In an effort to investigate the influence of a more cushioned apron material on nappe vibration, a 3 inch thick open-cell foam pad was secured to the floor of the flume. In addition to cushioning the impact zone, the porous foam pad influenced the hydraulics on the apron by making it more difficult for water in the air pocket behind the nappe to escape, causing the water depth in the air pocket to increase.

The presence of the foam pad did not cause the vibration of the nappe to cease; in fact, vibration became more intense and occurred more easily with the foam pad in place. Also, while the foam pad was on the apron, the nappe displayed a unique behavior when vented. When the nappe was lightly vented by placing a stick between the edge of the nappe and the confining acrylic side wall of the flume (in a manner which terminated vibration for all other model #1 modification conditions), the vibration continued to occur. While the peak vibration amplitude was similar to that of the un-vented nappe, the overall amplitude was much more variable. Moving the stick toward the center of the nappe and increasing the amount of venting eventually caused the vibration to cease. The frequency and magnitude of the measured acceleration for the non-vented nappe are shown in Fig. 36, with measurements of the vented nappe shown in Fig. 37.

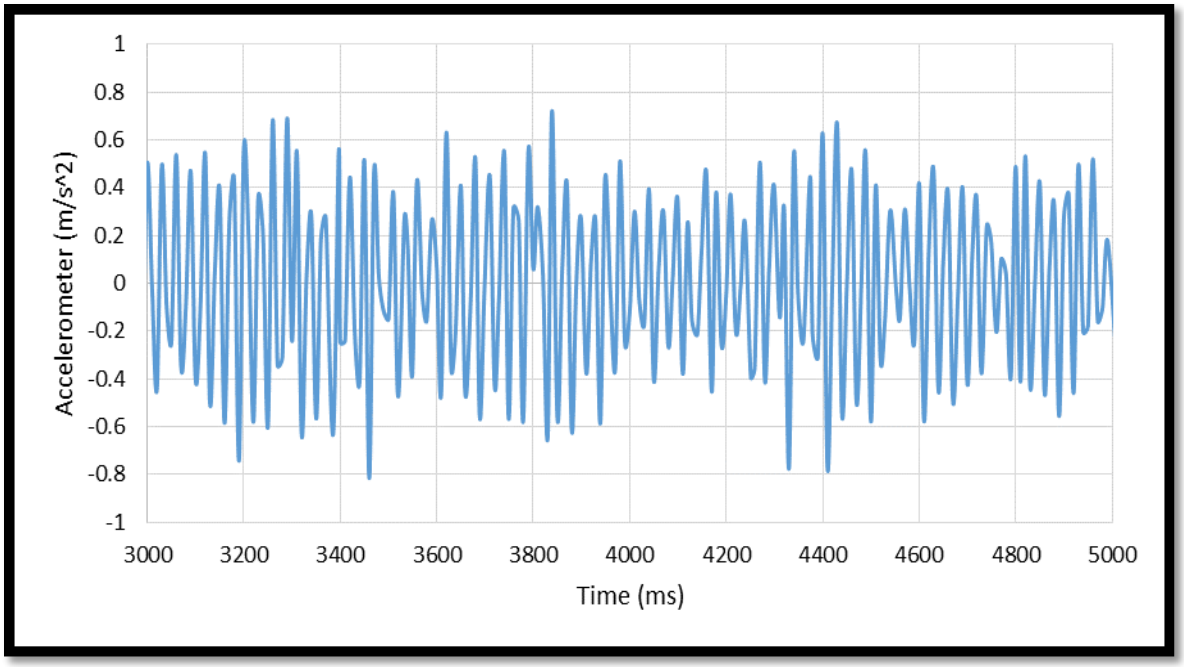

Fig. 36. Model #1d nappe vibration accelerometer data, non-vented (36 Hz)

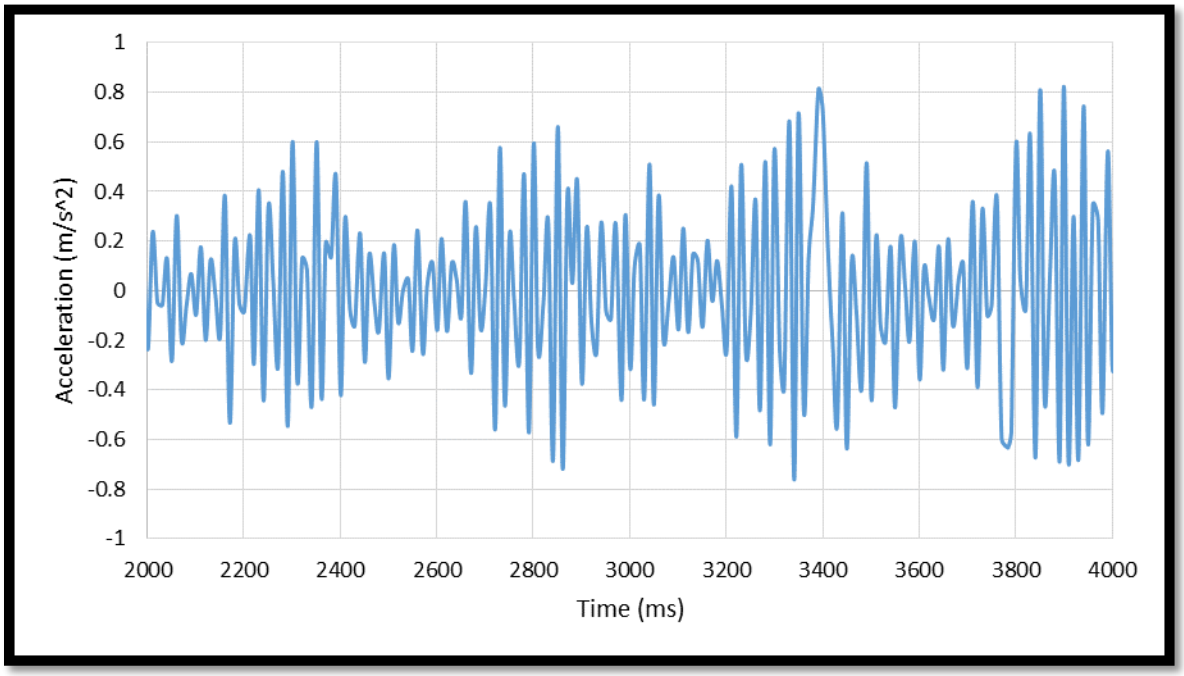

Fig. 37. Model #1d nappe vibration accelerometer data, vented (35 Hz)

Model #1e - Plate on the Apron
Angled 45° Toward Weir

The impact plate oriented 45° from horizontal toward the weir displayed interesting characteristics. The behavior of the nappe was dependent on how the nappe deflected off of the plate. If the nappe impacted the plate at an angle close to vertical, the water deflected upward at a steep angle on the downstream side of the nappe (Fig. 38 and Fig. 39). Under such conditions, strong vibration with an oscillating intensity would instantly begin and would sustain itself as long as the trajectory of the nappe remained constant. If the nappe impacted the plate at a less steep angle, water deflects downstream at a more flat trajectory. Mild vibration occurred under this condition, but the intensity did not match that of the previously stated condition (Fig. 40 and Fig. 41).

Fig. 38. Model #1e steep deflection angle

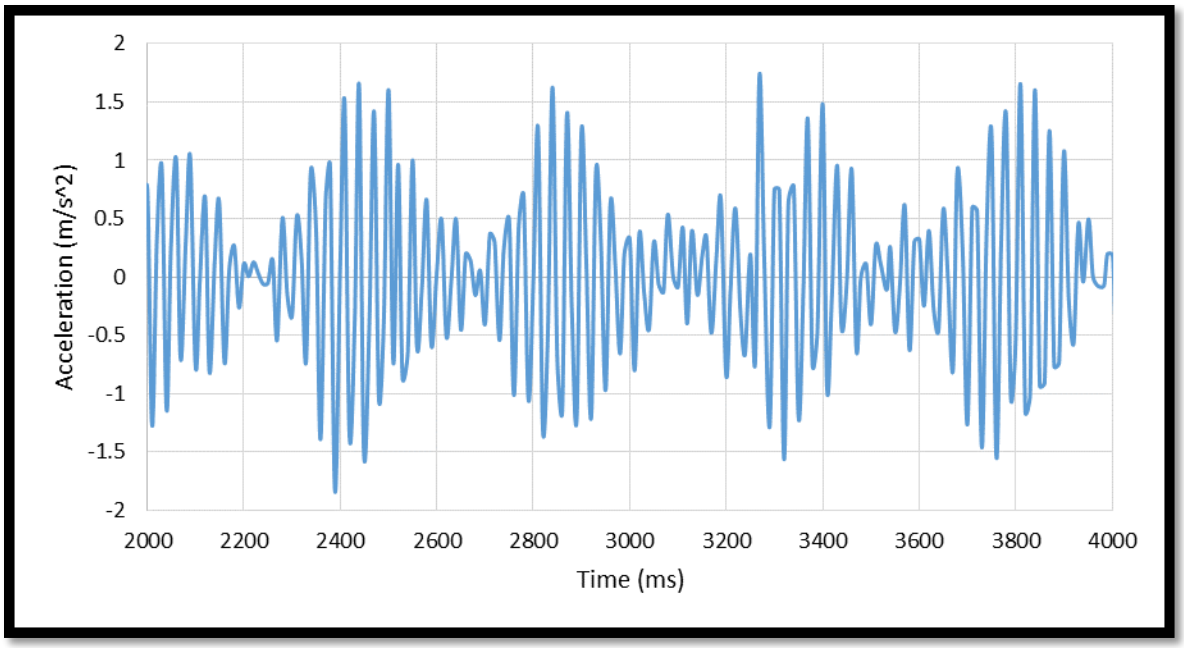

Fig. 39. Model #1e nappe vibration accelerometer data, steep deflection (35 Hz)

Fig. 40. Model #1e shallow deflection angle

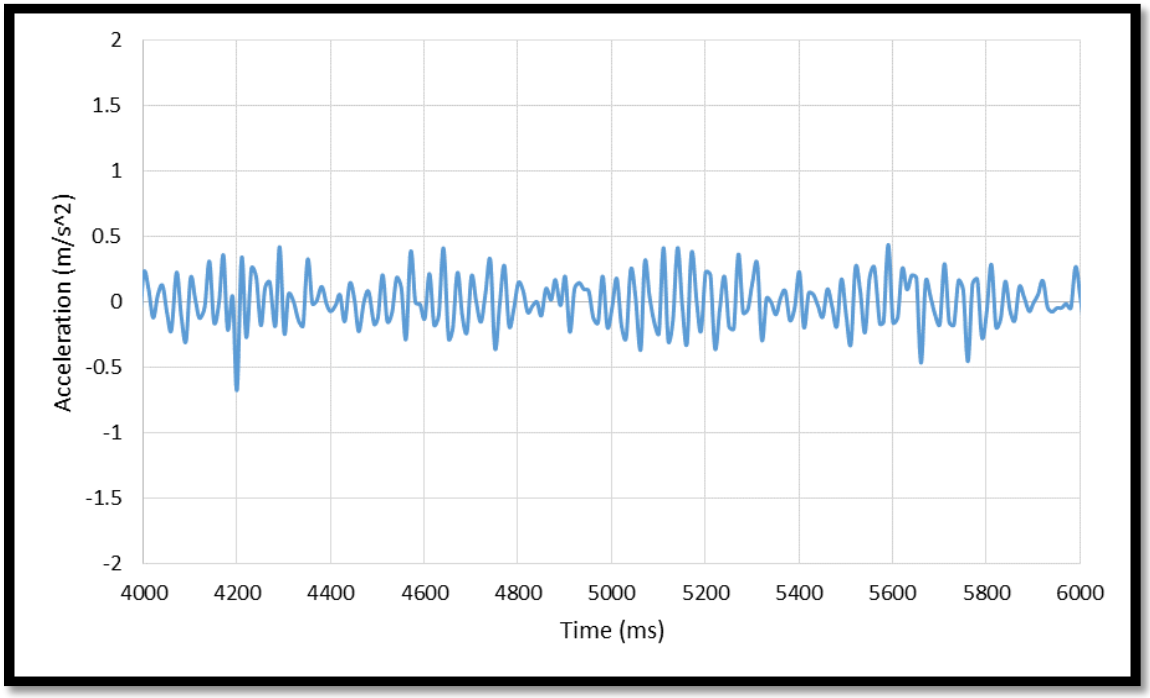

Fig. 41. Model #1e nappe vibration accelerometer data, shallow deflection (variable frequency)

Model #1f - Plate on Apron Angled 45° away from Weir

Orienting an angled plate on the apron away from the weir at a 45° angle had dichotomous results. Under certain conditions, the plate would deflect water back toward the weir, causing extremely intense vibration to ensue (see Fig. 42). But, if this deflection condition was not satisfied, the strong vibration did not occur. Fig. 40 displays the acceleration measured in the flume caused by the vibrating nappe. It is likely that the water jet impacting the wall has an effect on the vibration, potentially influencing the motion of the air pocket behind the nappe.

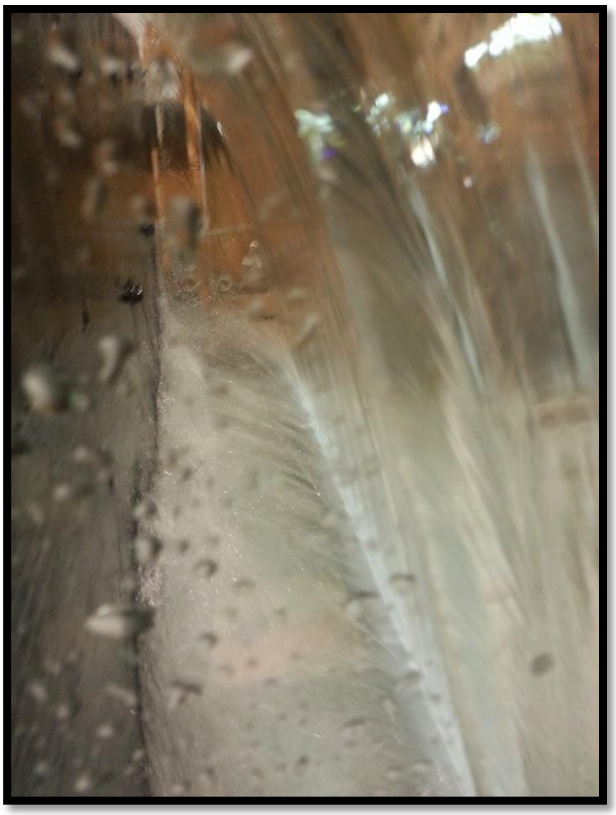

Fig. 42. Model #1f nappe deflecting back toward weir

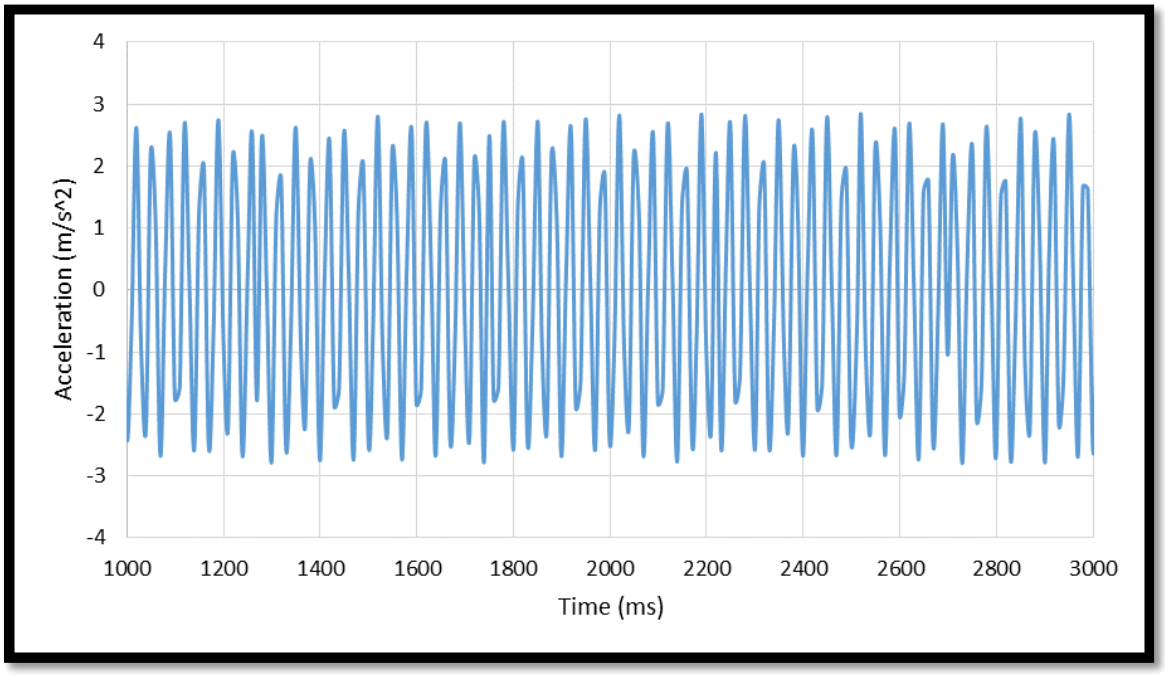

Fig. 43. Model #1f nappe vibration accelerometer data (30 Hz)

Model #1g - Plate Oriented Normal to the Nappe Impact Region

As the nappe lands on a plate oriented at an angle normal to the flow (9° from horizontal), water is deflected downstream at an angle near horizontal (see Fig. 44). This condition produces heavy vibration, shown in the accelerometer readings in Fig. 45. The results of tests with the angled plates in general were somewhat inconsistent. The behavior of the nappe varied significantly depending on the specific trajectory of the nappe and the angle that the water sheet deflected off of the plate. Tests with the variable angle plates at the point of impact produced the most intense vibration in the flume. The vibration witnessed during testing was truly astounding, and could at times be heard and felt throughout the large laboratory.

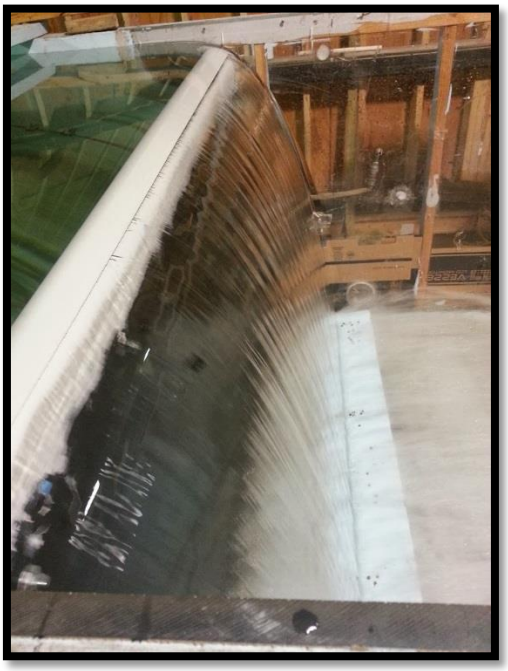

Fig. 44. Model #1g nappe deflection angle

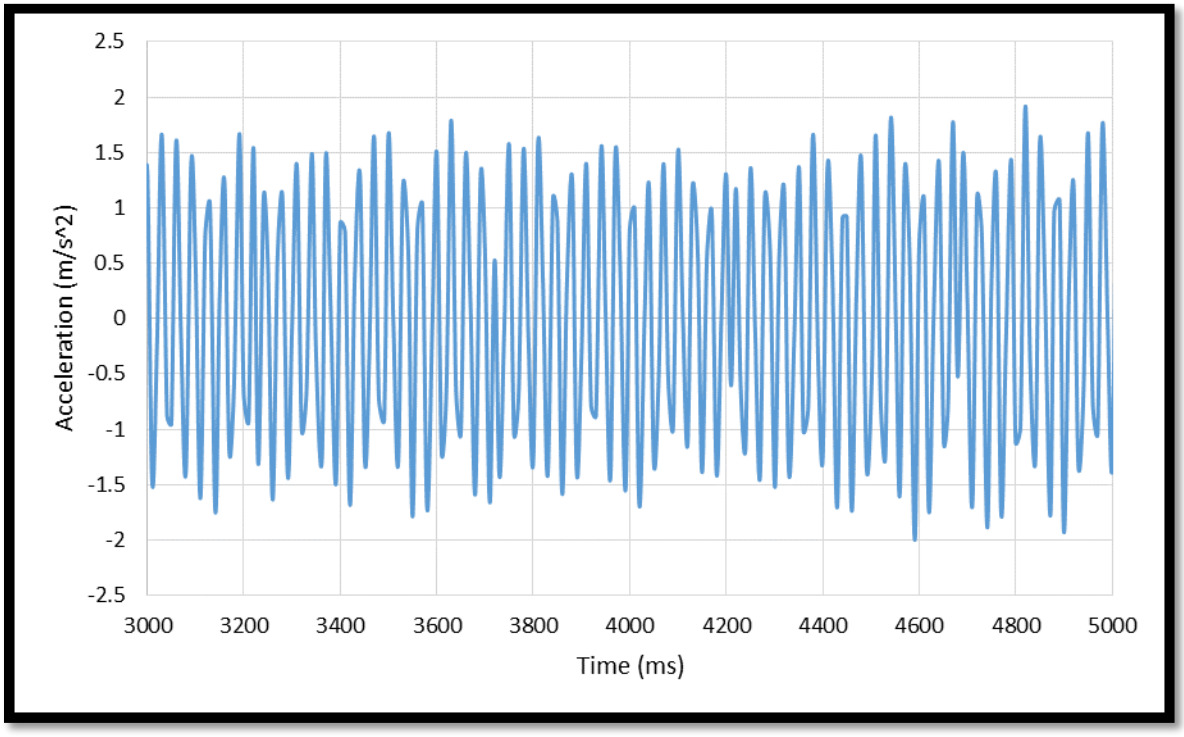

Fig. 45. Model #1g nappe vibration accelerometer data (32 Hz)

Model #1h - Increased Tail Water Depth

In many prototype spillway applications, discharge over a weir will fall into a plunge pool rather than a solid, bare surface. To produce tail water in model #1h, stop logs were installed at the downstream end of the flume. By raising the tail water in the flume (~8 inches deep), there was no detectable vibration, and the accelerometer readings were consistent with a "non-vibrating" nappe. While the addition of a plunge pool to the model reduced nappe vibration, as a side note, it was observed that dynamic tail water conditions, produced by damming and undamming the flume outlet repeatedly and quickly, can help initiate the vibration process. Fig. 46 shows the influence of increased tail water depth in model #1h.

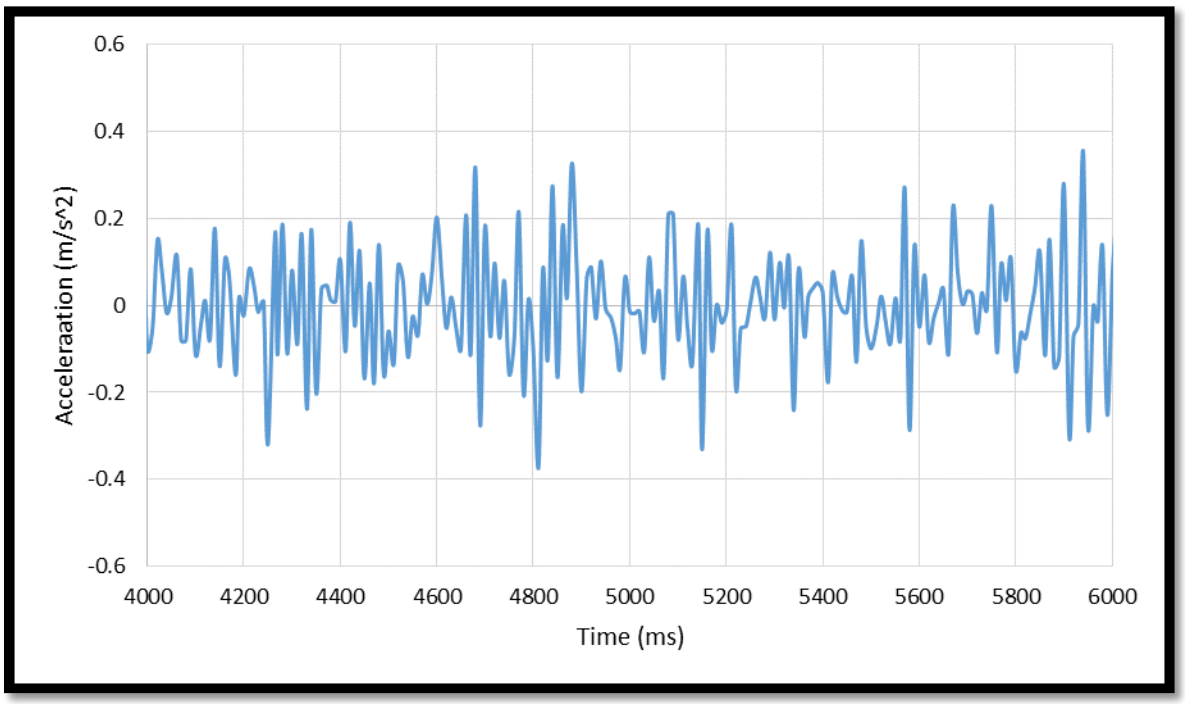

Fig. 46. Model #1h nappe vibration accelerometer data, (non-vibrating nappe)

Model #1i - Hardware Cloth Crest Modification with 45° Plate Toward Weir on Apron

It has been observed that nappe vibration can be attenuated or amplified by introducing different physical modifications to model #1. In an attempt to verify the sensitive location where nappe instability is initiated, a crest modification observed to eliminate vibration was paired with an apron modification observed to amplify vibration. The vertical hardware cloth prongs were installed on the downstream side of the weir, and the 45° plate (oriented toward the weir) was fastened to the apron. While the angled plate on the apron oriented at 45° toward the weir did not produce the strongest vibration in the nappe of all the tested apron modifications, it did provide the most consistent and repeatable vibration. Fig. 47 displays the accelerometer results of this test. Even with the angled plate on the apron, vibration in the flume was not observed.

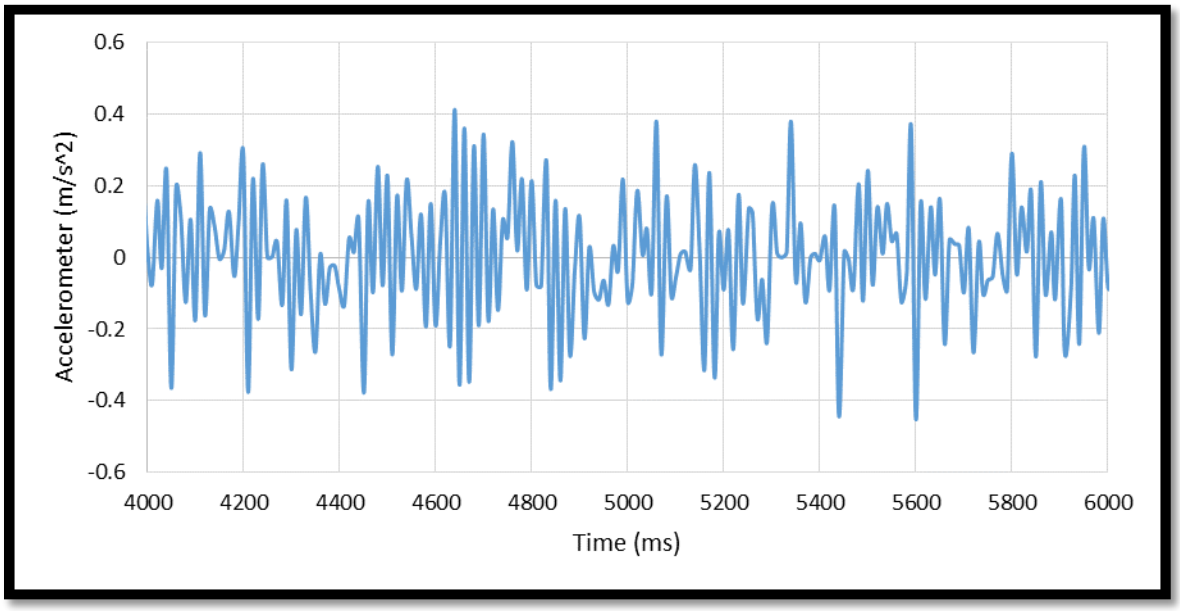

Fig. 47. Model #1i nappe vibration accelerometer data (non-vibrating nappe)

CHAPTER V

MODEL #2 RESULTS

General Observations

The majority of research regarding nappe vibration has focused on the conditions of a confined nappe. However, model #2 exhibited a vibrating nappe with unconfined nappe flow conditions (no sidewalls nor back wall to create a confined air volume behind the nappe). With nappe vibration occurring without a confined air pocket behind the nappe, it is difficult to conclude that the air behind the nappe is the only or primary driving force in self-induced nappe vibration.

The analysis of high-quality slow motion video of a vibrating nappe reveals some interesting characteristics about the nappe vibration process. By visually tracking a falling particle in the nappe flow, it appears as if individual particles are actually traveling in a continuous arcing path as opposed to oscillating back and forth in the nappe. This suggests that instability at the downstream edge of the crest causes a periodic variation in the nappe trajectory, which causes the wavy nappe flow pattern rather than oscillatory force that actually causes the nappe to vibrate while falling. This wavy nappe pattern is likely amplified by the Helmholtz effect, as the wave amplitudes tend to increase with fall distance. The intense vibration energy and sound waves generated by the falling nappe are the result of the oscillating, cyclical nappe waves impacting the downstream apron. Evidence that the instability originates at the crest exists in the form of visual banding that appears in a vibrating nappe. The probable causes of this instability at the crest are

discussed in Chapter VII. Due to the increased fall height of model #2, sheet breakup occurs near the base of the nappe for the lower discharges (<0.28 ft^2/s, see Fig. 48).

Fig. 48. Model #2b sheet breakup at the bottom of the nappe

As the nappe freely falls, gravitational acceleration causes an increase in velocity and an associated decrease in sheet thickness, which leads to break up. At the breakup region, several small water sheets, or "slices", oriented perpendicular to the flow will form, as seen in Fig. 49. Kyotoh (2002) referred to these formations as "ligaments". Kyotoh describes these ligaments as the result of transverse instabilities in the nappe at the location of break up.

Fig. 49. Model #2b ligaments or "slices" forming at the base of the nappe (image taken from downstream of the nappe)

Model #2 Results

Model #2b – Broad Crest with Upstream Rounded Edge

In order to test the effectiveness of certain countermeasures to nappe vibration, the weir configuration which included the rounded fillet (model #2b) was used to determine base levels of vibration. Flows were tested in 0.06 ft^2/s increments, starting at 0.22 ft^2/s and increasing to 0.47 ft^2/s. Vibration occurred at each of the flow rates tested. Oscillation frequency for each flow rate is displayed in Table 1. Fig. 50 is an audio recording for the unit discharge of 0.47 ft^2/s, which displays a physical representation of the vibration produced by the falling nappe.

Table 1. Model #2b vibration frequencies

Unit Discharge (ft^2/s)	Frequency (Hz)
0.22	16.5
0.28	17
0.34	17
0.40	17
0.47	16

Fig. 50. Model #2b nappe vibration audio recording, 0.47 ft^2/s
(x-axis = time in seconds, y-axis = decibel measurement)

Model #2c - Expanded Metal Roughness

An expanded metal sheet was fastened to the weir crest in order to provide roughness, similar to the test performed on model #1b. However, unlike model #1, the model #2 spillway lacked the confined air pocket behind the nappe, meaning that the nappe vibration was independent of pressure variations in the air pocket. Five flow rates were tested with the expanded metal crest modification, ranging from 0.22 ft^2/s to 0.47 ft^2/s in 0.06 ft^2/s increments. For a complete set of audio file for all flow rates on model #2b, #2c, and #2d, refer to Appendix A. To demonstrate the effect of the roughness on the crest, data is presented for a unit discharge of 0.34 ft^2/s. Fig. 51 displays the frequency of the vibration as recorded by the microphone before the expanded metal is added to the crest

(model #2b). Fig. 52 displays the audio recording for the same discharge of 0.34 ft^2/s, but with the expanded metal roughness on the crest (model #2c). As demonstrated from these results, the addition of roughness via expanded metal on the crest attenuates the vibration, eliminating the visible sound waves in the recorded audio file. The periodic oscillations of the sound pressure waves are no longer detected by the microphone. To further demonstrate the effect of crest roughness, two images of the nappe without (model#2b) and with the hardware cloth roughness (model #2c) on the crest are shown below in Fig. 53 and Fig. 54, respectively.

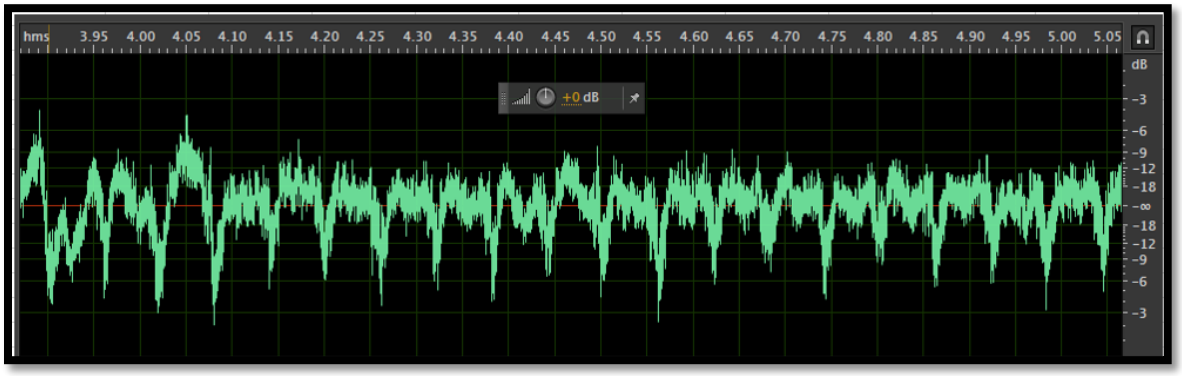

Fig. 51. Model #2b nappe vibration audio recording, 0.34 ft^2/s
(x-axis = time in seconds, y-axis = decibel measurement)

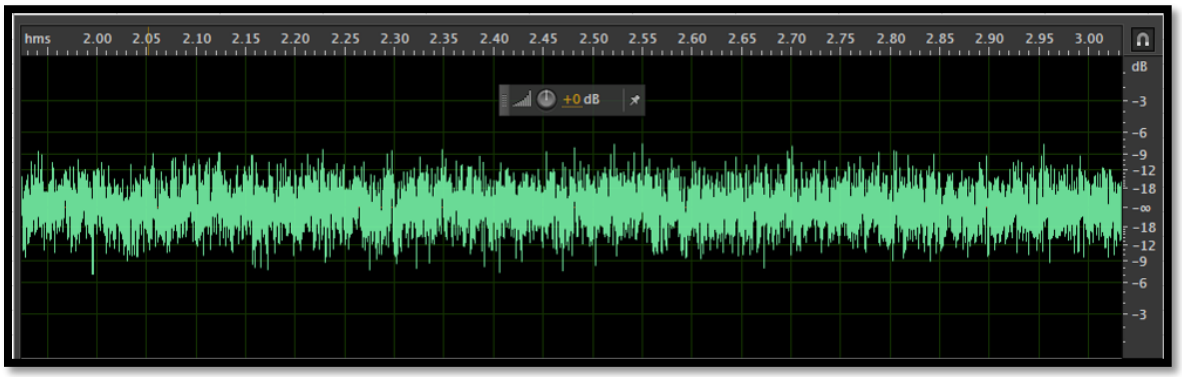

Fig. 52. Model #2c nappe vibration audio recording, 0.34 ft^2/s
(x-axis = time in seconds, y-axis = decibel measurement)

Fig. 53. Model #2b nappe appearance

Fig. 54. Model #2c nappe appearance

Fig. 54 and Fig. 55 demonstrate how roughness on the crest effects the unconfined nappe. While waves still appeared, they were no longer in phase. Waves in the nappe no longer impacted the apron in a cyclical manner, so the oscillating sound pressure waves were replaced with continuous noise. Even though the impact of the nappe on the apron was still loud for model #2c, the continuous noise did not produce the characteristic pressure pulses that could be felt and heard with model #2b.

Model #2d - Nappe Splitters

Nappe splitters installed on the crest spaced at a regular interval is a remedy used on prototype spillways to eliminate nappe oscillation. Nappe splitters create a break in the continuous lateral nappe profile, venting the confined air pocket (if one exists) behind the nappe to atmospheric pressure (see Fig. 55). However, in the case of a fully unconfined nappe, venting is not an issue, which brings into question what vibration mechanism nappe splitters are actually interrupting.

Results of the nappe splitter test showed that adding more splitters and shortening the spacing is most effective at disrupting the vibration. This, of course, is a general statement on what was observed on this model, and does not provide specific nappe splitter spacing design parameters for any given weir spillway. The same five flow rates tested with the roughness modification were tested with splitters. To demonstrate the influence of nappe splitters, the results of the 0.40 ft^2/s unit discharge test run are presented (see Fig. 56-59). As splitters are added, the vibration becomes less detectable for the audio recording device.

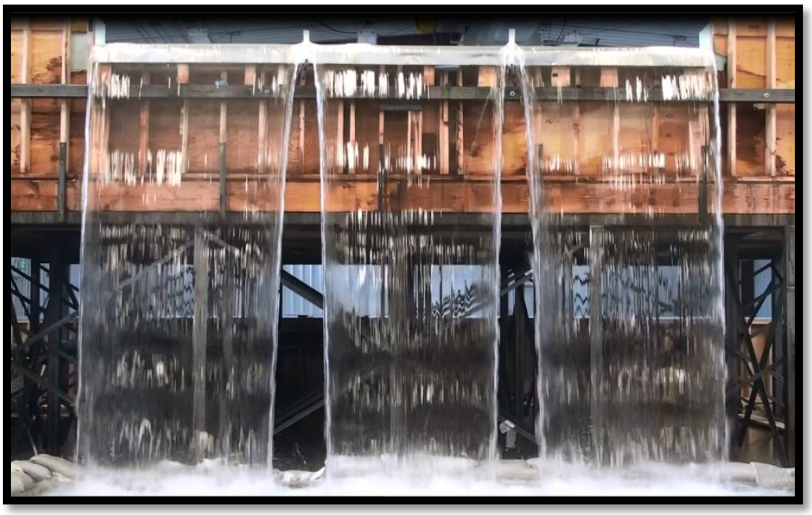

Fig. 55. Model #2d with two nappe splitters

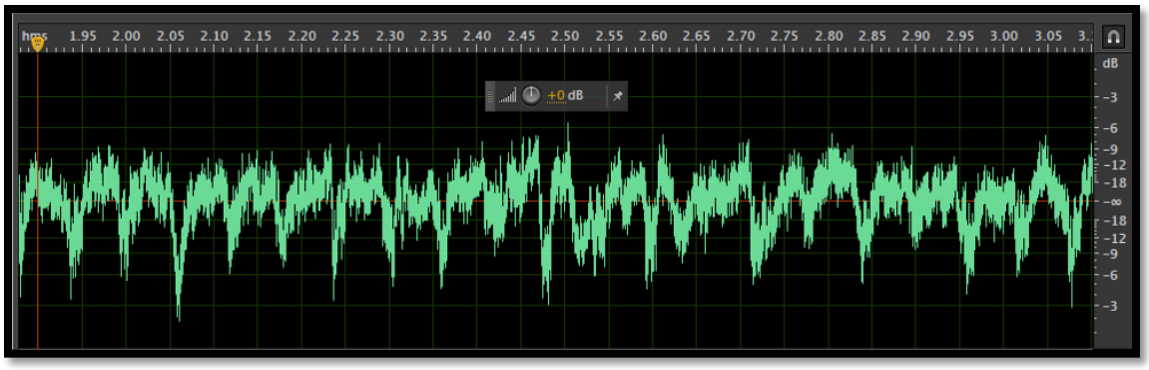

Fig. 56. Model #2b nappe vibration audio recording, 0.40 ft^2/s
(x-axis = time in seconds, y-axis = decibel measurement)

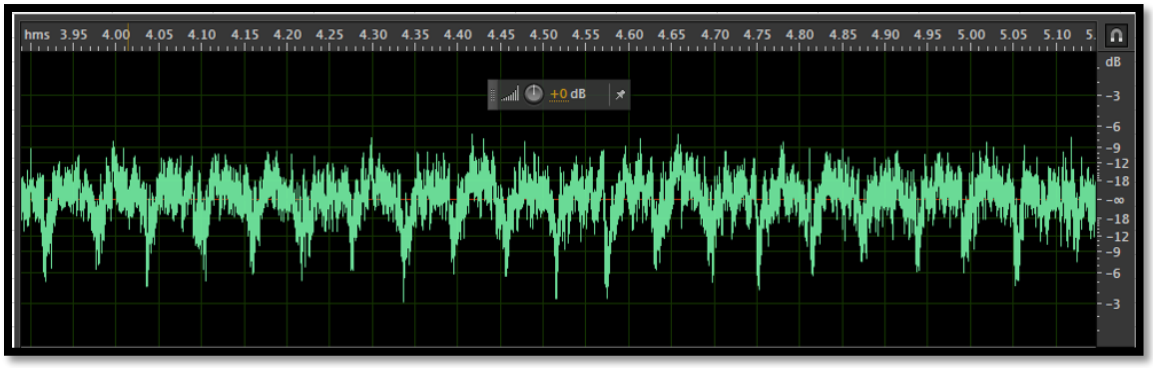

Fig. 57. Model #2d nappe vibration audio recording with one splitter, 0.40 ft^2/s
(x-axis = time in seconds, y-axis = decibel measurement)

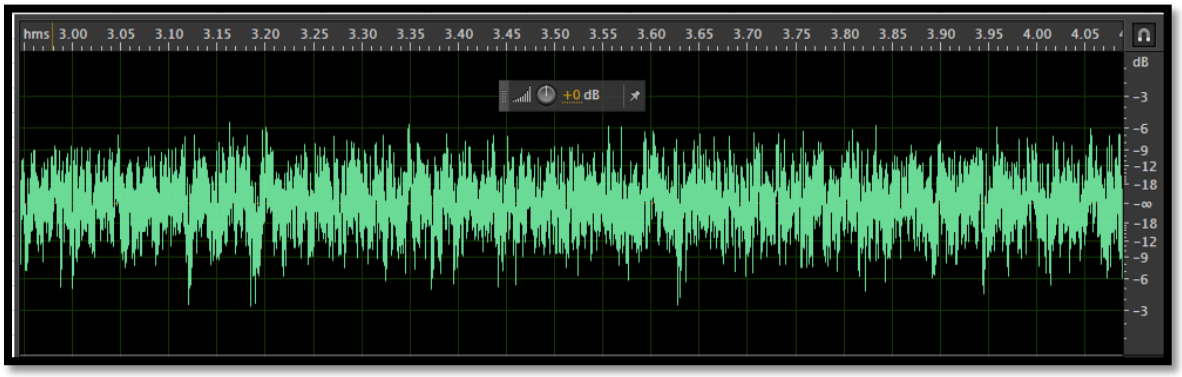

Fig. 58. Model #2d nappe vibration audio recording with two splitters, 0.40 ft^2/s (x-axis = time in seconds, y-axis = decibel measurement)

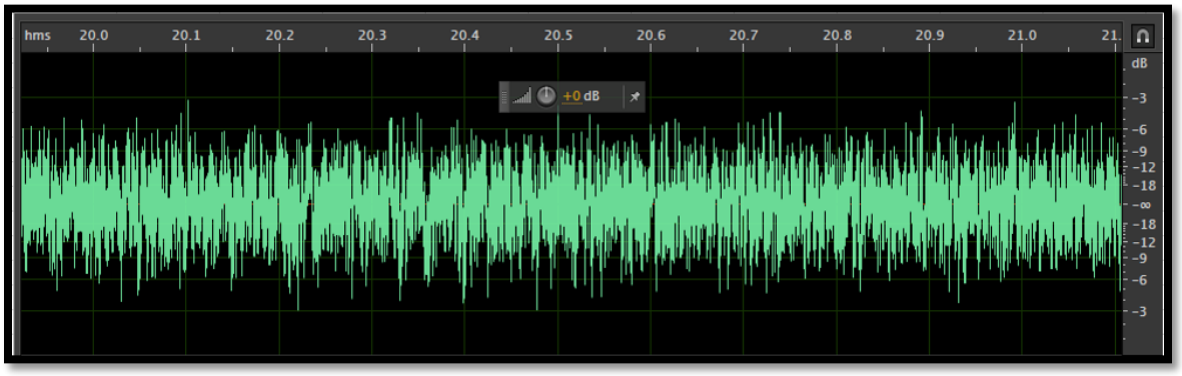

Fig. 59. Model #2d nappe vibration audio recording with three splitters, 0.40 ft^2/s (x-axis = time in seconds, y-axis = decibel measurement)

Results of this test revealed an important aspect about nappe splitters on the crest of a weir. By increasing the number of splitters, the range of flow rates under which detectable vibration occurred was reduced, even though the nappe is unconfined. The interesting discovery is that increasing the number of splitters on the crest has a greater effect on reducing nappe vibration for higher discharges. For example, the unit discharge of 0.40 ft^2/s required 2 splitters to effectively reduce the vibration of the nappe, while the unit discharge of 0.47 ft^2/s only required 1 splitter. This suggests a possible relationship

between flow depth exiting the crest and a required minimum nappe width in order to produce periodic vibration waves.

CHAPTER VI

MODEL #3 RESULTS

General Observations

While the dimensions of model #3 are slightly larger than model #2, the overall scale is approximately the same. Like model #2, model #3a featured an unconfined nappe geometry, and produced similar nappe behavior to model #2b, but the sound energy and frequency increased significantly. The cause of the increased amplitude is unknown, but possible reasons include:

- Change of weir crest shape
- Increased fall height (by 1 foot)
- Increase weir width (by 6 inches)
- Different impact conditions
- A more confined area around the nappe which may have reflected acoustical energy back toward the vibrating nappe and instrumentation

Flow rates tested for model #3 range from 0.14 ft^2/s to 0.42 ft^2/s at increments of 0.06 ft^2/s. For model #3e and model #3f, which involved roughness elements on the top of the crest, lower range discharges (up to 0.25 ft^2/s) were observed to produce gaps in the nappe, resulting in the a non-continuous water sheet. A set of higher discharges, ranging from 0.27 ft^2/s – 0.81 ft^2/s were tested for model #3c, #3e and #3f in order to create flow conditions which produced a continuous, unbroken nappe. This was done to verify the

effectiveness of these countermeasures without allowing excessive passage of air to and from the confined air pocket behind the nappe.

Model #3 Results

Model #3a - Porous Apron (Grating) vs. Solid Apron Impact, Fully Aerated Smooth Crest

As water discharges over the crest of model #3a, the falling nappe makes contact with a metal grate before falling into a pool (laboratory sump) below. This condition was altered by placing a long wooden plank (2 inch x 12 inch) onto the grate, creating a solid surface where the nappe impacts the apron. Although not always obvious in the recorded audio files, impact condition had a significant visual effect on the vibration of the nappe. Fig. 60 and Fig. 61 display the typical behavior of the nappe under the two different apron conditions.

Fig. 60. Model #3a impacting on the metal grating, 0.31 ft^2/s

The solid apron impact condition increased the amplitude of the vibration, and was especially noticeable at the point of impact on the apron. The water sheet also broke up at a point higher up on the nappe when the wooden plank was in place over the grating. Table 2 displays the estimated frequency of vibration for each flow rate with the two impact conditions. The difference in behavior between the two different impact conditions is believed to be a result of water or sound waves rebounding off of the wooden plank back up toward the base of the nappe.

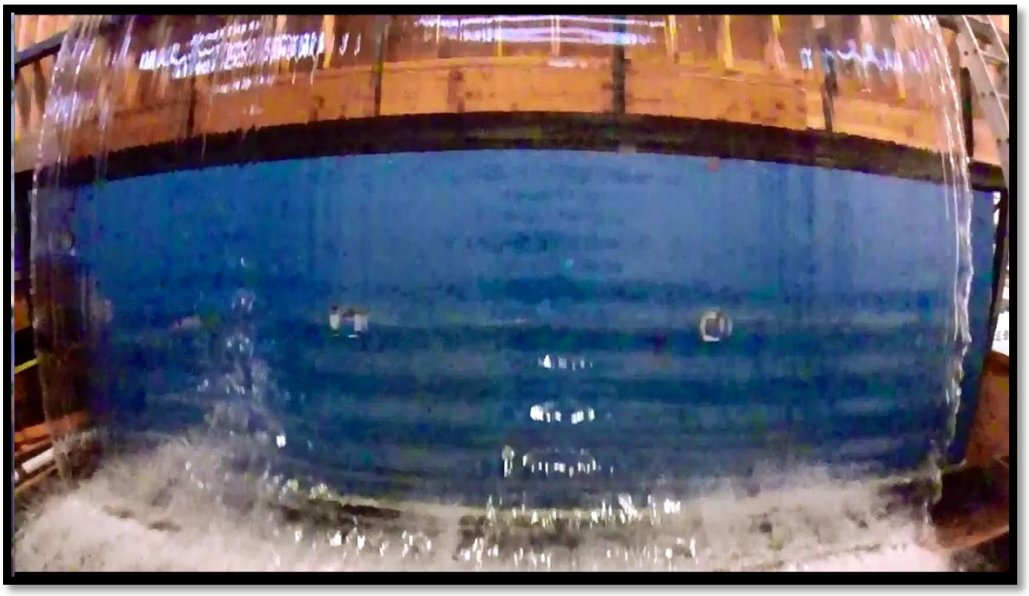

Fig. 61. Model #3a impacting on the wooden plank, 0.31 ft^2/s

Table 2. Model #3a vibration frequencies

Unit Discharge (ft^2/s)	Grate (Hz)	Wood (Hz)
0.14	NA	NA
0.20	39	47
0.25	40	40
0.31	40	NA
0.36	37	35
0.42	37	37

The vibration frequency estimates shown in Table 2 were generated by inspection of the audio files recorded with model #3a (see Appendix B for a complete set of audio figures). With estimated frequencies ranging between 39 Hz and 47 Hz, model #3a produces a much higher frequency nappe vibration than model #2b.

Model #3b - Partially Roughened Crest, Unconfined Nappe

Partially roughening the upstream portion of the weir crest with stones (model #3b) in conjunction with an unconfined nappe had a similar effect to that seen in the full crest roughness tested for model #2c. Fig. 62 and Fig. 63 compare the audio recordings for the unit discharge of 0.36 ft^2/s without the roughness elements and with the roughness elements, respectively, which displays a good representation of what occurred for most flow rates.

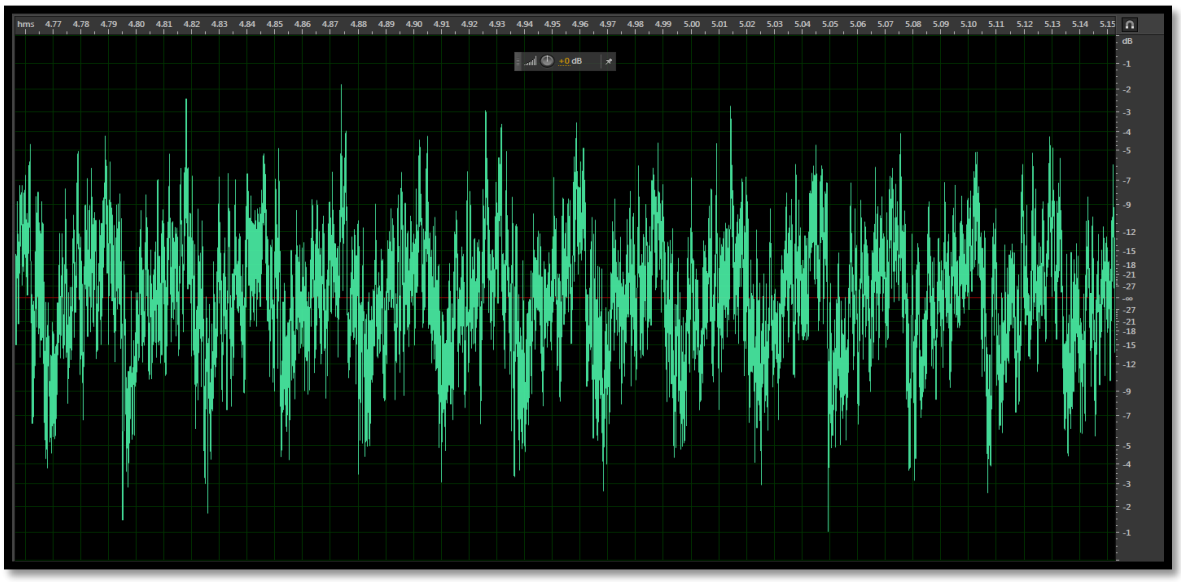

Fig. 62. Model #3a nappe vibration audio recording, 0.36 ft^2/s
(x-axis = time in hundredths of seconds, y-axis = decibel measurement)

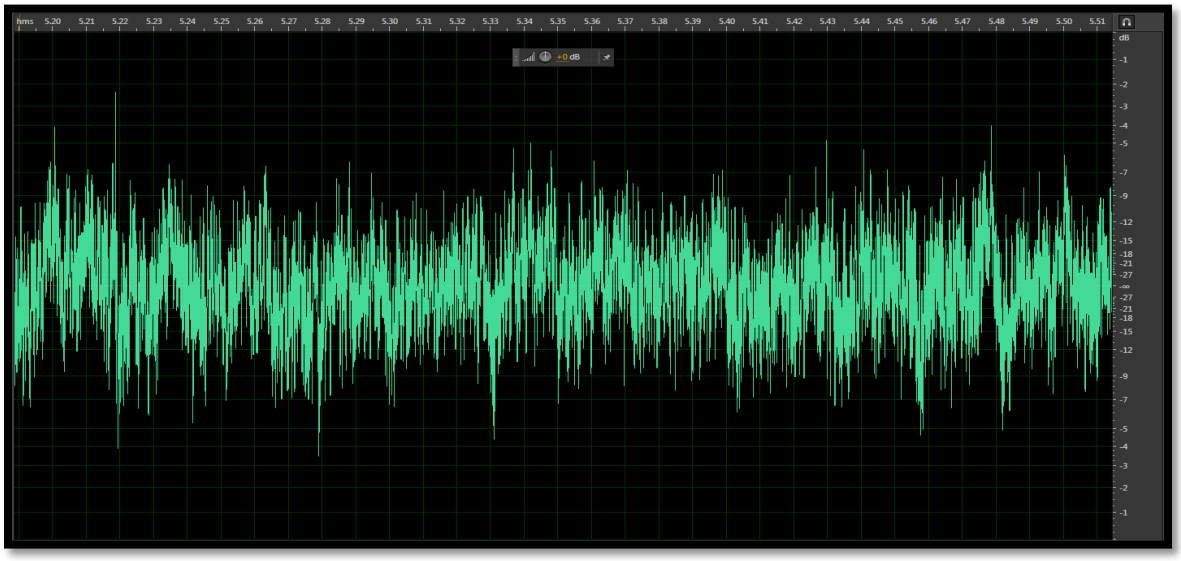

Fig. 63. Model #3b nappe vibration audio recording, 0.36 ft^2/s
(x-axis = time in hundredths of seconds, y-axis = decibel measurement)

The only exception was discovered for the maximum discharge tested of 0.42 ft^2/s. While testing Model #3b with the unit discharge of 0.42 ft^2/s, vibration was not audibly noticeable to the naked ear. However, analysis of audio recordings (Fig. 64 and Fig. 65) at this flow rate with the solid impact reveals that, while the vibration amplitude had been reduced, it was not mitigated as much as with the lower flow rates.

Visually, the stones glued on the upstream side of the crest (Model #3b) had a similar effect on the nappe as Model #2c. Waves were still visible in the nappe, but they were now out of phase; Figs. 66 and Fig. 67 display this observed nappe behavior. However, for the unit discharge of 0.42 ft^2/s, analysis of slow motion video revealed the presence of unbroken, in-phase waves running across the nappe, which agreed with what was observed in the audio recordings. The partial roughness on the upstream side of the crest was not sufficient to completely eliminate traces of nappe vibration.

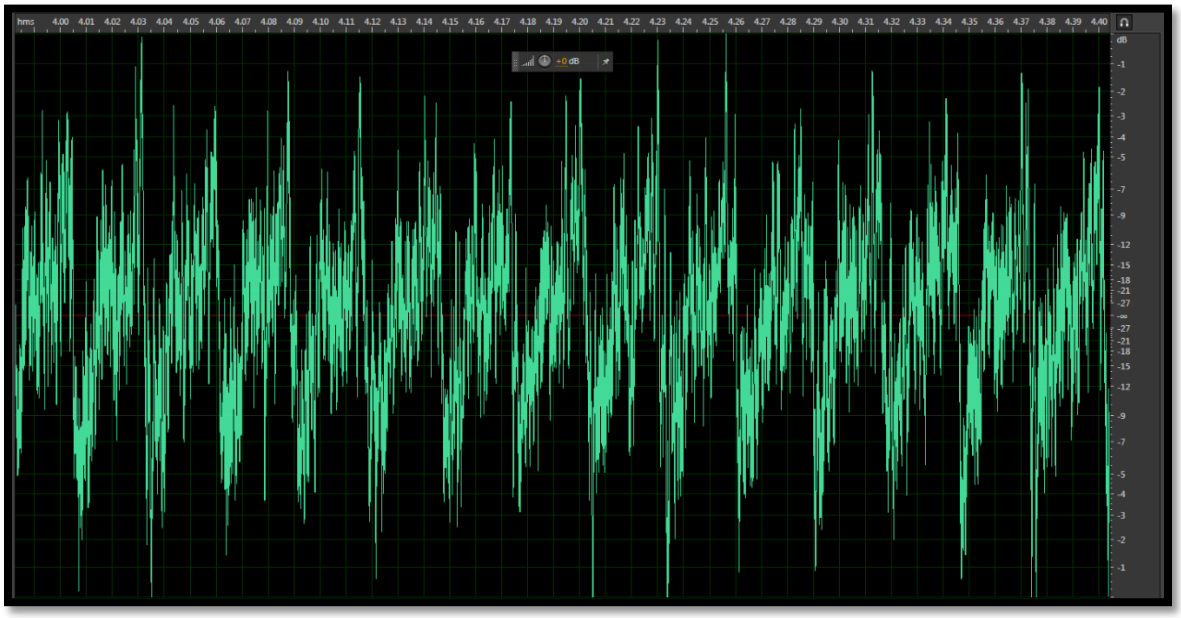

Fig. 64. Model #3a (solid impact) nappe vibration audio recording, 0.42 ft^2/s (x-axis = time in hundredths of seconds, y-axis = decibel measurement)

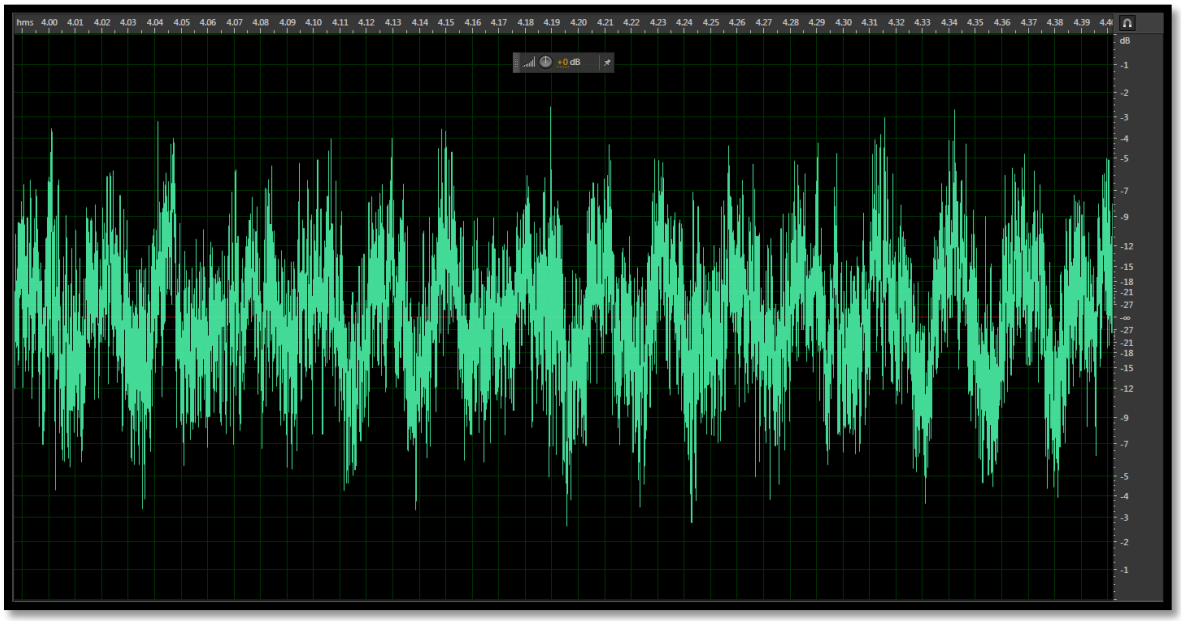

Fig. 65. Model #3b (solid impact) nappe vibration audio recording, 0.42 ft^2/s (x-axis = time in hundredths of seconds, y-axis = decibel measurement)

Fig. 66. Model #3a in-phase nappe waves

Fig. 67. Model #3b out of phase nappe waves

Model #3c - Unmodified Crest, Confined Nappe

The addition of containment walls around the nappe had a significant effect on the behavior of nappe with the smooth unmodified crest. While the frequency of the vibration in the nappe appeared to decrease slightly, the overall intensity of the sound pressure waves increased more dramatically. The existence of the confined air volume behind the nappe had an influence on the trajectory of the nappe, especially at the lower discharges. Rather than following a normal parabolic path from crest to apron, the air pressure behind the nappe would often push on the nappe, causing the nappe to follow a more straight line path and impact on the apron at a point further downstream. In addition, the trajectory of the nappe would often shift forward and backward with no definite frequency, demonstrating a variation of pressure behind the nappe. In order to verify the effectiveness of particular nappe vibration countermeasures (model #3e and #3f), a wider range of flows was tested under the model #3c configuration. Table 3 displays the range of observed vibration frequencies with the corresponding unit discharge.

Over the range of discharges for model #3c, the nappe displayed an interesting variation in vibration wave amplitude and consistency. Three different wave amplitude patterns were observed in data recorded by the accelerometer:

- Consistent amplitude (see Fig. 68)
- Oscillation in amplitude with symmetry about the axis (see Fig. 69)
- Oscillation in amplitude with asymmetry about the axis (see Fig. 70)

The vibration patterns tended to increase in amplitude and become unstable as the flow rates were increased. Model #1 and model #2 also exhibited variations of in the wave amplitude characteristics, but model #3 was the only one that was known to produce the asymmetric wave pattern shown in Fig. 70.

Table 3. Model #3c vibration frequencies

Unit Discharge (ft^2/s)	Frequency (Hz)
0.14	NA
0.20	37
0.25	35
0.31	35
0.36	34
0.42	34
0.48	35
0.59	34
0.70	30
0.81	NA

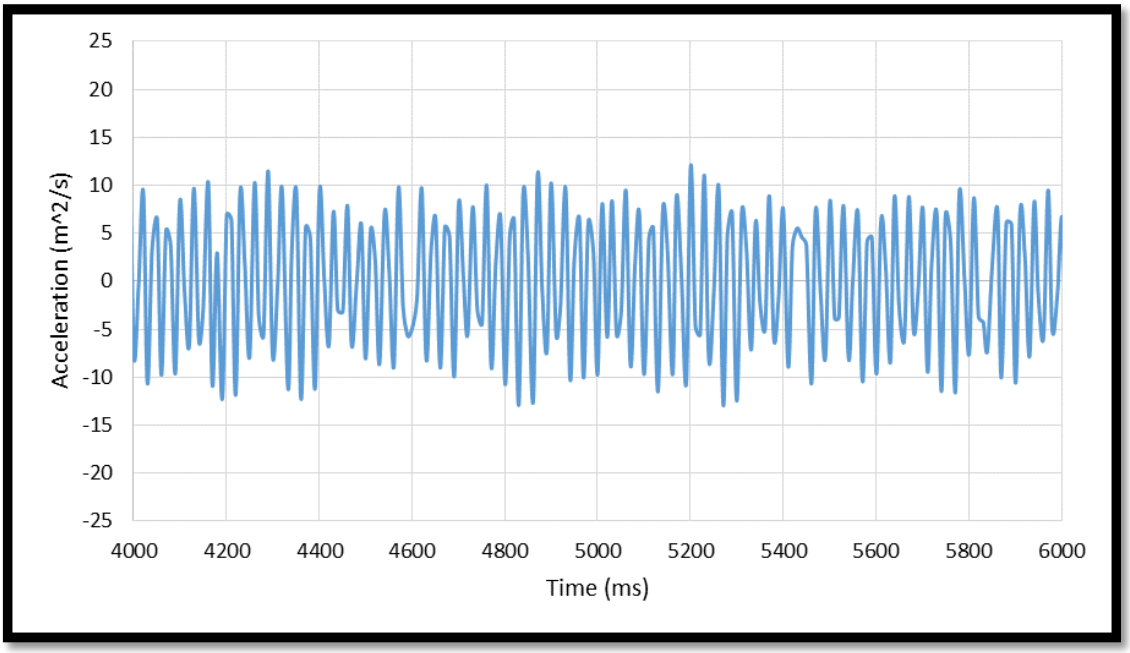

Fig. 68. Model #3c consistent amplitude vibration, 0.31 ft^2/s

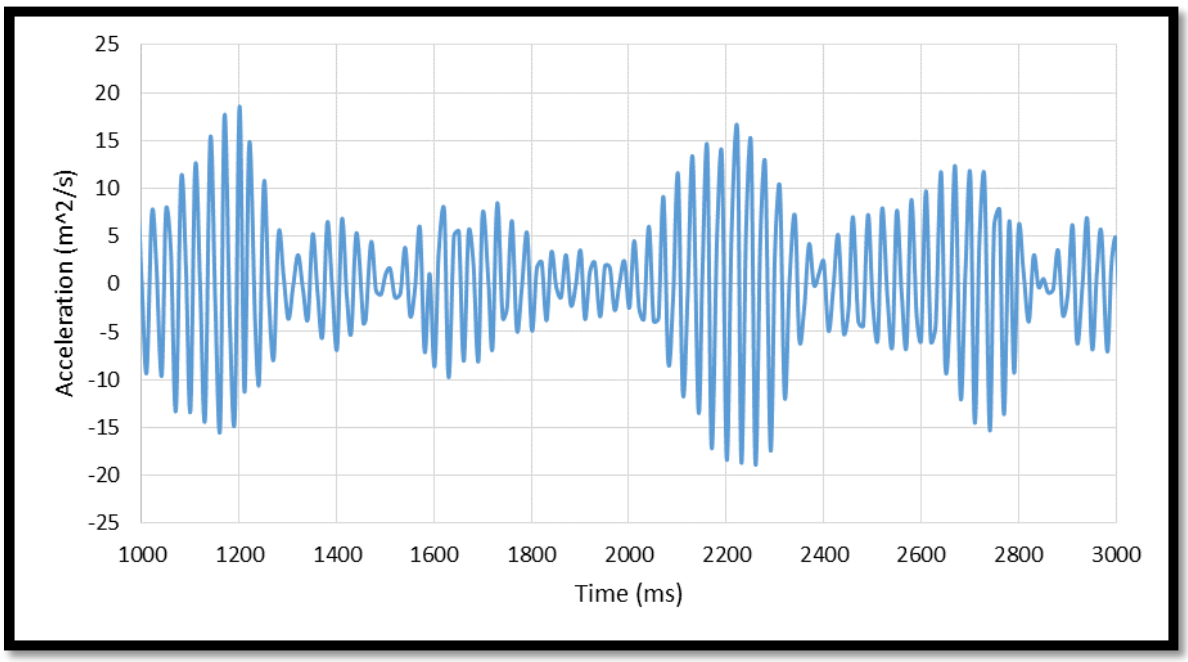

Fig. 69. Model #3c time variable amplitude with symmetry about the x-axis, 0.36 ft^2/s

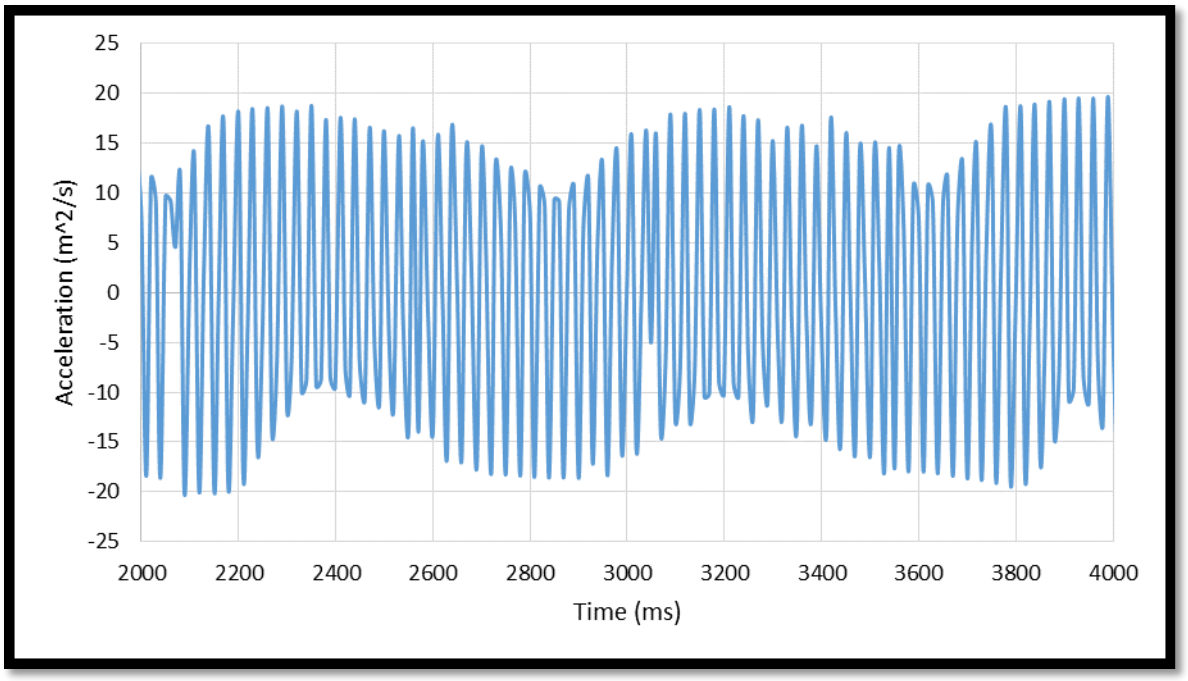

Fig. 70. Model #3c time variable amplitude with asymmetry about the x-axis, 0.59 ft^2/s

Model #3d - Partially Roughened Crest, Confined Nappe

The addition of sidewalls and a back wall to the partially roughened weir crest configuration on model #3d produced significantly different results than the fully aerated conditions of model #3b. While model #3b showed faint signs of vibration at the high unit discharge of 0.42 ft^2/s, model #3d displayed heavy vibration beginning with a unit discharge of 0.25 ft^2/s and continuing up to the maximum discharge of 0.42 ft^2/s (see Table 4). At 0.25 ft^2/s, the vibration of the nappe exhibited a pulsing variation in wave amplitude; as the discharge increased, the vibration became more consistent and constant in amplitude (see Fig. 68). See Appendix B for a complete set of figures for vibration measurements taken on model #3d.

Model #3b showed traces of nappe vibration during the high discharge run, but the presence of the confined air pocket behind the nappe provided the means by which full on nappe vibration could occur. Enough turbulence on the crest was present on the unconfined nappe of model #3b to interfere with the waves up to a certain limit (0.42 ft^2/s), but the crest roughness was unable to impede the nappe oscillations when the confined air pocket was added.

Table 4. Model #3d vibration frequencies

Unit Discharge (ft^2/s)	Frequency (Hz)
0.14	NA
0.20	NA
0.25	32
0.31	35
0.36	35
0.42	36

Fig. 71. Model #3d nappe vibration, 0.36 ft^2/s

Model #3e – Fully Roughened Crest, Confined Nappe

While the partially roughened crest was moderately successful at attenuating nappe vibration (model #3b), the addition of the confining walls (model #3d) proved the limitations of that modification. However, adding more stones in order to fully roughen the crest produced better results. Fig. 72 displays the accelerometer results for the unit discharge of 0.59 ft^2/s, and comparing with Fig. 70 for the un-roughened crest, vibration was interrupted and eliminated. Fig. 73 displays the typical appearance of the nappe for model #3e. The waves that appeared in the nappe of model #3e were of minimal amplitude and completely out of phase. Even under the influence of the confined air pocket, the model #3e modification eliminated periodic oscillations. Results were similar for each discharge tested (see Appendix B for a full set of accelerometer output figures for model #3e).

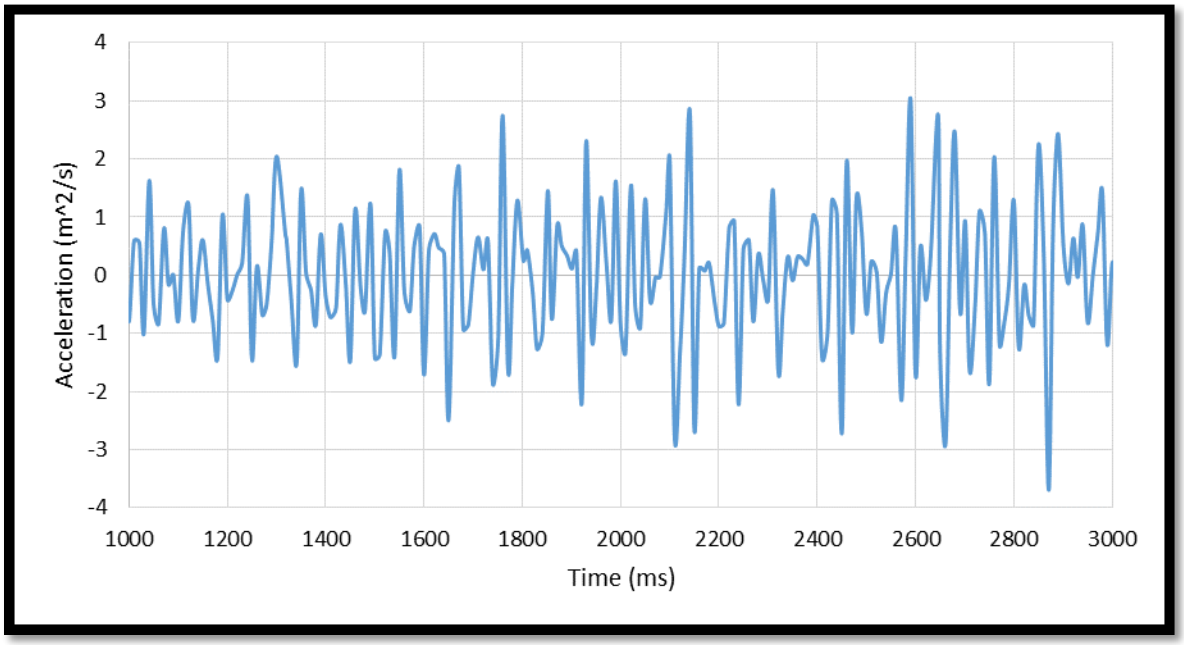

Fig. 72. Model #3e nappe vibration accelerometer data, 0.59 ft^2/s

Fig. 73. Model #3e nappe appearance

As shown in Fig. 73, and as could be expected, the overall appearance of the nappe was much rougher, and no wave patterns were visible. It is important to note that increased roughness naturally decreases the efficiency of the weir, but the randomness of the shapes of the rocks on the crest make it difficult to determine a reliable estimate as to how much the efficiency was actually reduced.

Model #3f – One Row of Stones at Edge of Weir Crest

The model #3e modification was successful at remediating nappe vibration, while model #3d had its limitations. Considering these results, model #3f aimed to determine if a single row of stones at the edge of the crest would provide sufficient roughness and provide similar results to model #3e. Interestingly enough, model #3f was successful at eliminating nappe vibration at each tested discharge. Comparing the same discharge (0.59 ft^2/s) for model #3e (see Fig. 72) and model #3f (see Fig. 74), it is shown that both modifications produced very similar results.

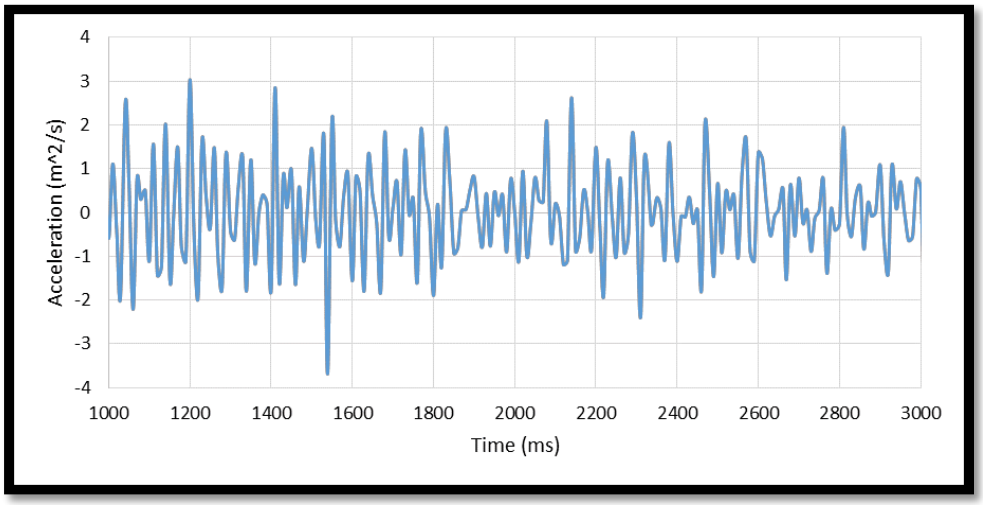

Fig. 74. Model #3f nappe vibration accelerometer data, 0.59 ft^2/s

Model #3g – Square Notches Cut into Weir Crest

While model #3e and #3f were successful at eliminating vibrations in the nappe, certain concerns arise about the application of said methods of remediation. Prototype weir structures which regularly pass large quantities of debris, such as large logs and trash, may run the risk of having stones on the crest dislodged over time, reducing the effectiveness of the countermeasure or requiring undesirable levels of maintenance. Model #3g attempted to provide sufficient turbulence in the flow to reduce or eliminate vibration in the nappe without having to add roughness elements to the crest, which effectively raise the weir crest elevation and negatively impact the weir efficiency. The first iteration of model #3g-a included the square notches located at 4 foot spacing on center. At 4 foot spacing, vibration was not successfully remediated by the notches. Because the first iteration showed no improvement toward interrupting the vibration, the next iteration drastically decreased the spacing between notches.

With a 1 foot spacing (model #3g-b) on center between the notches, there was some attenuation that occurred (see Table 5), but only at low discharges, interrupting the vibration at 0.14 ft^2/s and showing minor improvements in wave disruption at a unit discharge of 0.20 ft^2/s. Higher discharges displayed strong nappe vibration very similar to the results seen for model #3c (see Fig. 75). Due to limitations of the model, the notches in the crest had to be cut relatively small. Results may have differed had the notches been larger. For a full set of figures with the measured accelerometer data for model #3g-a, refer to Appendix B.

Table 5. Model #3g-b vibration frequencies

Unit Discharge (ft^2/s)	Frequency (Hz)
0.14	NA
0.20	35
0.25	36
0.31	36
0.36	34
0.42	35

Fig. 75. Model #3g-b nappe appearance, 0.36 ft^2/s

Model #3h – Square Notches Projecting Upward from Crest

Upward notches oriented parallel to the flow showed moderate nappe vibration attenuation at the lower discharges, and performed slightly better than model #3g-b (see Table 6). Nappe vibration was interrupted up to a unit discharge of 0.25 ft^2/s, but strong nappe vibration ensued at higher discharges. Fig. 76 shows the nappe for the unit discharge

of 0.36 ft^2/s, and similar results were seen for other discharges exceeding 0.25 ft^2/s (see Appendix B for a complete set of figures).

Table 6. Model #3h vibration frequencies

Unit Discharge (ft^2/s)	Frequency (Hz)
0.14	NA
0.2	NA
0.25	36
0.31	37
0.36	37
0.42	36

Fig. 76. Model #3h nappe appearance, 0.36 ft^2/s

CHAPTER VII

DISCUSSION

Experimentation has shown that distinct differences exist between models 1, 2 and 3, and while there may be similarities regarding the initiation of instability leading to self-excited vibration, the predominant physical mechanisms which sustain or amplify the vibration are not the same (Kyotoh, 2002). In the discussion of the cause of nappe vibration, it is important to distinguish between forces which initiate instabilities and those that amplify and sustain the instability. Results of this research indicate that the initiation of the instability most likely occurs at the weir crest. Support of this argument is found in the following observations:

- Waves (also referred to as banding) are seen directly after flow separation from the weir crest occurs, even for models #2 and #3 with a fully unconfined nappe.
- Roughness elements, or elements that in general introduce turbulence, added to the crest can partially or completely terminate the vibration.
- Pairing a crest countermeasure with an apron vibration amplifier exhibited little to no vibration on the small scale model (model #1).

What causes this instability has not been determined definitely, and may vary from spillway to spillway, but plausible causes include:

- The boundary layer that forms on the crest flow profile develops a negative pressure. When the boundary layer reaches the downstream end of the crest, a sudden pressure discontinuity occurs between the ambient air pressure behind the

nappe and the boundary layer of the flow. This pressure discontinuity may contribute to instability leading to nappe vibration (Chanson, 1996).

- Sound pressure waves that travel from the impact of the nappe back up to the crest (Falvey, 1997).

The function of a confined air pocket behind the nappe with regards to nappe vibration was shown to vary with size-scale. Model #1 required the enclosed air pocket in order to vibrate, but the larger models (model #2 and model #3) did not. However, it was observed in model #3 that the confined air pocket behind the nappe acted as a means of amplification, demonstrated most strongly in the results of model #3b and model #3d.

This study has revealed that modifications to the apron can affect how the vibration of the nappe behaves, specifically on model #1 and model #3. Certain apron modifications amplify and intensify the vibration while others attenuate the mechanism, but apron modifications become less capable of attenuation as the size-scale of the weir increases. The addition of tail water to model #1 eliminated the vibration, indicating that, for the small-scale model, the energy associated with the nappe impacting a solid surface may be a factor. While the results of the apron modifications on model #1 were somewhat scattered and at times inconsistent, the general takeaway was that apron modifications can and do influence the vibration mechanism.

Traditionally, the success of nappe splitters in terminating nappe vibration has been attributed to the fact that they provide air flow to and from the confined air pocket behind the nappe. While this process of venting does aid in reducing or eliminating vibrations, nappe splitters were also seen to reduce vibrations even when there was no finite air pocket

present (model#2). This suggests a possible required aspect ratio of flow depth over the crest to nappe width in order for nappe vibration to occur, which would explain similar observations by the U.S. Bureau of Reclamation (1964).

CHAPTER VIII

CONCLUSIONS

Nappe vibration is a fascinating phenomenon, and this research has furthered the knowledge of the topic as well as supported previous findings by other researchers. While some aspects of nappe vibration remain unclear, evidence supports that nappe vibration is initiated by an instability originating at the weir crest. The source of this instability is found at either the boundary layer of the flow of the weir crest or due to pressure waves created at the impact location of the nappe on the downstream apron. The nappe vibration mechanism is dependent on size-scale, and conditions on the apron have a much greater effect on small scale weirs.

Generally speaking, roughness elements or elements that create turbulence at the weir crest were successful at interfering with nappe vibration. Nappe splitters located on the weir crest have proven to be an effective countermeasure, but specific spacing of splitters for a weir of a given height and width has not been determined and would be a valuable focus of future research, along with further investigation of the aspect ratio of flow depth to nappe width conducive to nappe vibration. A better understanding of the causes and preventative measures of nappe vibration will aid engineers in the design of dam spillways structures.

REFERENCES

Binnie, A.M. (1971). "The stability of a falling sheet of water." *Proceedings of the Royal Society of London. Series A, Mathematical and Physical,* 326(1565), 149-163.

Casperson, Lee W. (1991). "Fluttering fountains." *J. Sound and Vibration,* 162(2), 251-262.

Casperson, Lee. W. (1994). "Fluttering fountains: stability criteria." *J. Applied Physics,*75(10), 4892-4894.

Casperson, Lee W. (1995). "Fluttering fountains: annular geometry." *J. Applied Physics,* 79(3), 1275-1278.

Chanson, Hubert. (1996). "Some hydraulic aspects during overflow above inflatable flexible membrane dam." Department of Civil Engineering, The University of Queensland, Australia, Report CH47/96, 3-3-3-9.

De Luca, Luigi, and Costa, Michela. (1997). "Instability of a spatially developing liquid sheet." *J. Fluids Mechanics,* 331, 127-144.

Falvey, Henry T. (1980). "Bureau of reclamation experience with flow-induced vibrations." *Practical Experiences with Flow-Induced Vibrations,* Denver, CO, 386-398.

Knisely, Charles W. (1994). "Nappe oscillation countermeasure." *Fusion Engineering and Design,* 182, 17-24.

Kolkman, P.A. (1972). "Instability of a vertical-curtain closing an air-chamber." *Symp. on Flow-Induced Structural Vibrations,* Karlsruhe, Germany, 17-33.

Kyotoh, H. (2002). "Incipient oscillations of a sheet of falling water and the instability mechanisms." *J. Hydroscience and Hydr. Engrg,* 20(1), 77-93.

Metropolitan Water, Sewage and Drainage Board. (1980). "Investigation into spillway discharge noise at avon dam." *ANCOLD Bull.,* (57), 31-36.

Naudascher, E. (1974). "Flow-induced structural vibrations." *Symp. of the International Union of Theoretical and Applied Mechanics (I.U.T.A.H.) and the International Association of Hydraulic Research (I.A.R.P.),* 167-182.

Naudascher, Eduard, and Rockwell, Donald. (1994). "Flow-induced vibrations: an engineering guide." Dover Publications Inc., Mineaola, New York, 142-146.

Rayleigh. (1878). “On the instability of jets.” *Proceedings of the London Mathematical Society,* 10, 4-13.

Sato, Y., Miura, S., Morii, S., and Ohkubo, S. (2007). “Behavior of a falling water sheet.” *J. Environment and Engrg.*, 2(2), 394-406.

Schmid, Peter J. and Henningson, Dan S. (2002). “On the stability of a falling liquid curtain.” *J. Fluid Mechanics,* 463, 163-171.

Schwartz, H.I. (1966). “Edgetones and nappe oscillation.” *J. Acoustical Society of America,* 39(3), 579-582.

Squire, H.B. (1953). “Investigation of the instability of a moving liquid film.” *Br. J. Applied Physics,* 4, 167-169.

Sumi, Tetsuya. (1990). “Three-dimensional characteristic of nappe oscillation and the estimation of sound pressure levels.” *J. Hydroscience and Hydr. Engrg,* 8(1), 89-99.

United States Bureau of Reclamation. (1964). “Experiences of the Bureau of Reclamation with flow-induced vibrations.” (538), 11-13.

von Helmholtz, Hermann. (1868). "Über discontinuierliche flüssigkeits-bewegungen [On the discontinuous movements of fluids]". *Monatsberichte der Königlichen Preussische Akademie der Wissenschaften zu Berlin* [Monthly Reports of the Royal Prussian Academy of Philosophy in Berlin], (23), 215–228.

APPENDICES

Appendix A. Model #2 Figures

Fig. A1. Model #2b nappe vibratio audio recording, 0.22 ft^2/s
(x-axis = time in seconds, y-axis = decibel measurement)

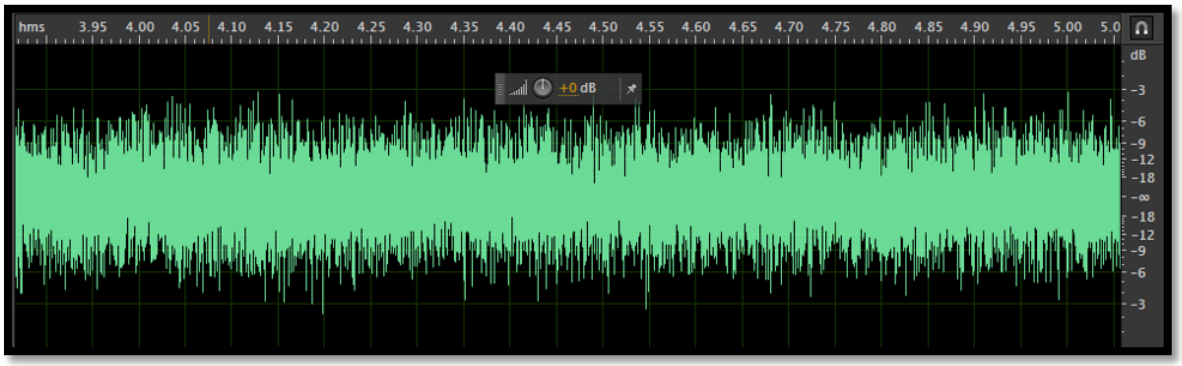

Fig. A2. Model #2c nappe vibration audio recording, 0.22 ft^2/s
(x-axis = time in seconds, y-axis = decibel measurement)

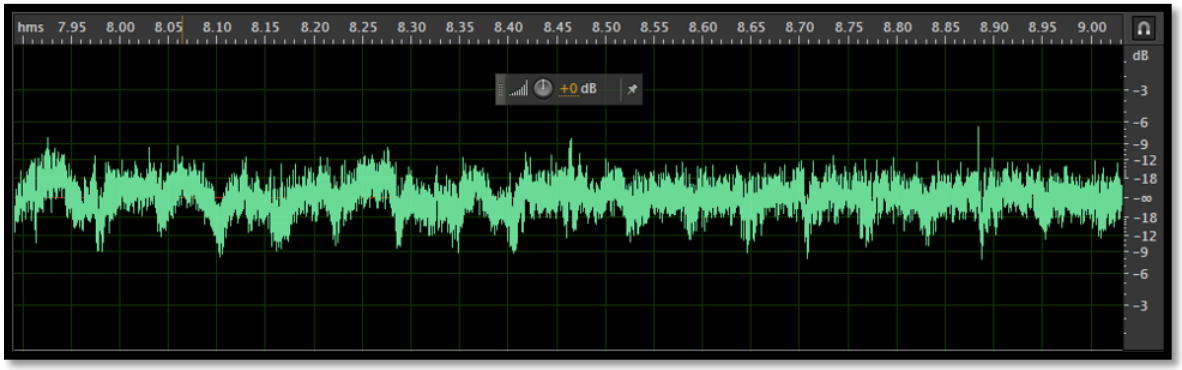

Fig. A3. Model #2d nappe vibration audio recording with one splitter, 0.22 ft^2/s
(x-axis = time in seconds, y-axis = decibel measurement)

Fig. A4. Model #2d nappe vibration audio recording with two splitters, 0.22 ft^2/s (x-axis = time in seconds, y-axis = decibel measurement)

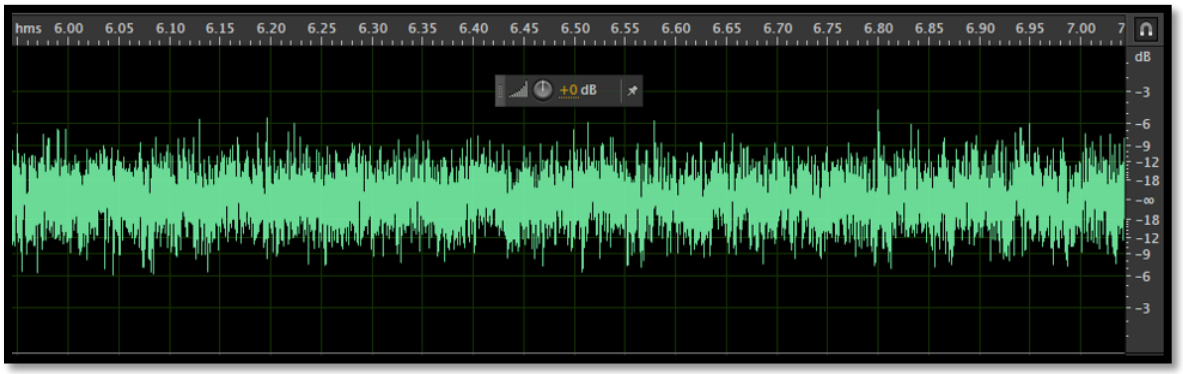

Fig. A5. Model #2d nappe vibration audio recording with three splitters, 0.22 ft^2/s (x-axis = time in seconds, y-axis = decibel measurement)

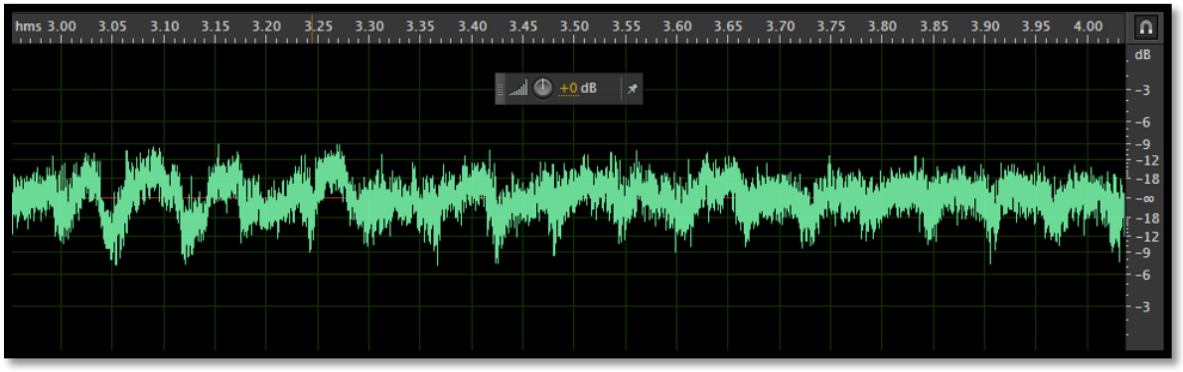

Fig. A6. Model #2b nappe vibration audio recording, 0.28 ft^2/s (x-axis = time in seconds, y-axis = decibel measurement)

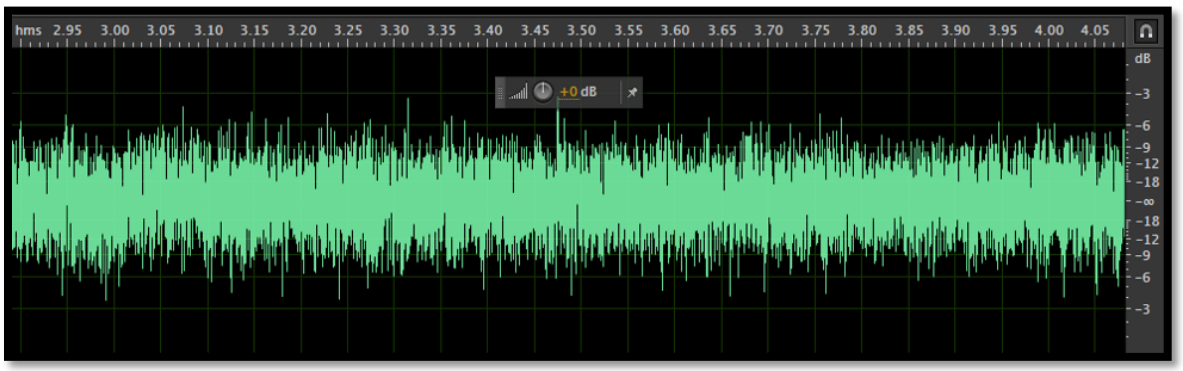

Fig. A7. Model #2c nappe vibration audio recording, 0.28 ft^2/s
(x-axis = time in seconds, y-axis = decibel measurement)

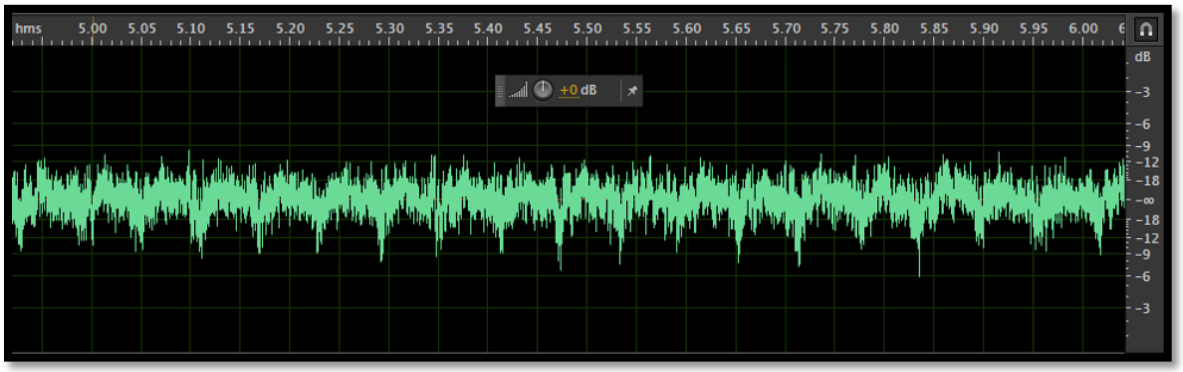

Fig. A8. Model #2d nappe vibration audio recording with one splitter, 0.28 ft^2/s
(x-axis = time in seconds, y-axis = decibel measurement)

Fig. A9. Model #2d nappe vibration audio recording with two splitters, 0.28 ft^2/s
(x-axis = time in seconds, y-axis = decibel measurement)

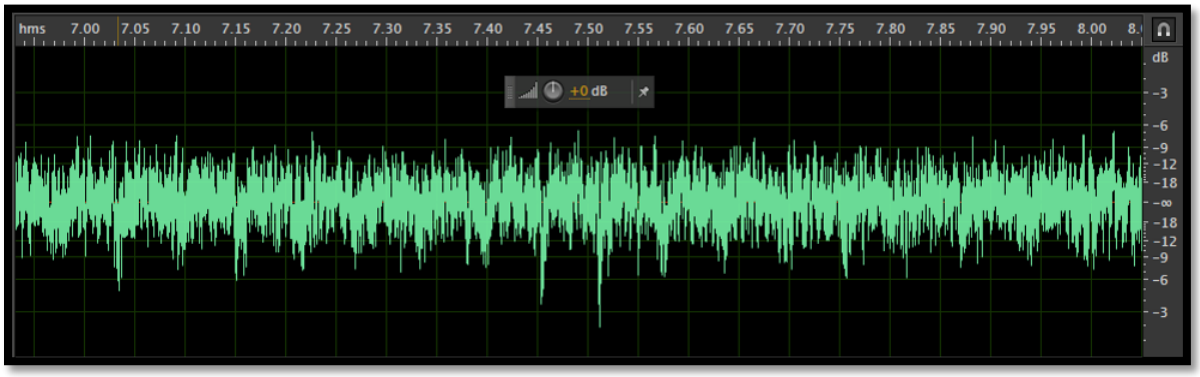

Fig. A10. Model #2d nappe vibration audio recording with three splitters, 0.28 ft^2/s
(x-axis = time in seconds, y-axis = decibel measurement)

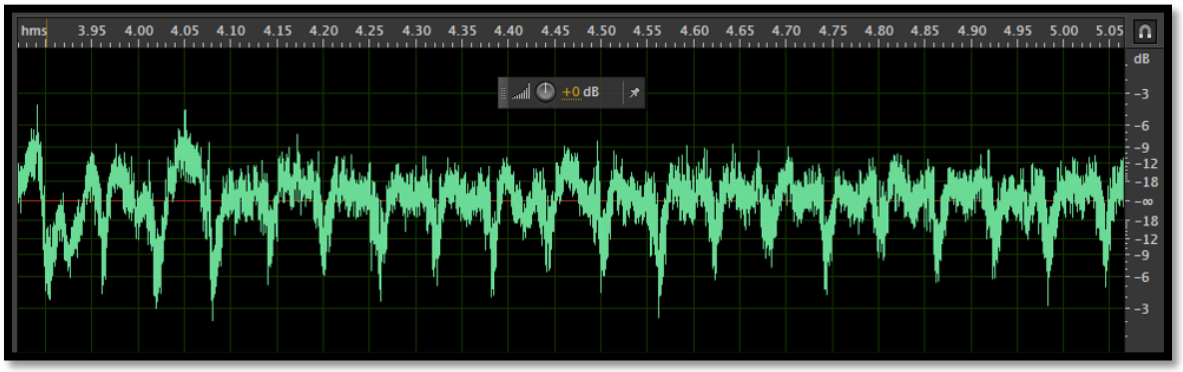

Fig. A11. Model #2b nappe vibration audio recording, 0.34 ft^2/s
(x-axis = time in seconds, y-axis = decibel measurement)

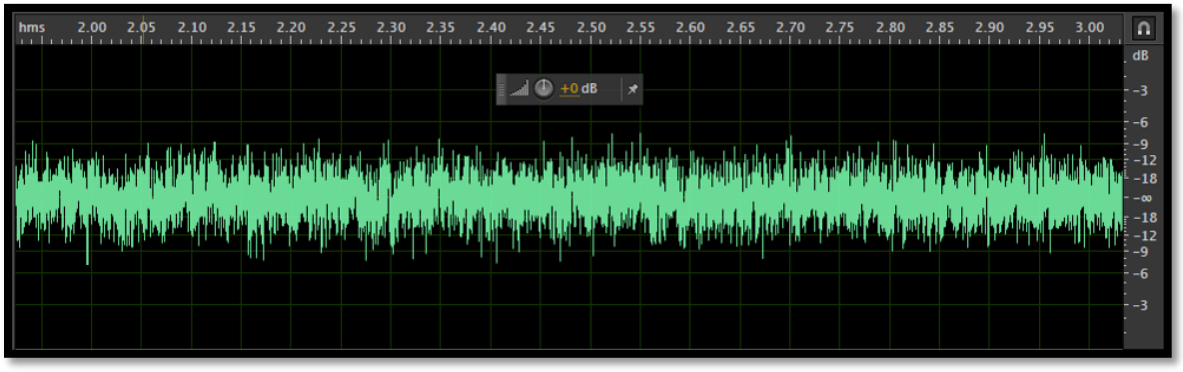

Fig. A12. Model #2c nappe vibration audio recording, 0.34 ft^2/s
(x-axis = time in seconds, y-axis = decibel measurement)

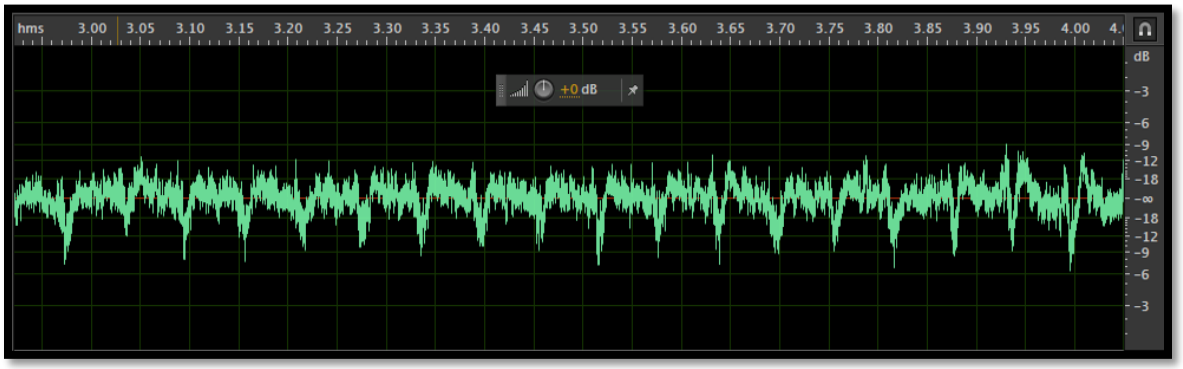

Fig. A13. Model #2d nappe vibration audio recording with one splitter, 0.34 ft^2/s (x-axis = time in seconds, y-axis = decibel measurement)

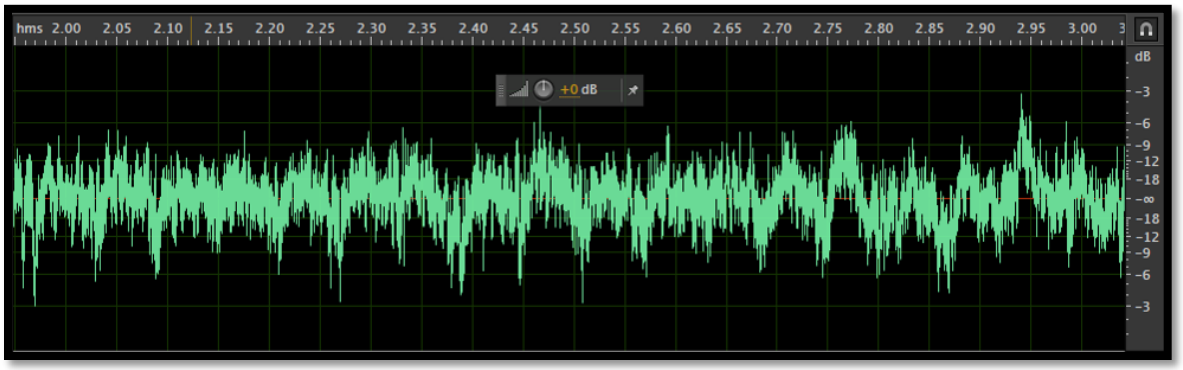

Fig. A14. Model #2d nappe vibration audio recording with two splitters, 0.34 ft^2/s (x-axis = time in seconds, y-axis = decibel measurement)

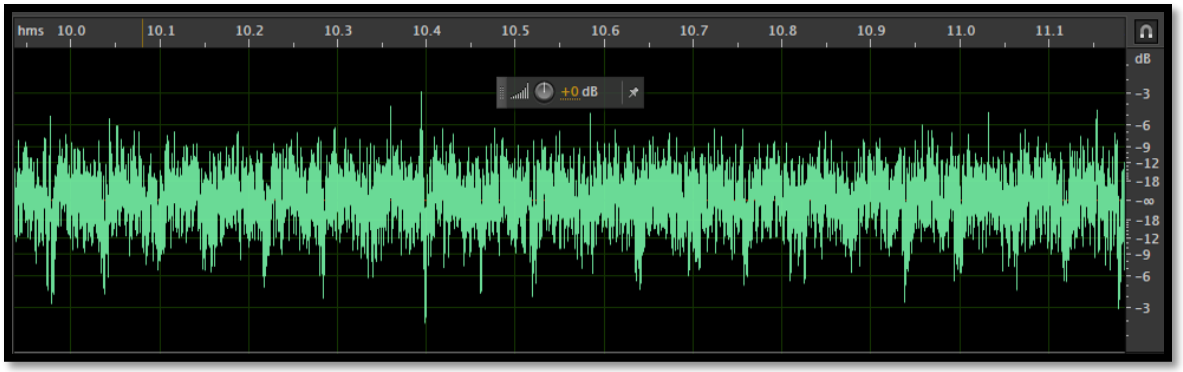

Fig. A15. Model #2d nappe vibration audio recording with three splitters, 0.34 ft^2/s (x-axis = time in seconds, y-axis = decibel measurement)

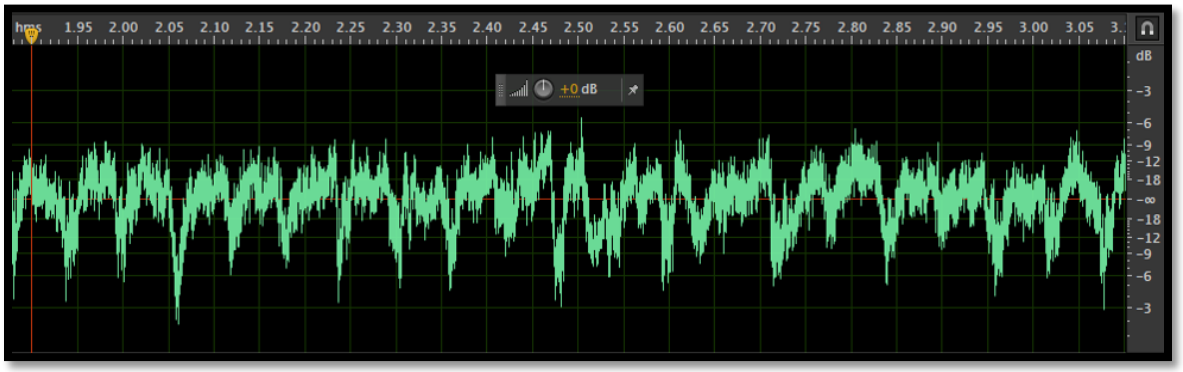

Fig. A16. Model #2b nappe vibration audio recording, 0.40 ft^2/s
(x-axis = time in seconds, y-axis = decibel measurement)

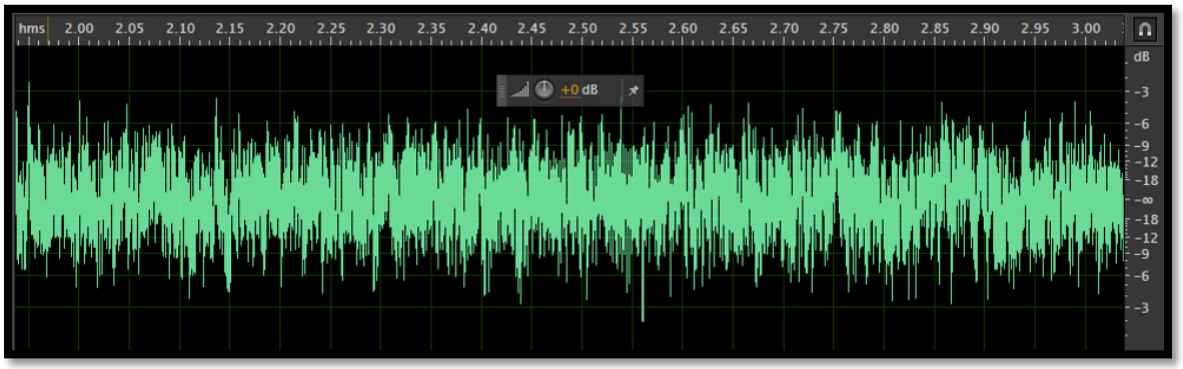

Fig. A17. Model #2c nappe vibration audio recording, 0.40 ft^2/s
(x-axis = time in seconds, y-axis = decibel measurement)

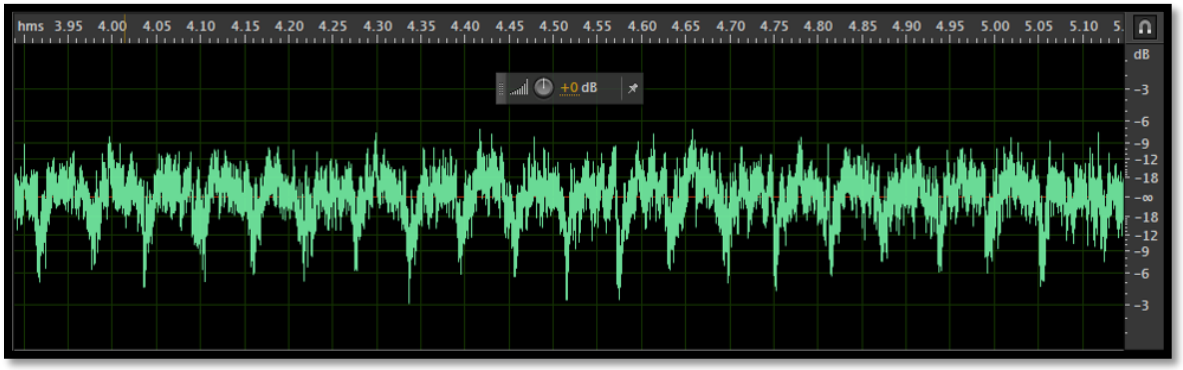

Fig. A18. Model #2d nappe vibration audio recording with one splitter, 0.40 ft^2/s
(x-axis = time in seconds, y-axis = decibel measurement)

Fig. A19. Model #2d nappe vibration audio recording with two splitters, 0.40 ft^2/s (x-axis = time in seconds, y-axis = decibel measurement)

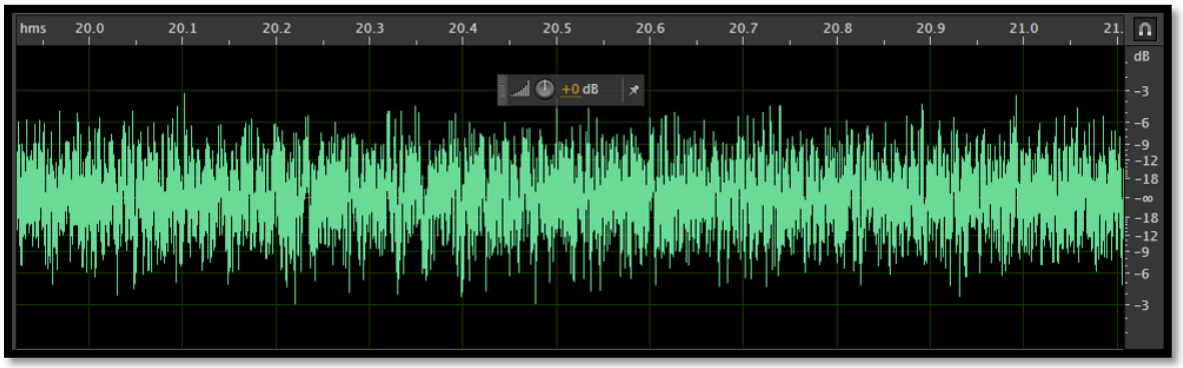

Fig. A20. Model #2d nappe vibration audio recording with three splitters, 0.40 ft^2/s (x-axis = time in seconds, y-axis = decibel measurement)

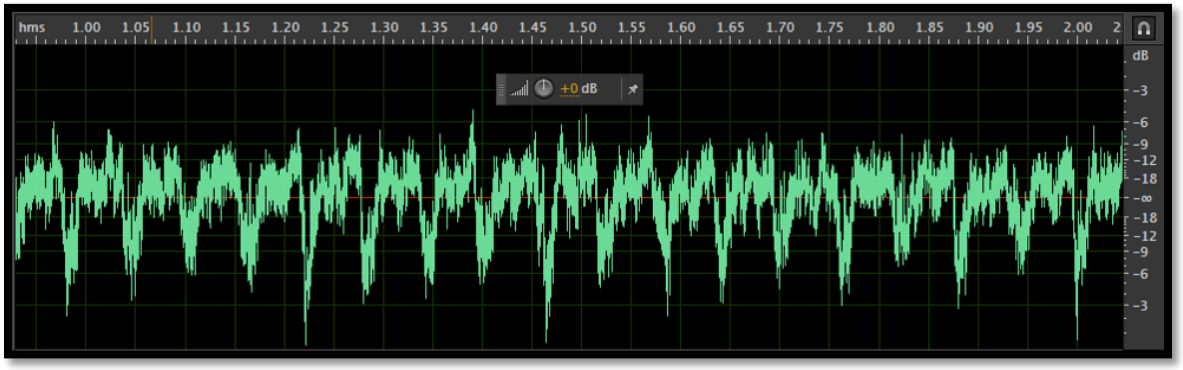

Fig. A21. Model #2b nappe vibration audio recording, 0.47 ft^2/s (x-axis = time in seconds, y-axis = decibel measurement)

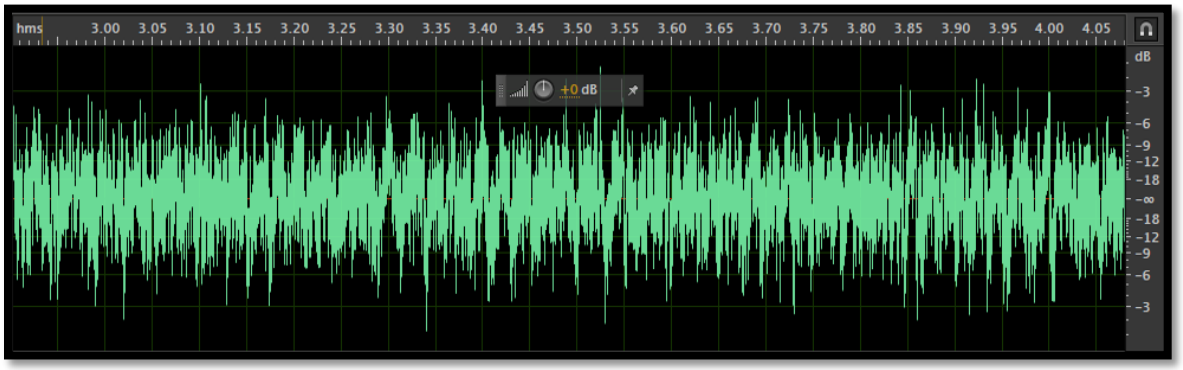

Fig. A22. Model #2c nappe vibration audio recording, 0.47 ft^2/s
(x-axis = time in seconds, y-axis = decibel measurement)

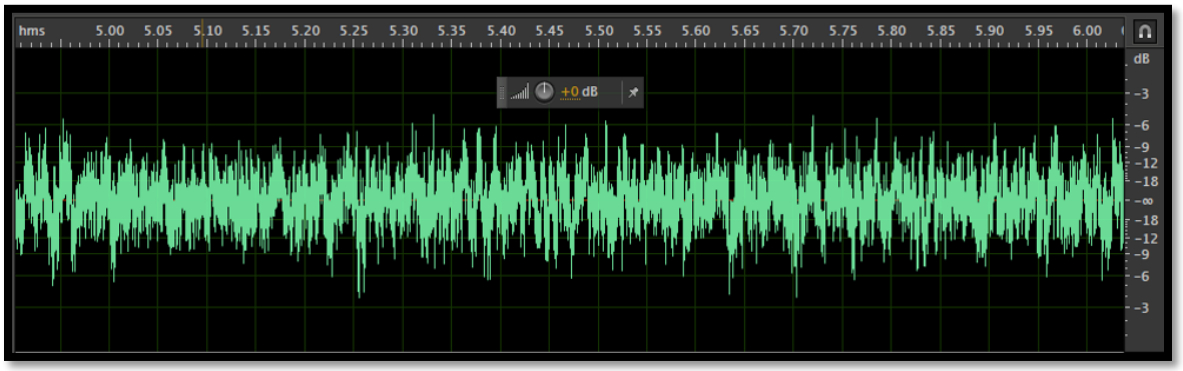

Fig. A23. Model #2d nappe vibration audio recording with one splitter, 0.47 ft^2/s
(x-axis = time in seconds, y-axis = decibel measurement)

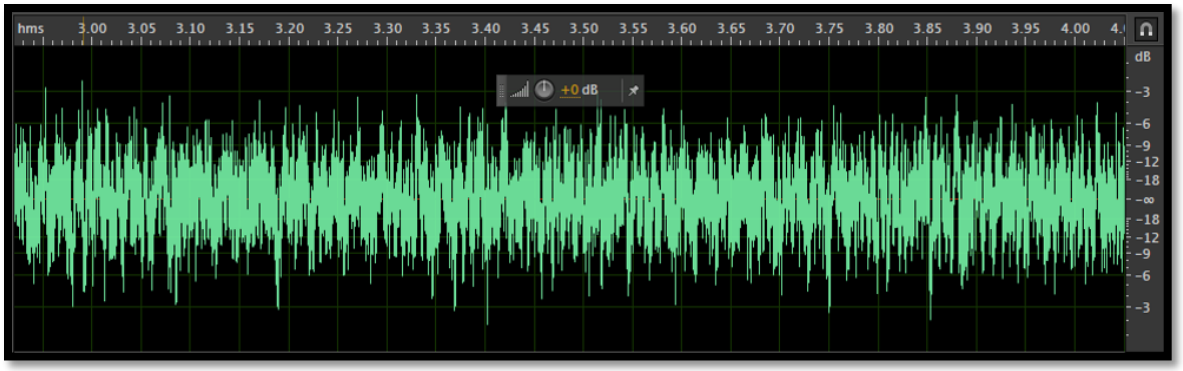

Fig. A24. Model #2d nappe vibration audio recording with two splitters, 0.47 ft^2/s
(x-axis = time in seconds, y-axis = decibel measurement)

Fig. A25. Model #2d nappe vibration audio recording with three splitters, 0.47 ft^2/s (x-axis = time in seconds, y=axis = decibel measurement)

Appendix B. Model #3 Figures

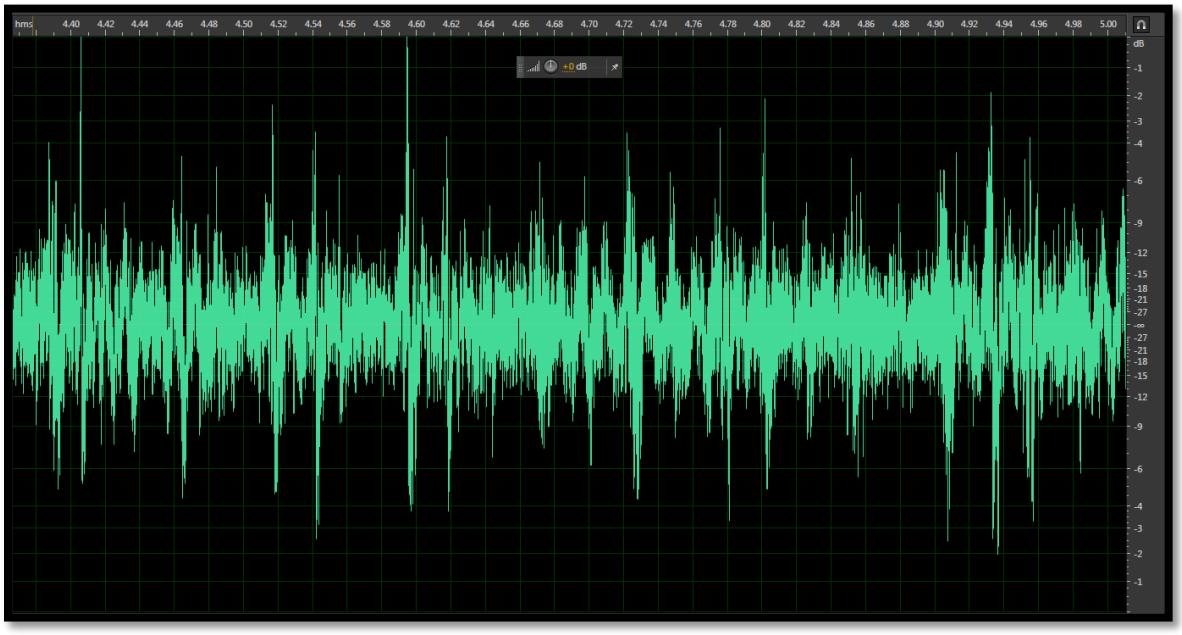

Fig. B1. Model #3a nappe vibration audio recording (grate impact), 0.14 ft^2/s
(x-axis = time in seconds, y-axis = decibel measurement)

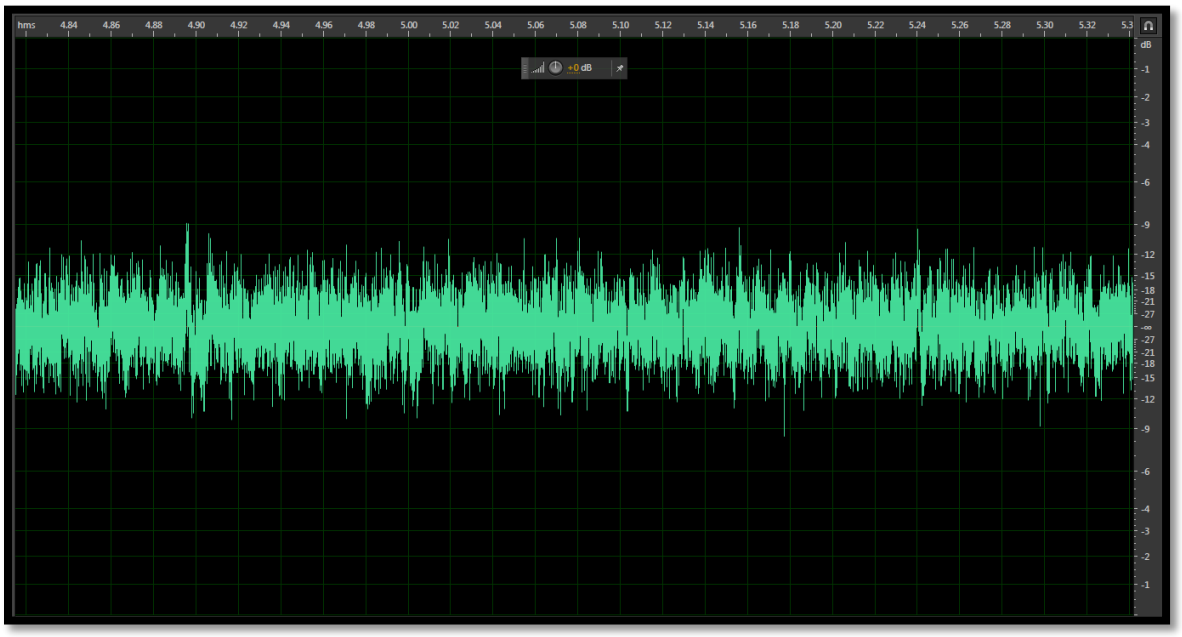

Fig. B2. Model #3a nappe vibration audio recording (solid impact), 0.14 ft^2/s
(x-axis = time in seconds, y-axis = decibel measurement)

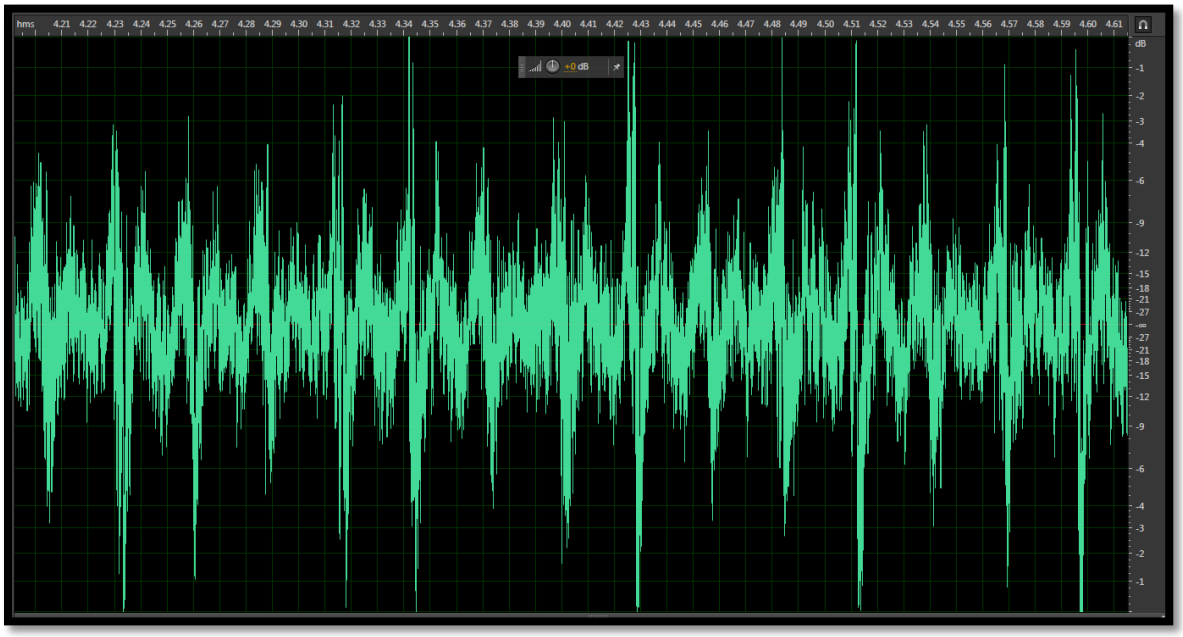

Fig. B3 Model #3a nappe vibration audio recording (grate impact), 0.20 ft^2/s
(x-axis = time in seconds, y-axis = decibel measurement)

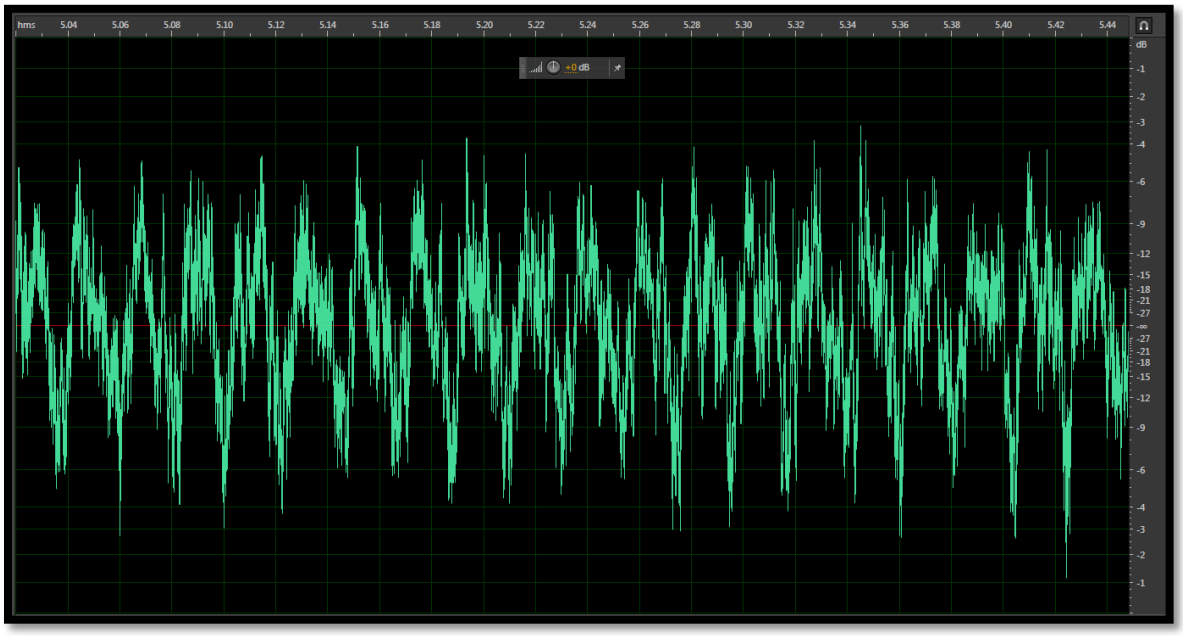

Fig. B4. Model #3a nappe vibration audio recording (solid impact), 0.20 ft^2/s
(x-axis = time in seconds, y-axis = decibel measurement)

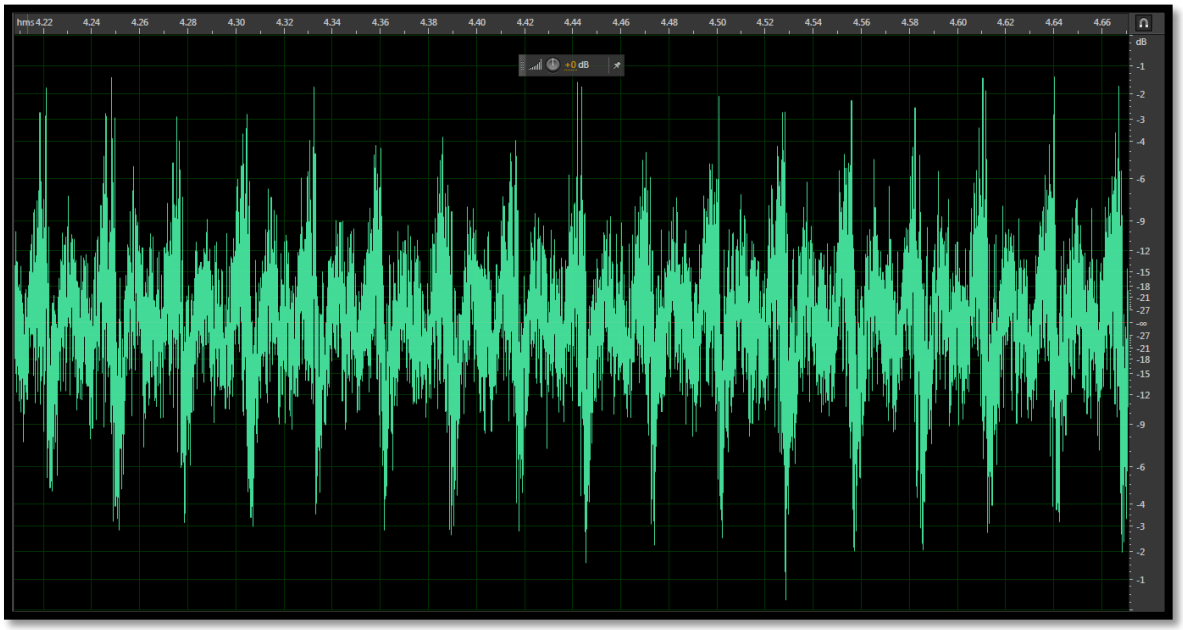

Fig. B5 Model #3a nappe vibration audio recording (grate impact), 0.25 ft^2/s
(x-axis = time in seconds, y-axis = decibel measurement)

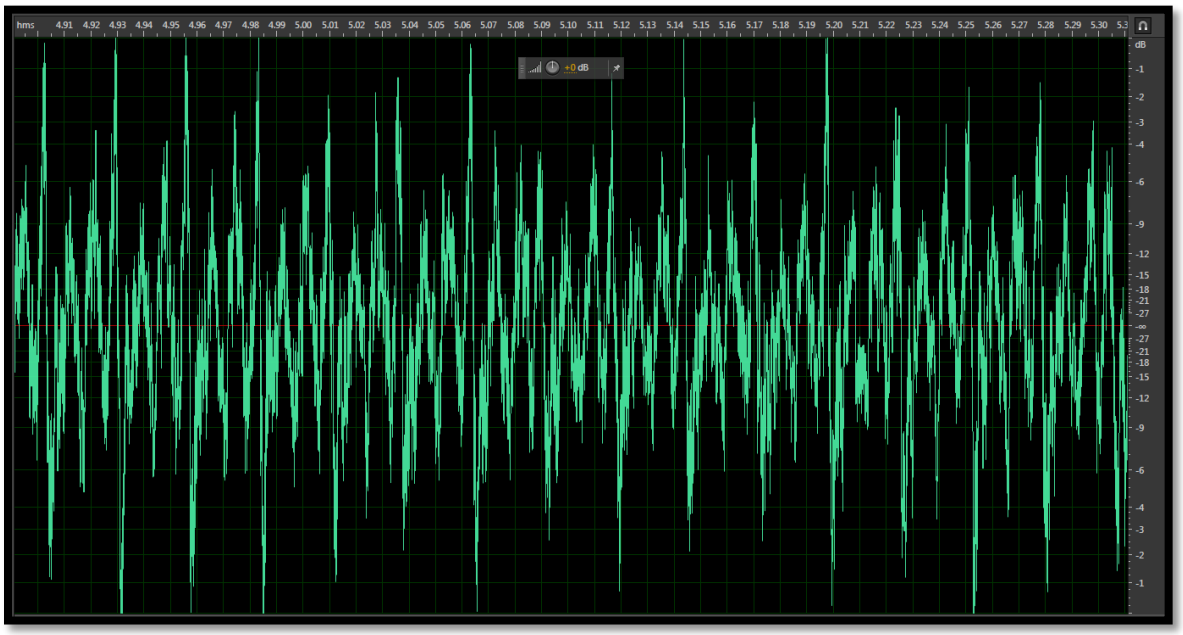

Fig. B6. Model #3a nappe vibration audio recording (solid impact), 0.25 ft^2/s
(x-axis = time in seconds, y-axis = decibel measurement)

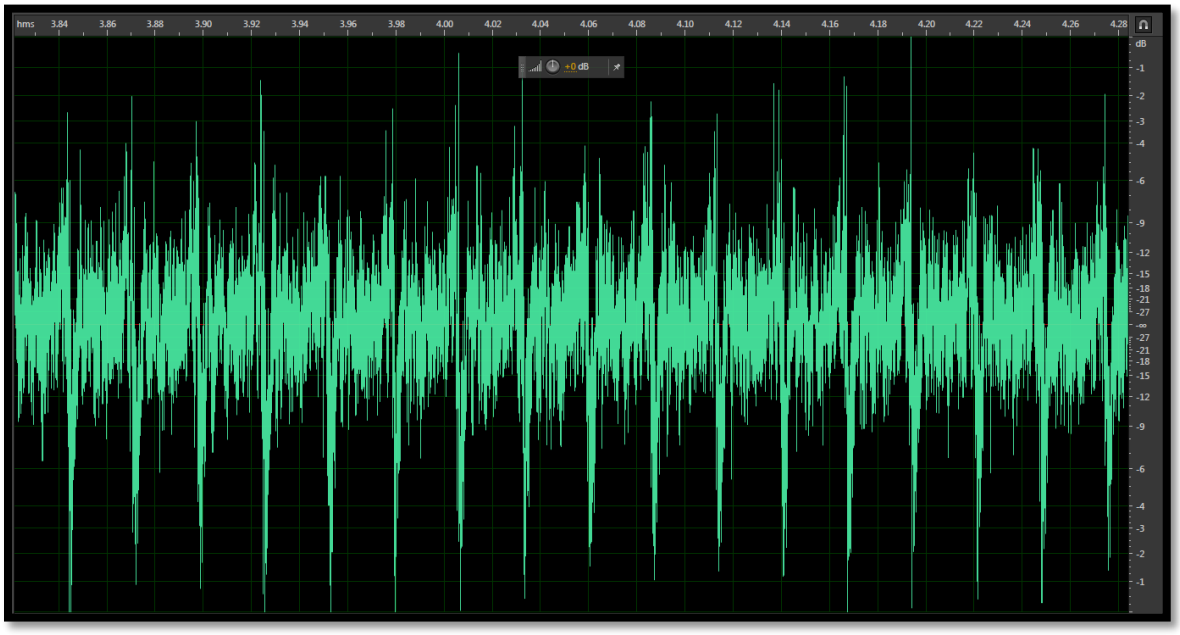

Fig. B7. Model #3a nappe vibration audio recording (grate impact), 0.31 ft^2/s (x-axis = time in seconds, y-axis = decibel measurement)

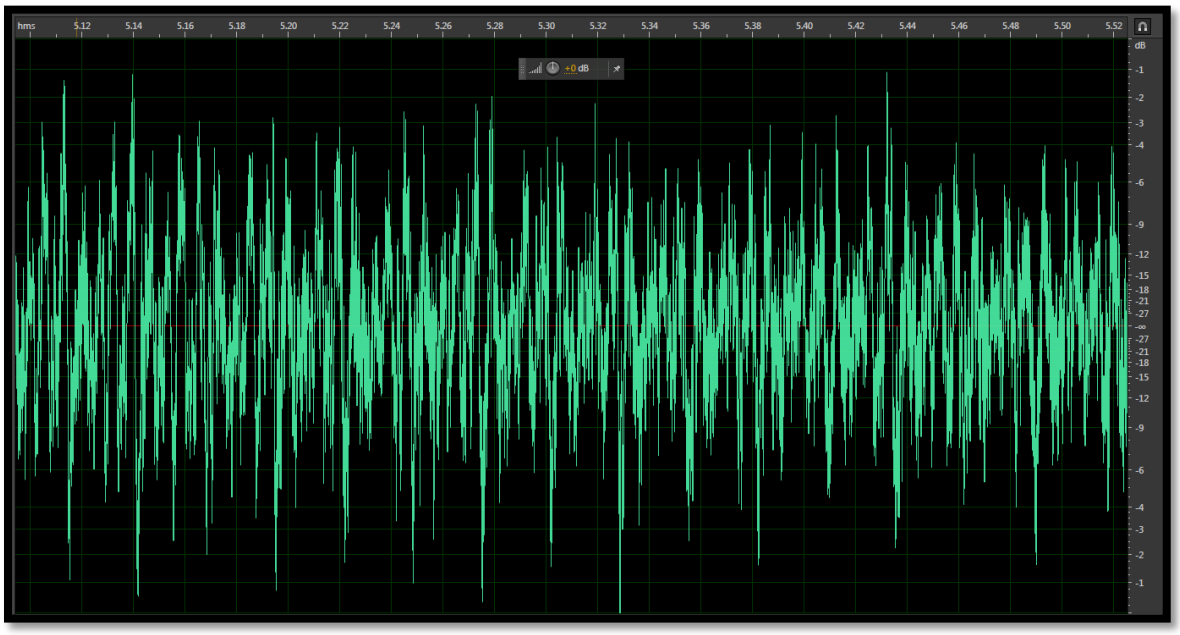

Fig. B8. Model #3a nappe vibration audio recording (solid impact), 0.31 ft^2/s (x-axis = time in seconds, y-axis = decibel measurement)

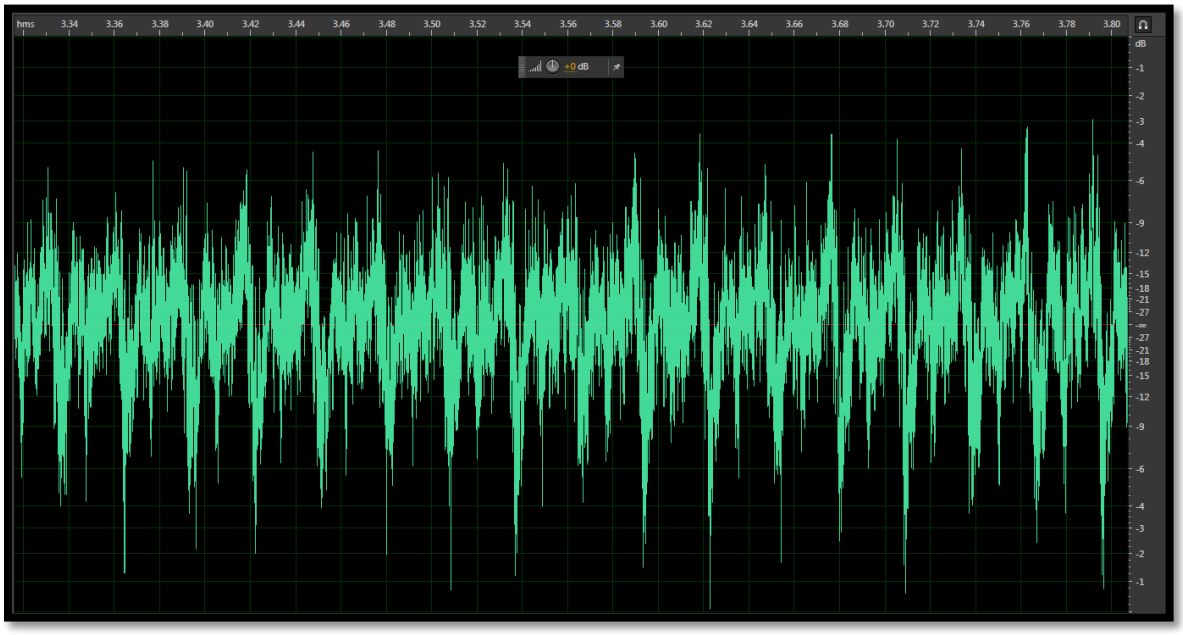

Fig. B9. Model #3a nappe vibration audio recording (grate impact), 0.36 ft^2/s
(x-axis = time in seconds, y-axis = decibel measurement)

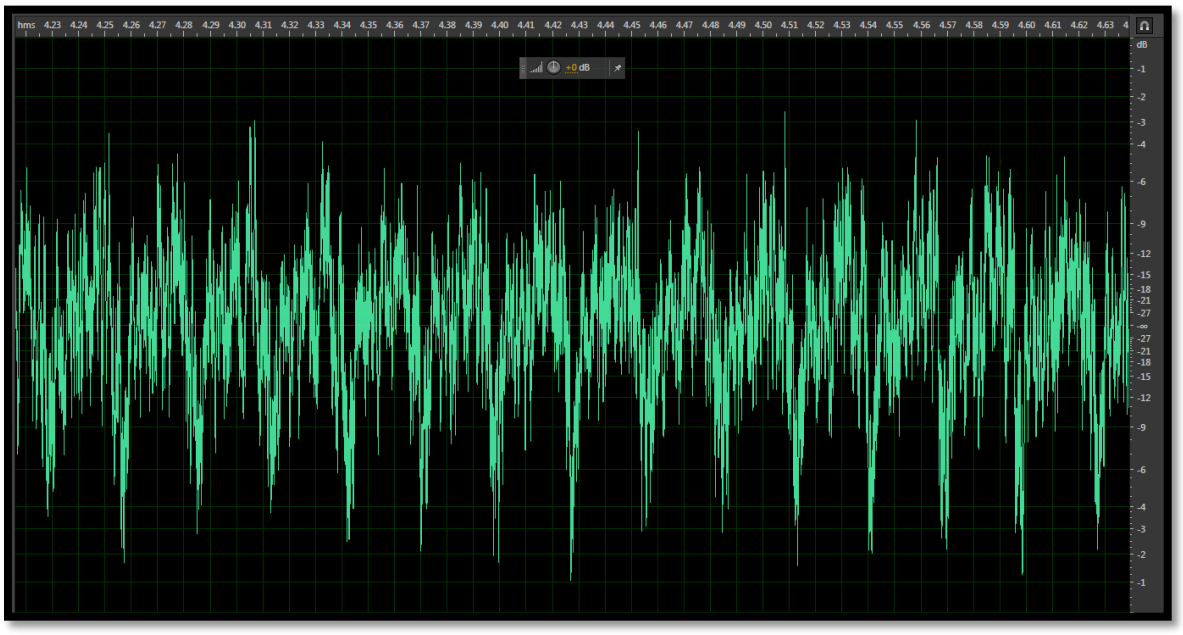

Fig. B10. Model #3a nappe vibration audio recording (solid impact), 0.36 ft^2/s
(x-axis = time in seconds, y-axis = decibel measurement)

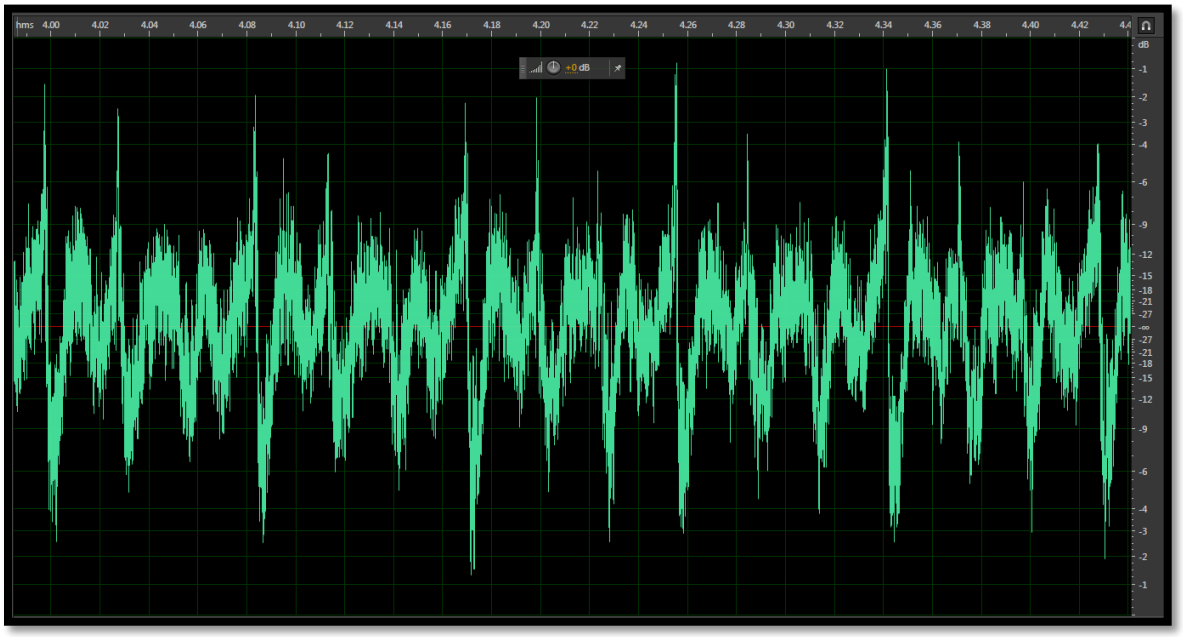

Fig. B11. Model #3a nappe vibration audio recording (grate impact), 0.42 ft^2/s (x-axis = time in seconds, y-axis = decibel measurement)

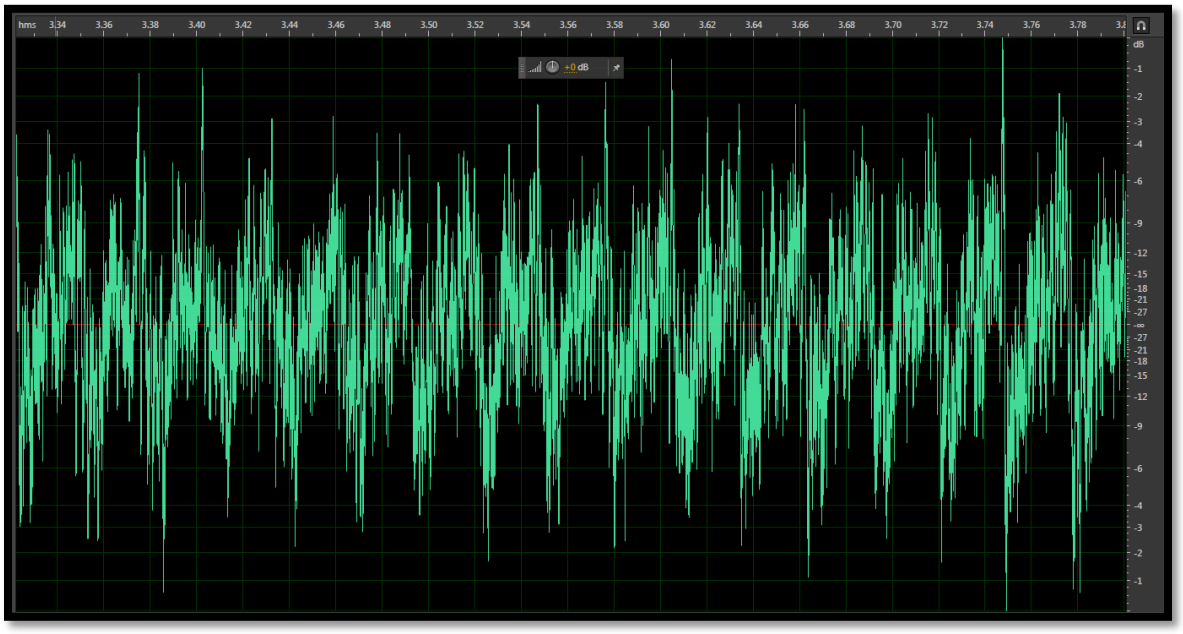

Fig. B12. Model #3a nappe vibration audio recording (solid impact), 0.42 ft^2/s (x-axis = time in seconds, y-axis = decibel measurement)

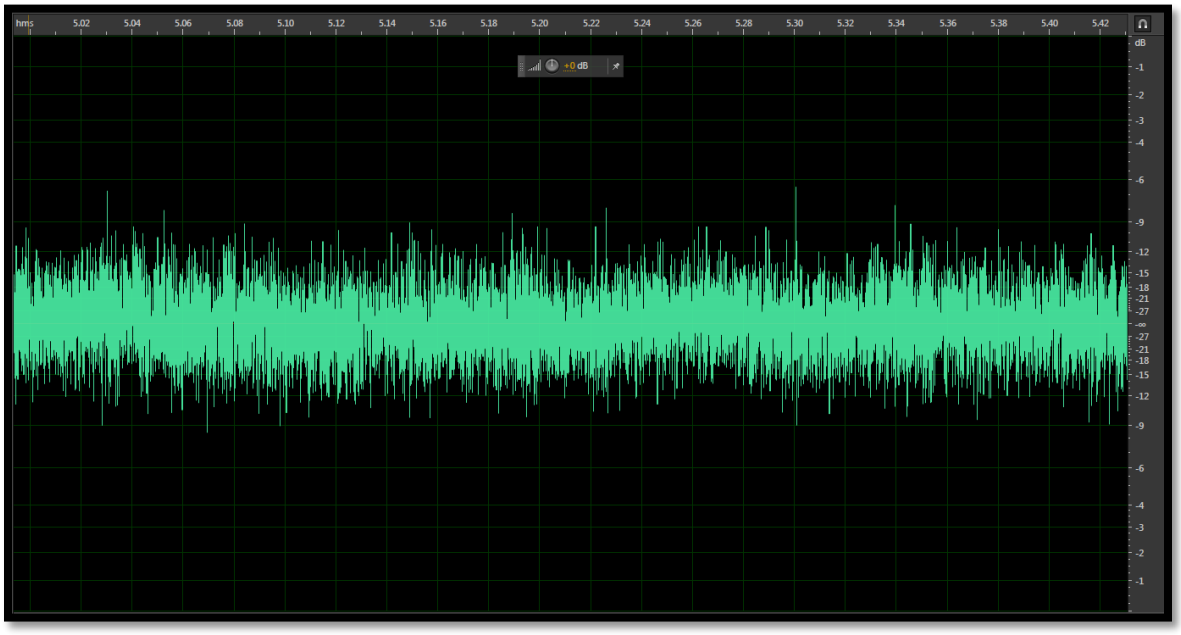

Fig. B13. Model #3b nappe vibration audio recording (grate impact), 0.14 ft^2/s (x-axis = time in seconds, y-axis = decibel measurement)

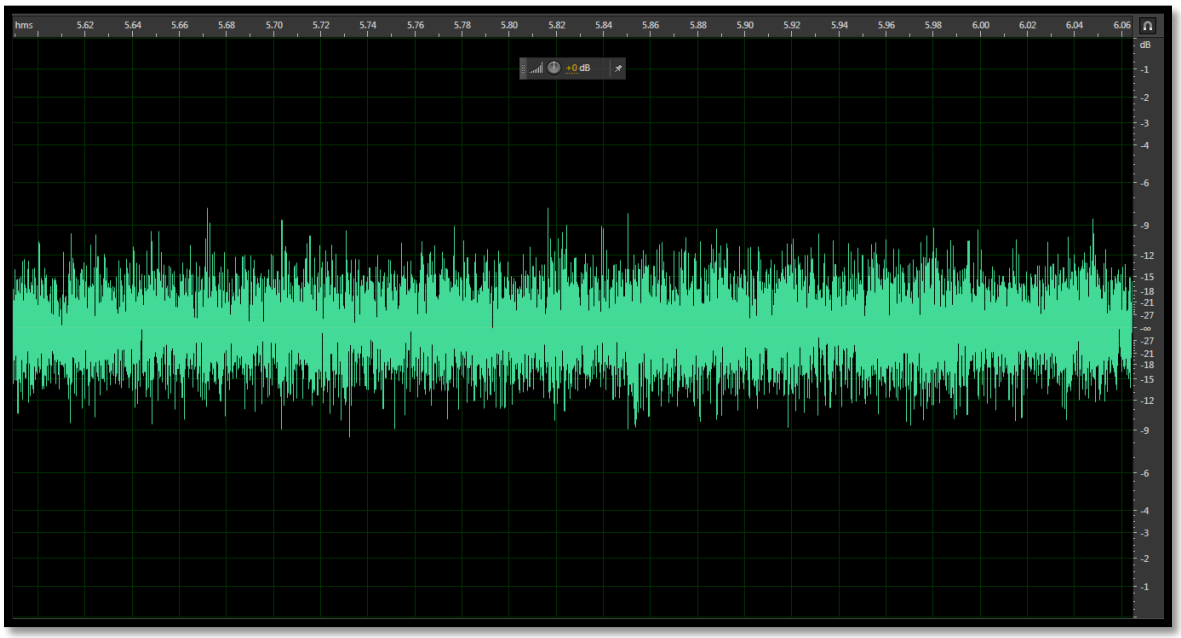

Fig. B14. Model #3b nappe vibration audio recording (solid impact), 0.14 ft^2/s (x-axis = time in seconds, y-axis = decibel measurement)

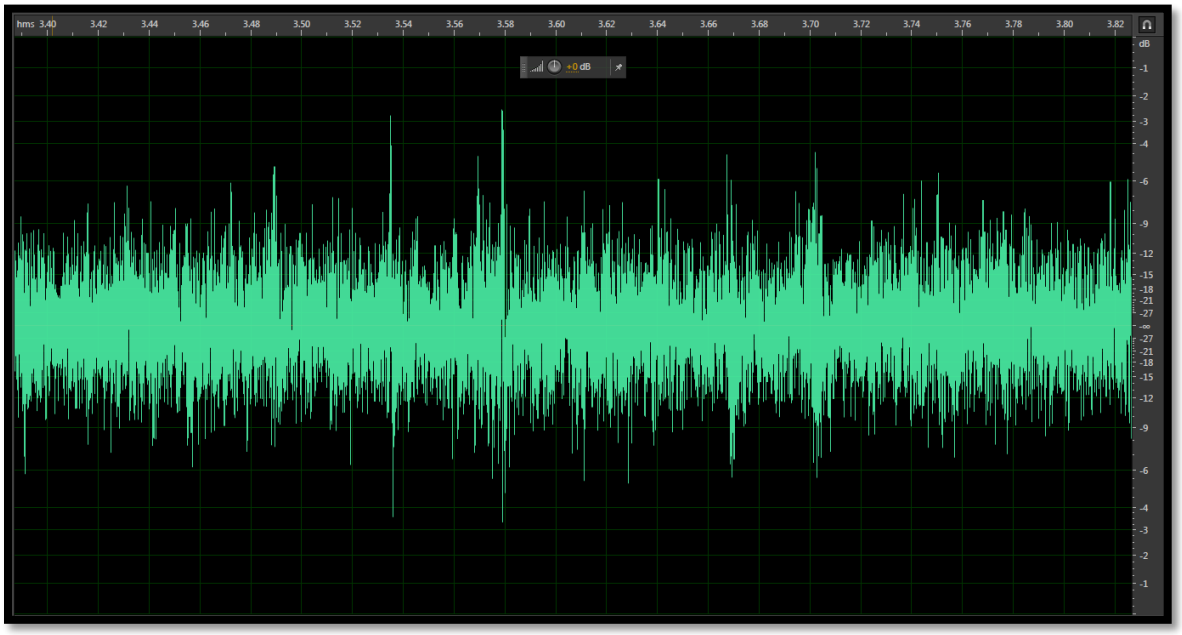

Fig. B15. Model #3b nappe vibration audio recording (grate impact), 0.20 ft^2/s (x-axis = time in seconds, y-axis = decibel measurement)

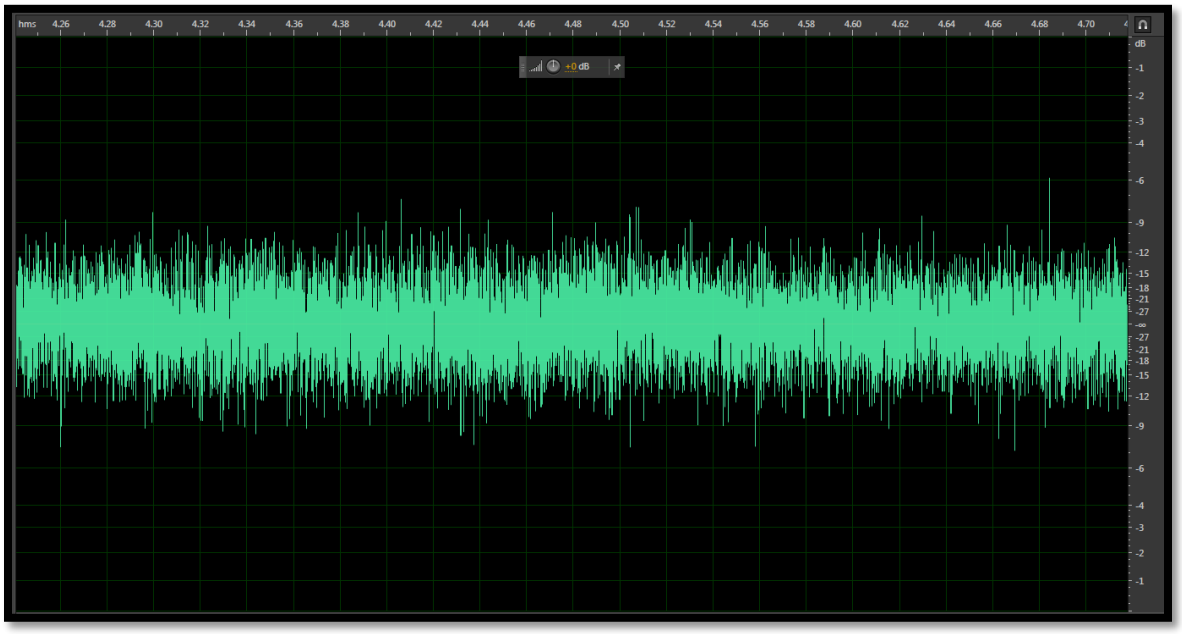

Fig. B16. Model #3b nappe vibration audio recording (solid impact), 0.20 ft^2/s (x-axis = time in seconds, y-axis = decibel measurement)

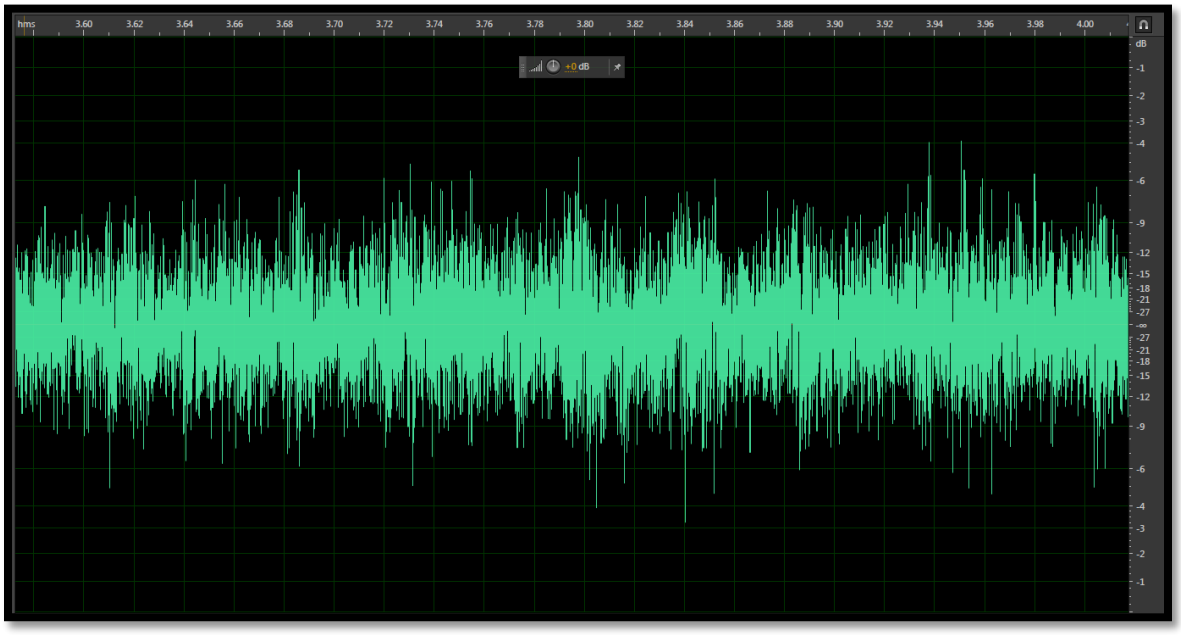

Fig. B17. Model #3b nappe vibration audio recording (grate impact), 0.25 ft^2/s (x-axis = time in seconds, y-axis = decibel measurement)

Fig. B18. Model #3b nappe vibration audio recording (solid impact), 0.25 ft^2/s (x-axis = time in seconds, y-axis = decibel measurement)

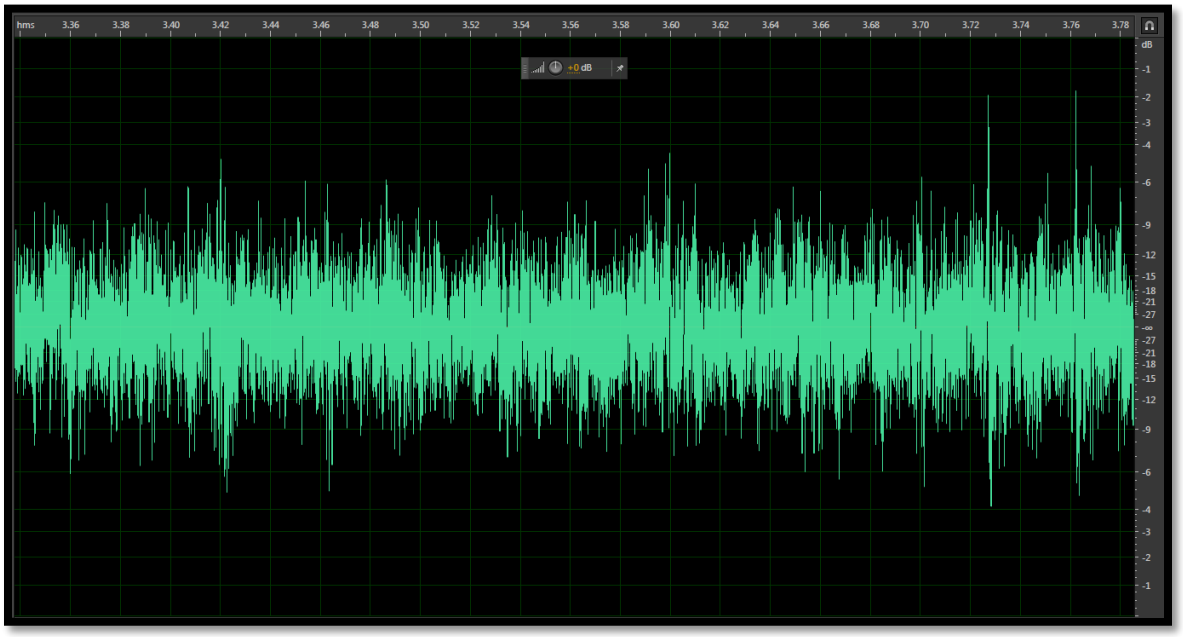

Fig. B19. Model #3b nappe vibration audio recording (grate impact), 0.31 ft^2/s (x-axis = time in seconds, y-axis = decibel measurement)

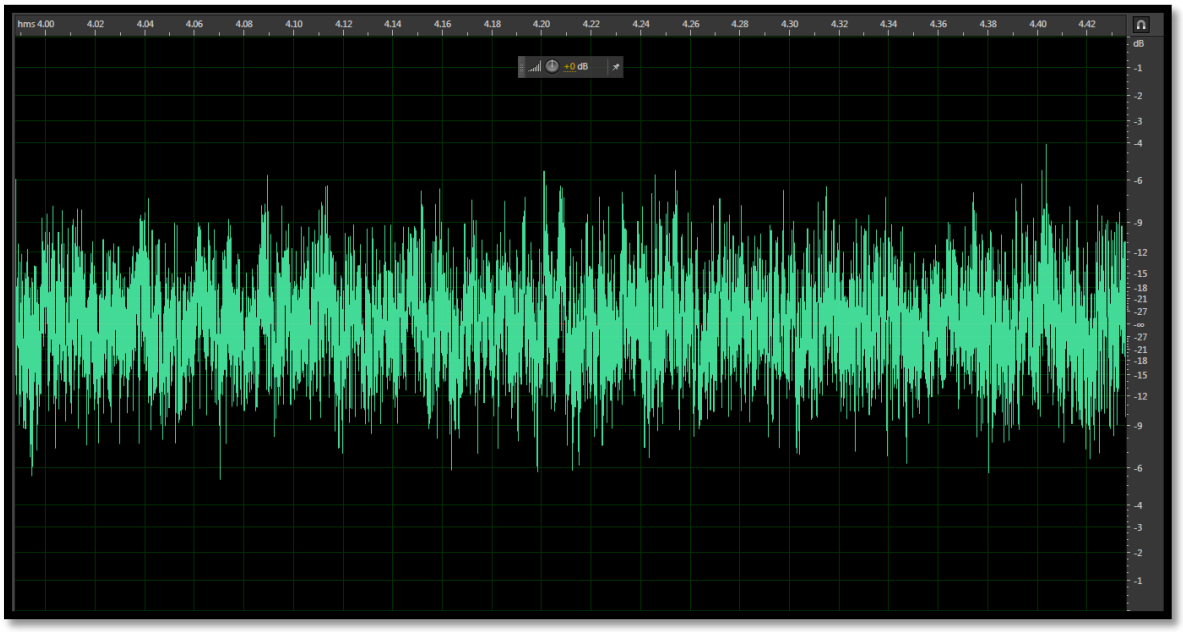

Fig. B20. Model #3b nappe vibration audio recording (solid impact), 0.31 ft^2/s (x-axis = time in seconds, y-axis = decibel measurement)

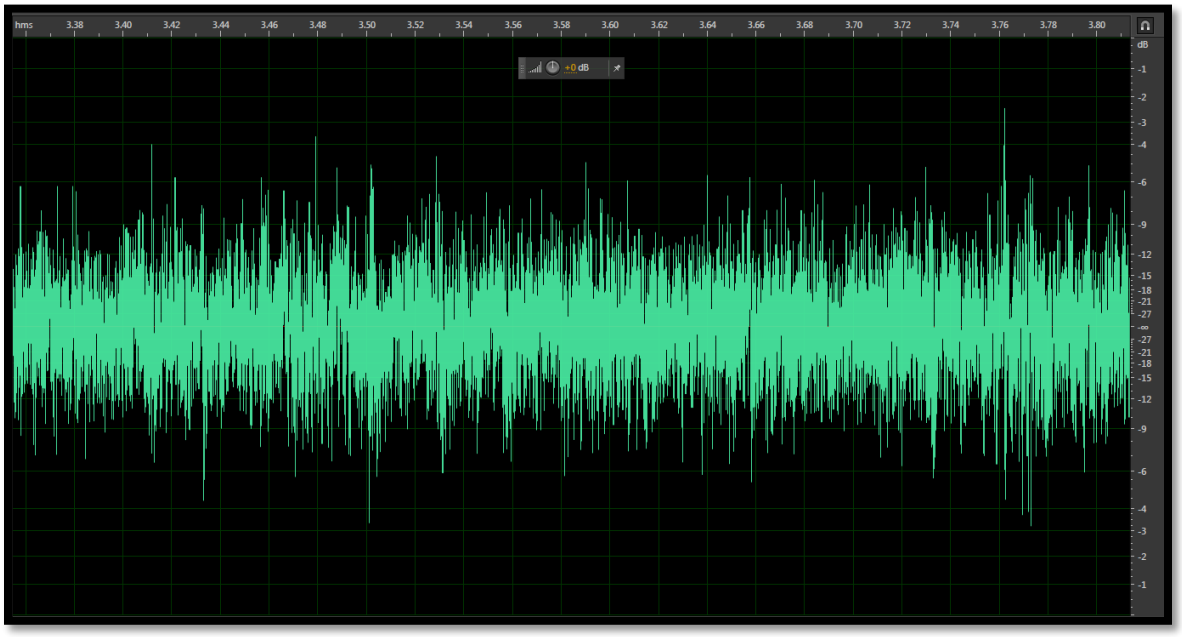

Fig. B21. Model #3b nappe vibration audio recording (grate impact), 0.36 ft^2/s (x-axis = time in seconds, y-axis = decibel measurement)

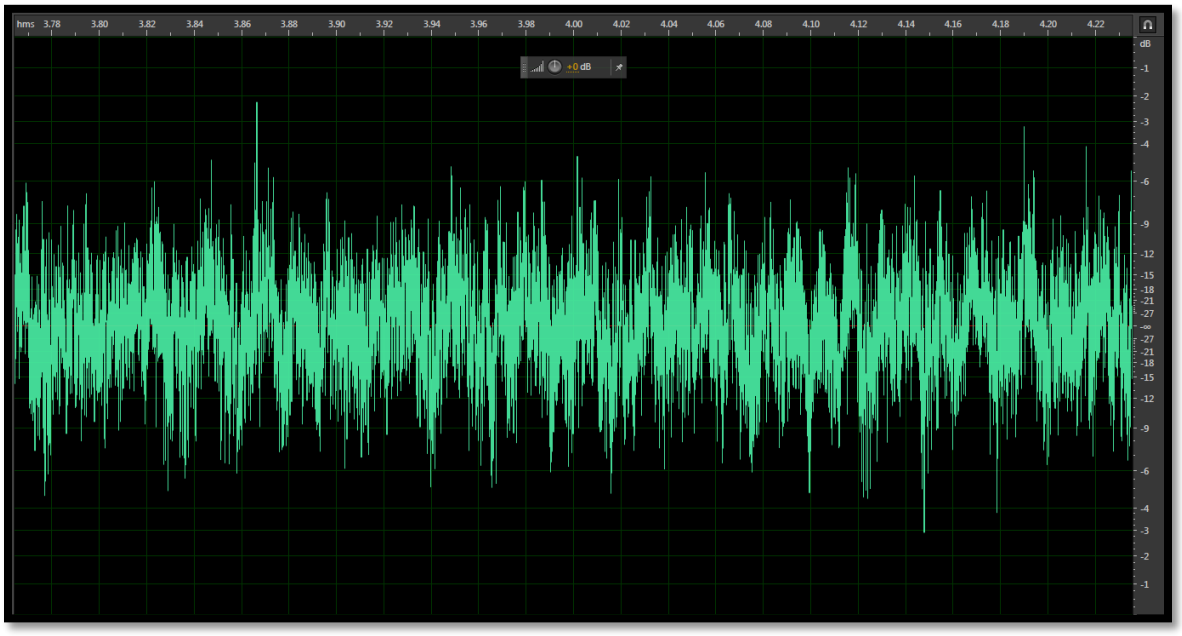

Fig. B22. Model #3b nappe vibration audio recording (solid impact), 0.36 ft^2/s (x-axis = time in seconds, y-axis = decibel measurement)

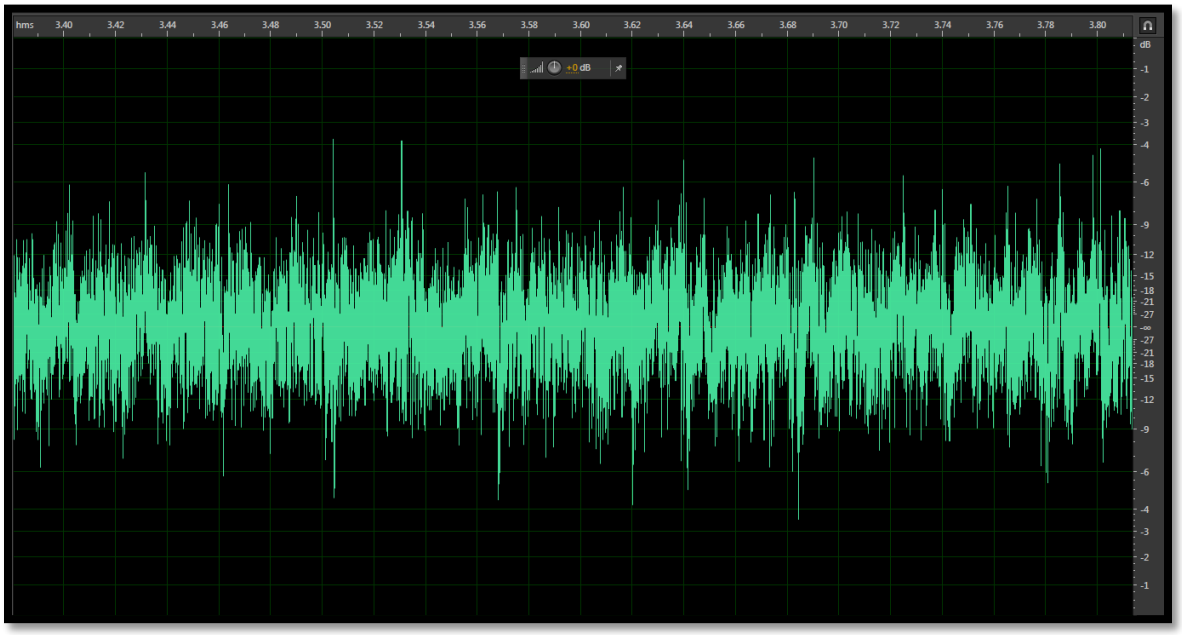

Fig. B23. Model #3b nappe vibration audio recording (grate impact), 0.42 ft^2/s (x-axis = time in seconds, y-axis = decibel measurement)

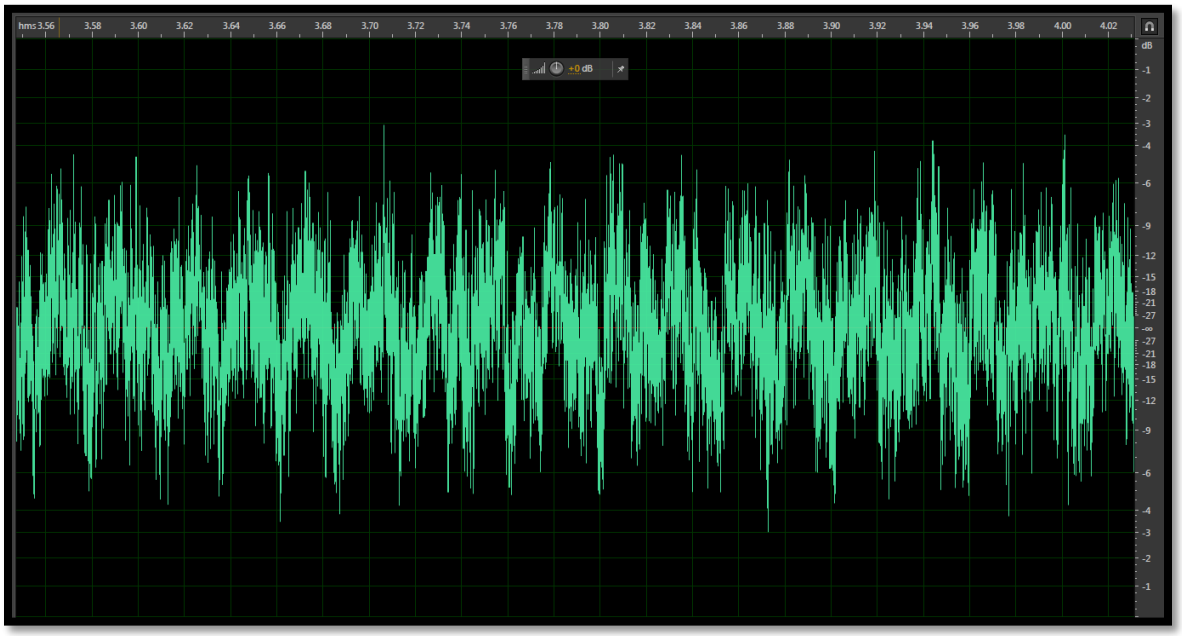

Fig. B24. Model #3b nappe vibration audio recording (solid impact), 0.42 ft^2/s (x-axis = time in seconds, y-axis = decibel measurement)

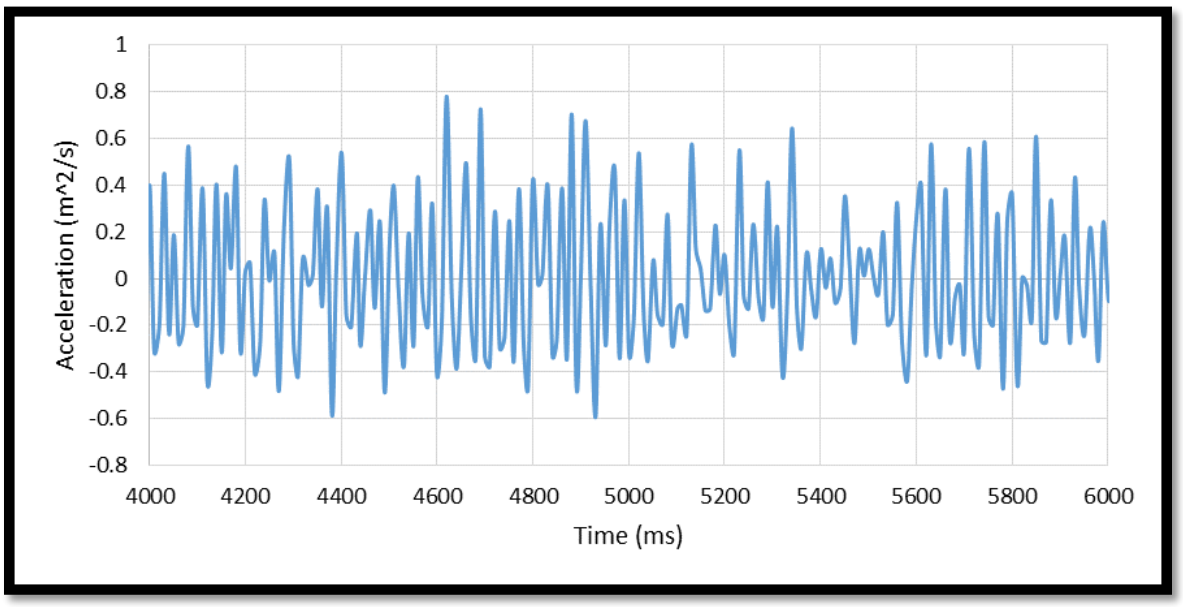

Fig. B25. Model #3c nappe vibration accelerometer data, 0.14 ft^2/s

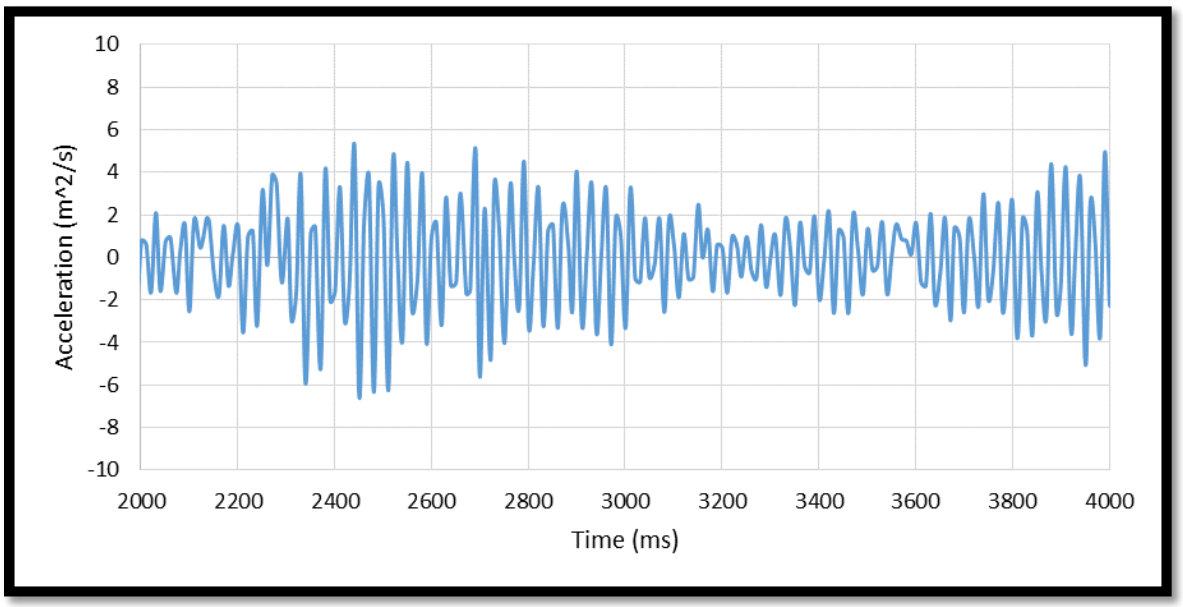

Fig. B26. Model #3c nappe vibration accelerometer data, 0.20 ft^2/s

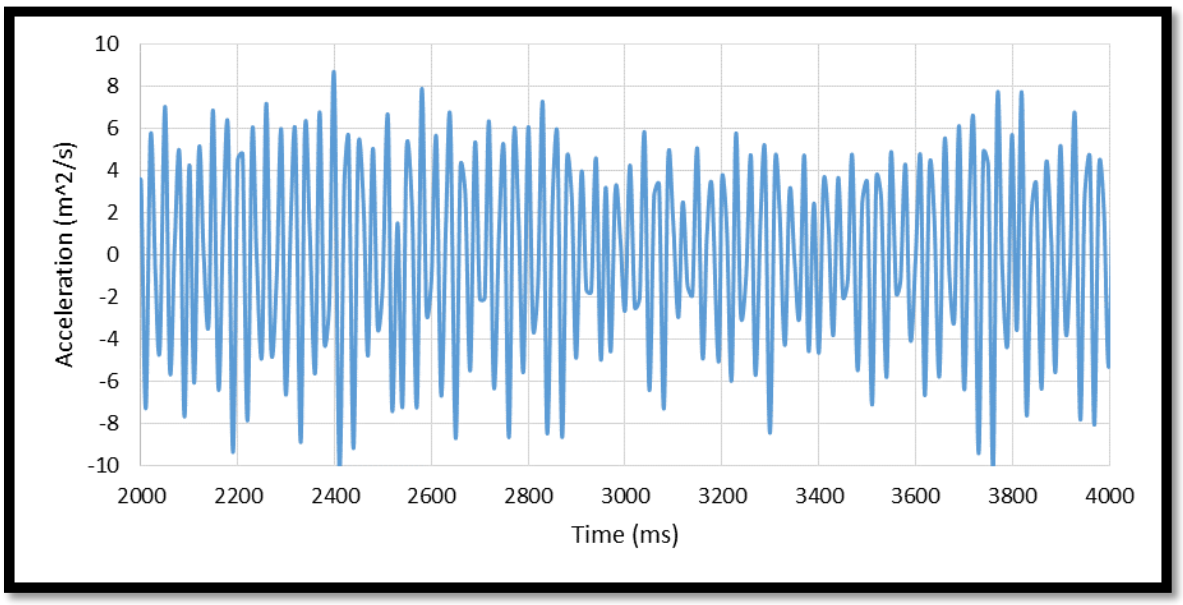

Fig. B27. Model #3c nappe vibration accelerometer data, 0.25 ft^2/s

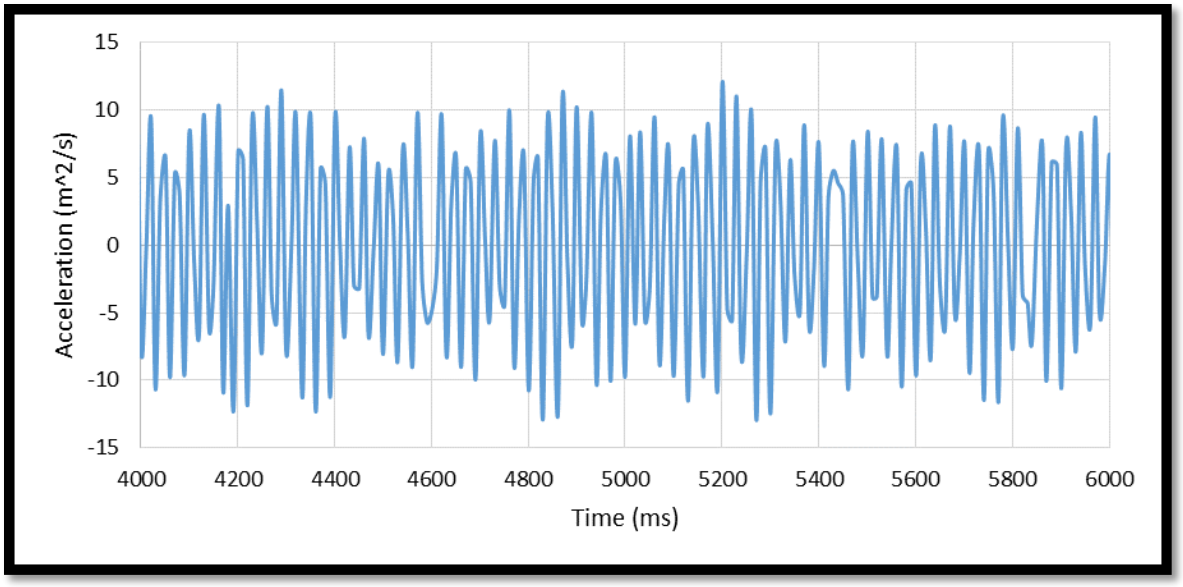

Fig. B28. Model #3c nappe vibration accelerometer data, 0.31 ft^2/s

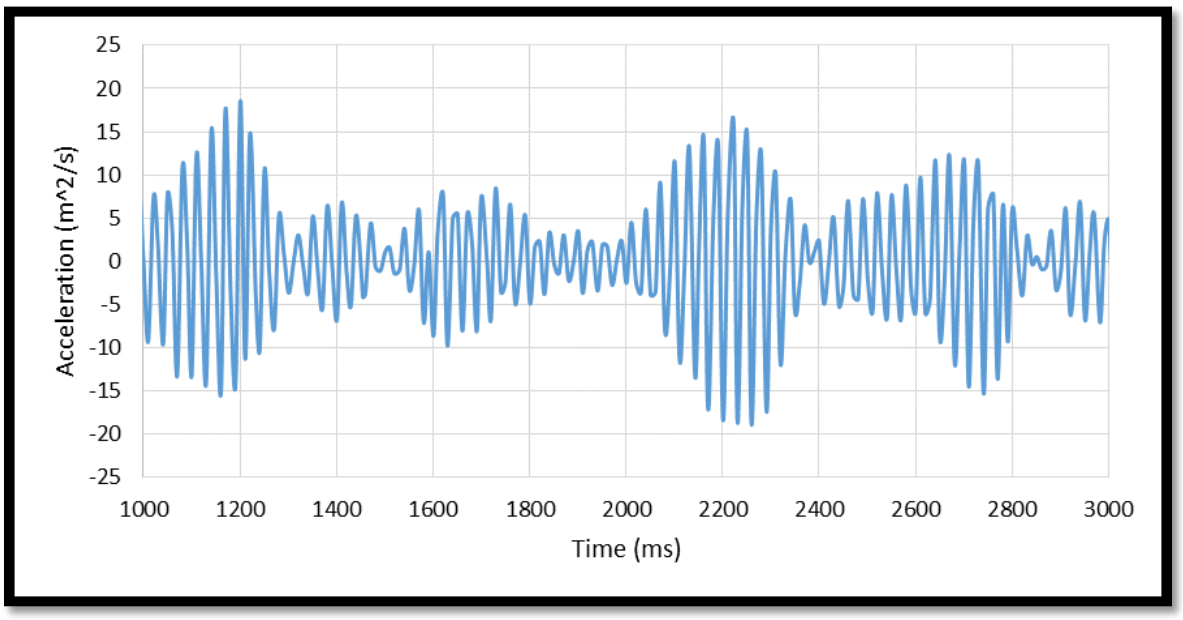

Fig. B29. Model #3c nappe vibration accelerometer data, 0.36 ft^2/s

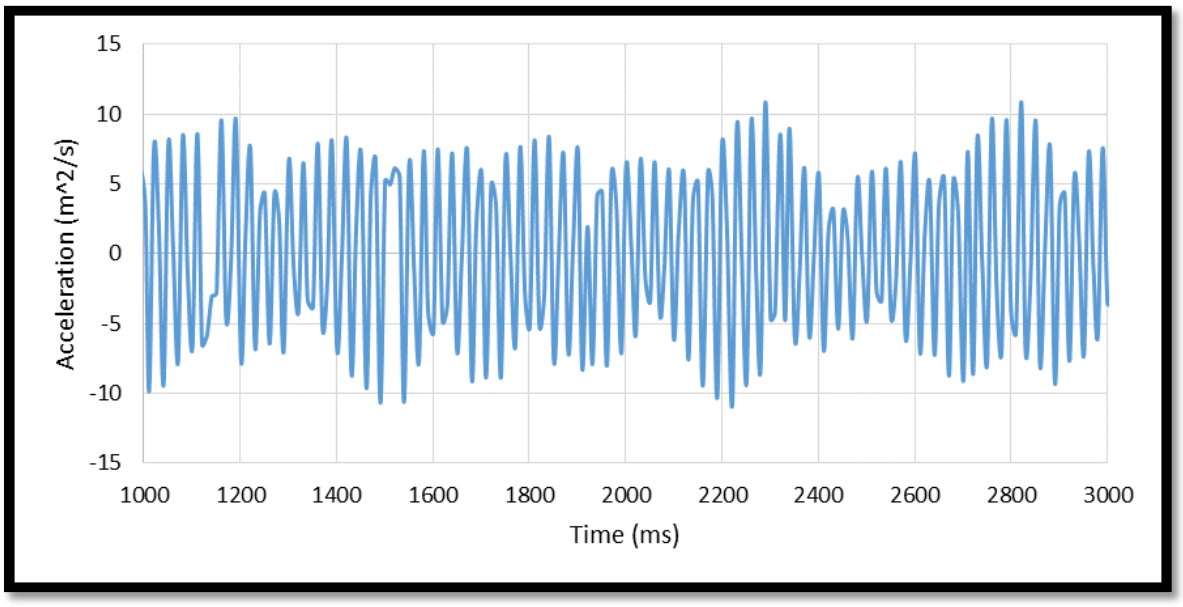

Fig. B30. Model #3c nappe vibration accelerometer data, 0.42 ft^2/s

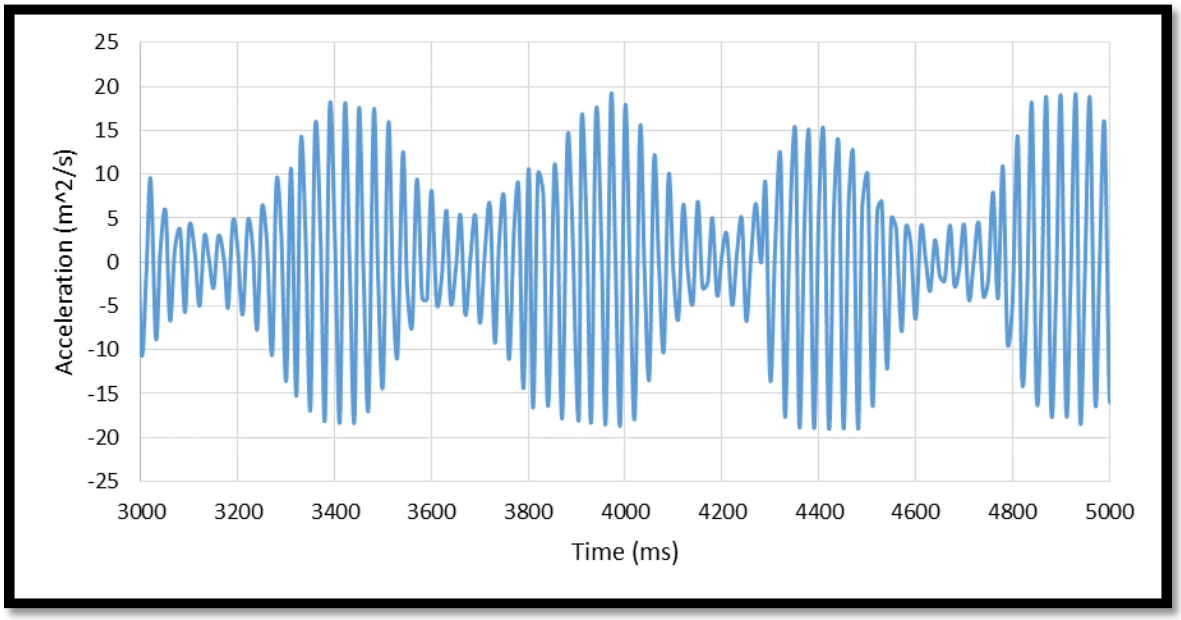

Fig. B31. Model #3c nappe vibration accelerometer data, 0.48 ft^2/s

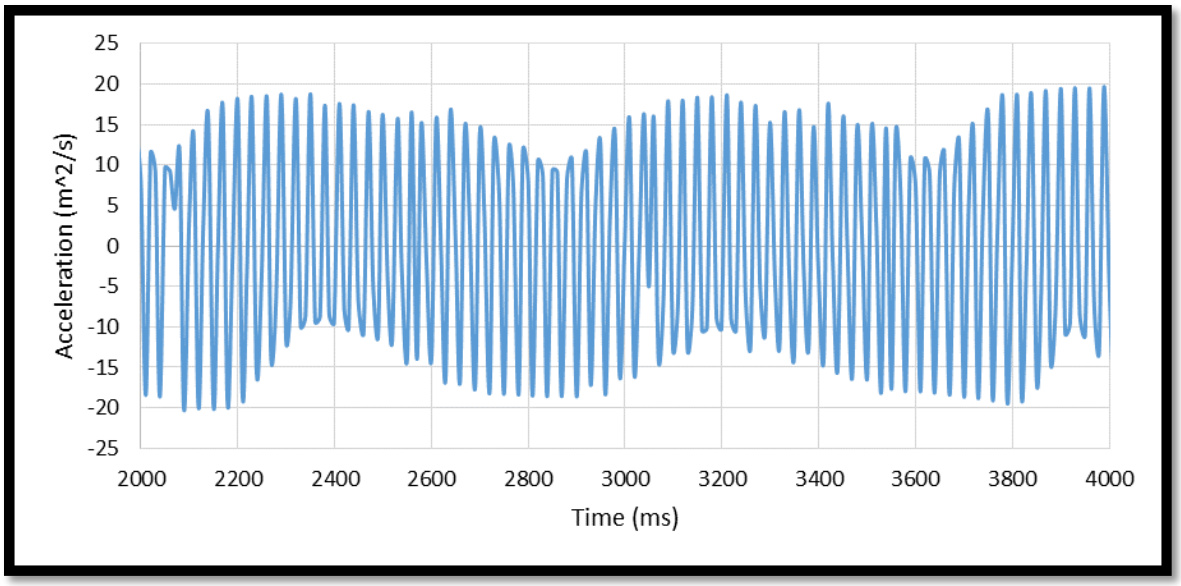

Fig. B32. Model #3c nappe vibration accelerometer data, 0.59 ft^2/s

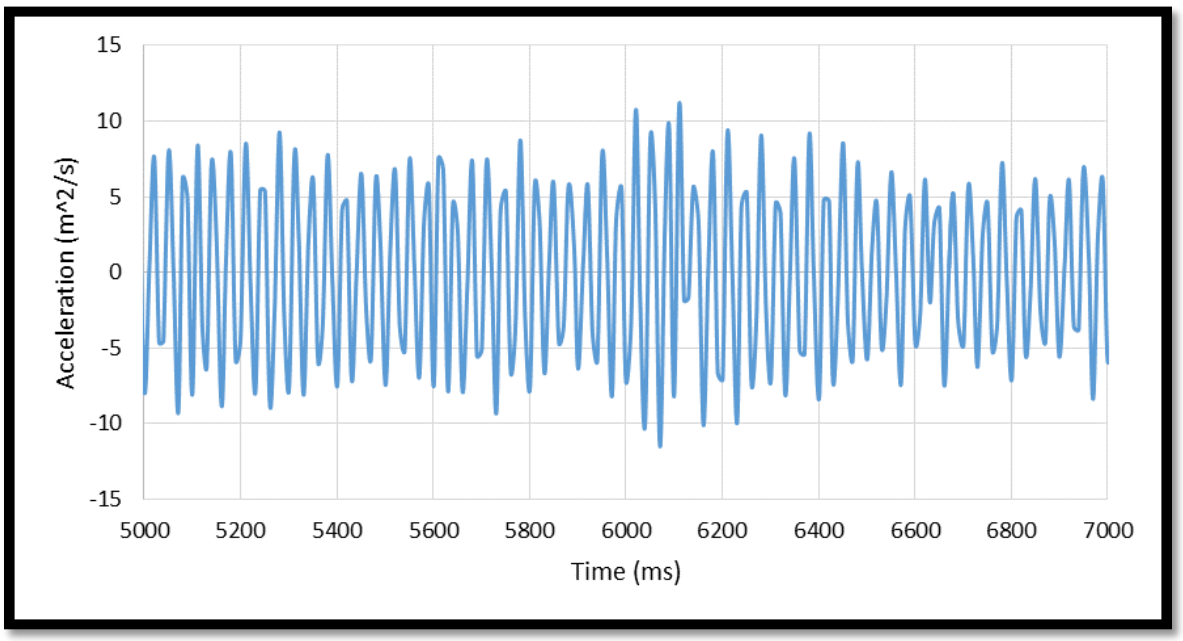

Fig. B33. Model #3c nappe vibration accelerometer data, 0.70 ft^2/s

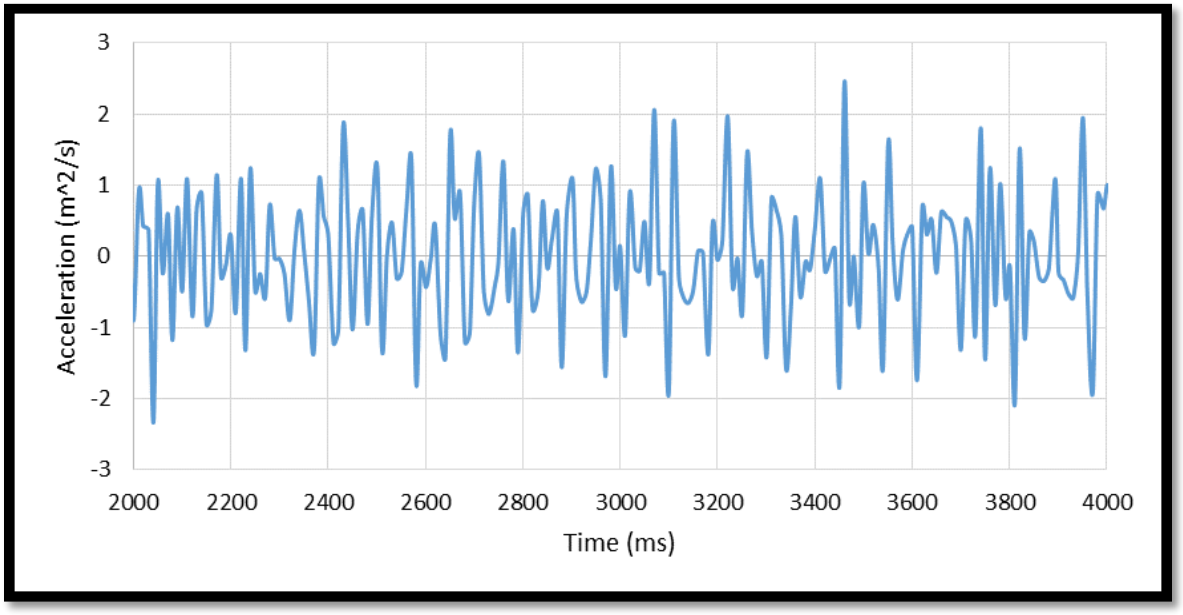

Fig. B34. Model #3c nappe vibration accelerometer data, 0.81 ft^2/s

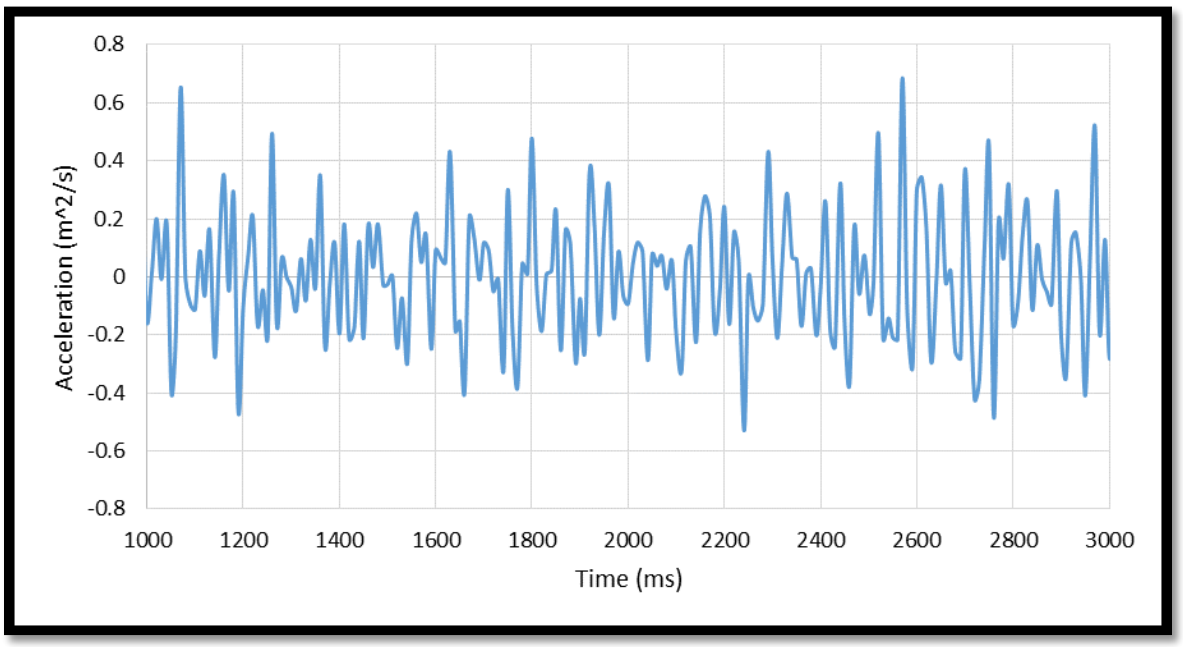

Fig. B35. Model #3d nappe vibration accelerometer data, 0.14 ft^2/s

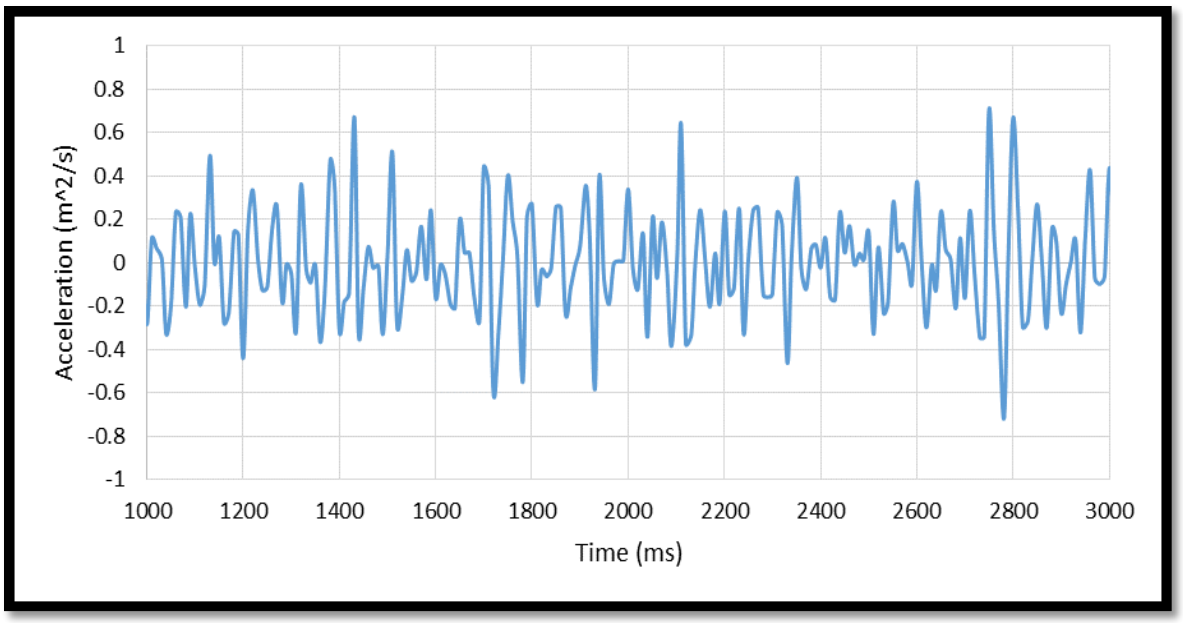

Fig. B36. Model #3d nappe vibration accelerometer data, 0.20 ft^2/s

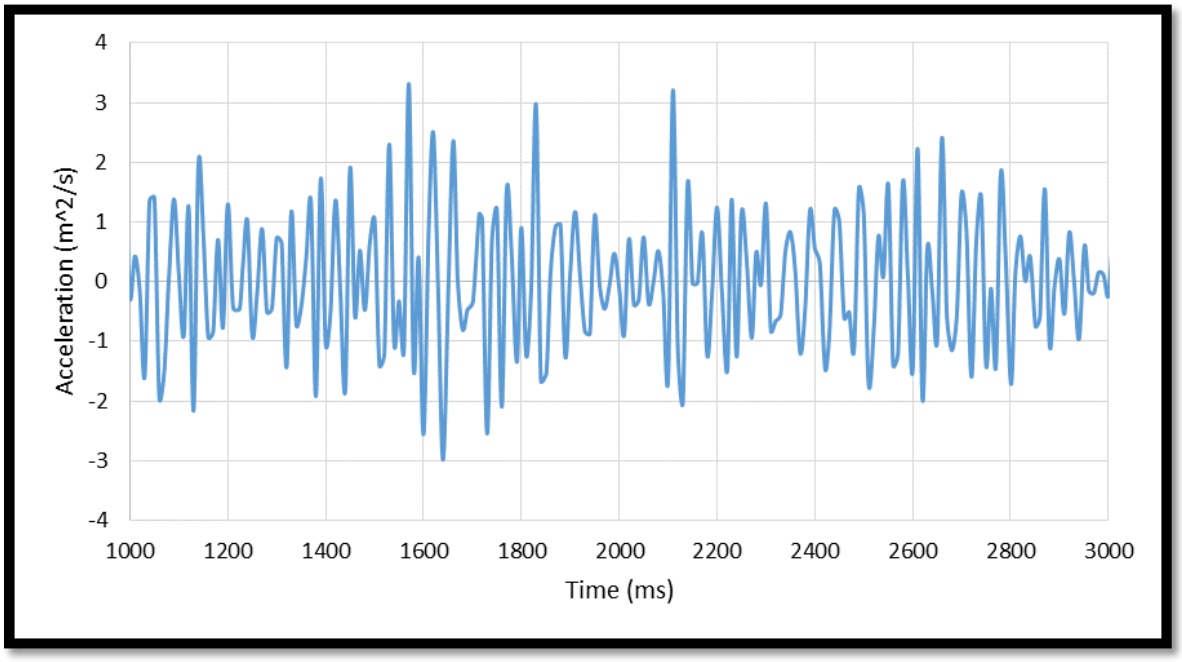

Fig. B37. Model #3d nappe vibration accelerometer data, 0.25 ft^2/s

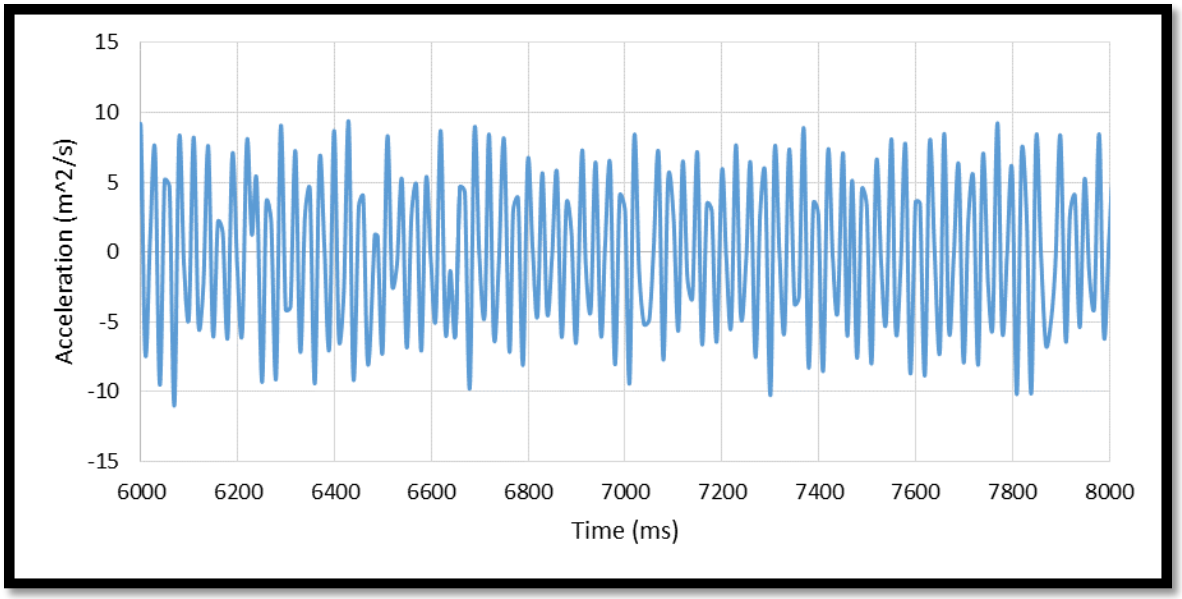

Fig. B38. Model #3d nappe vibration accelerometer data, 0.31 ft^2/s

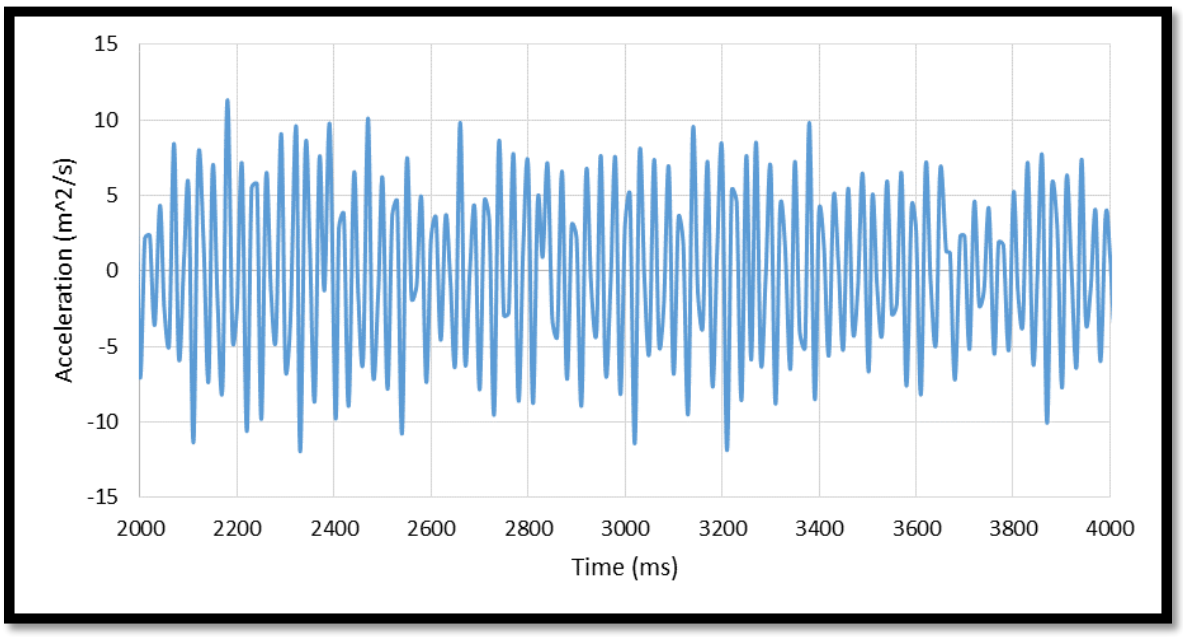

Fig. B39. Model #3d nappe vibration accelerometer data, 0.36 ft^2/s

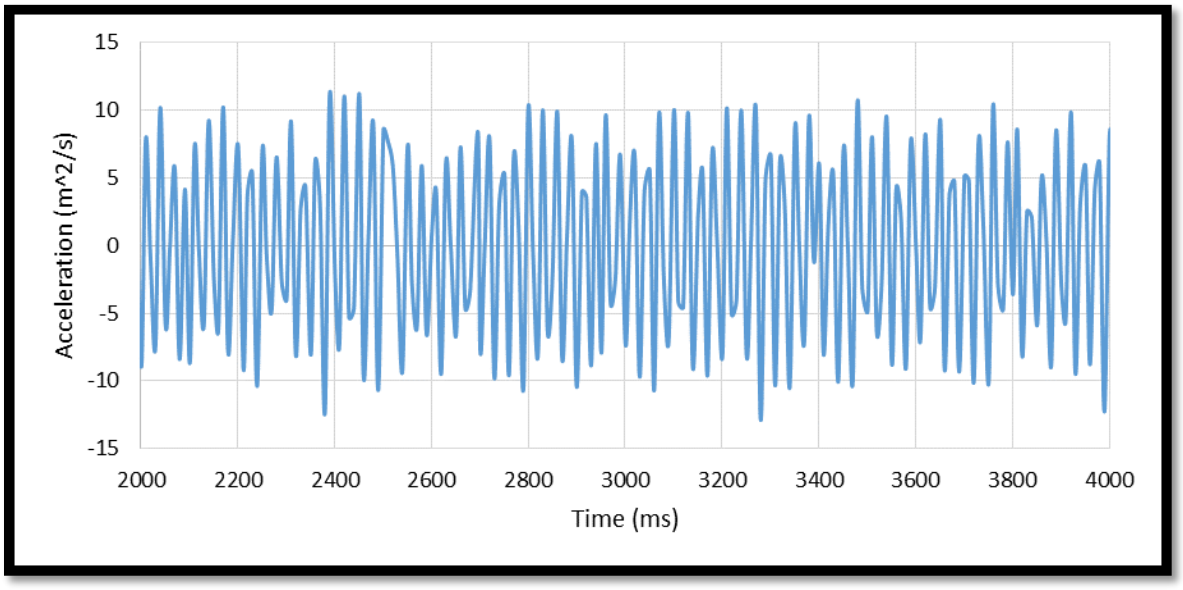

Fig. B40. Model #3d nappe vibration accelerometer data, 0.42 ft^2/s

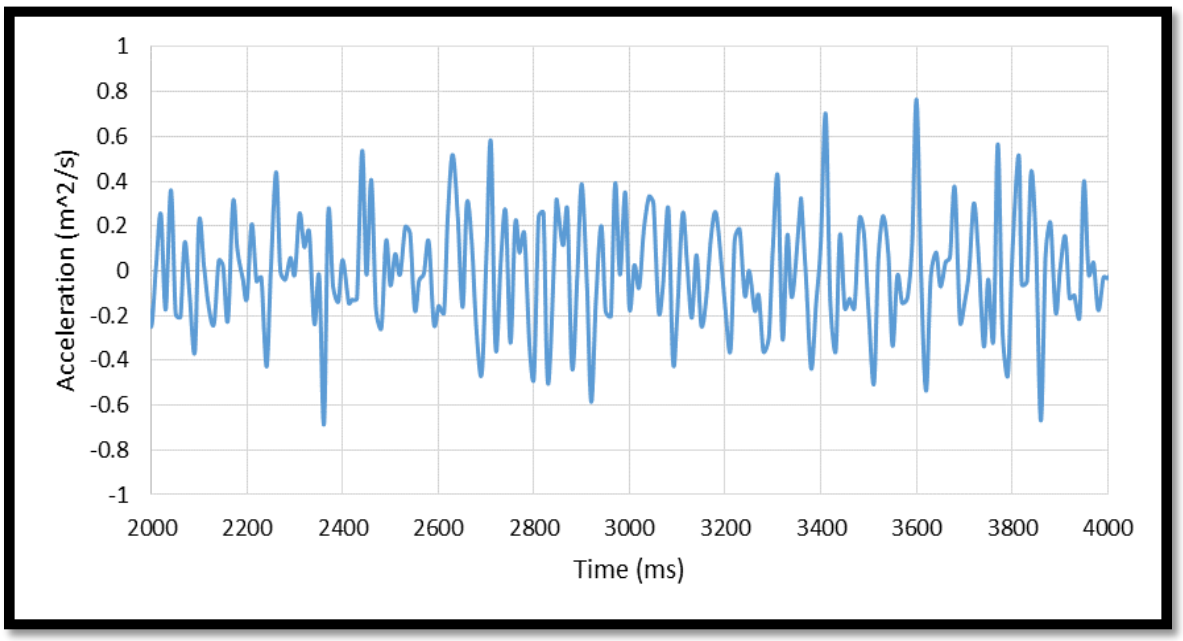

Fig. B41. Model #3e nappe vibration accelerometer data, 0.27 ft^2/s

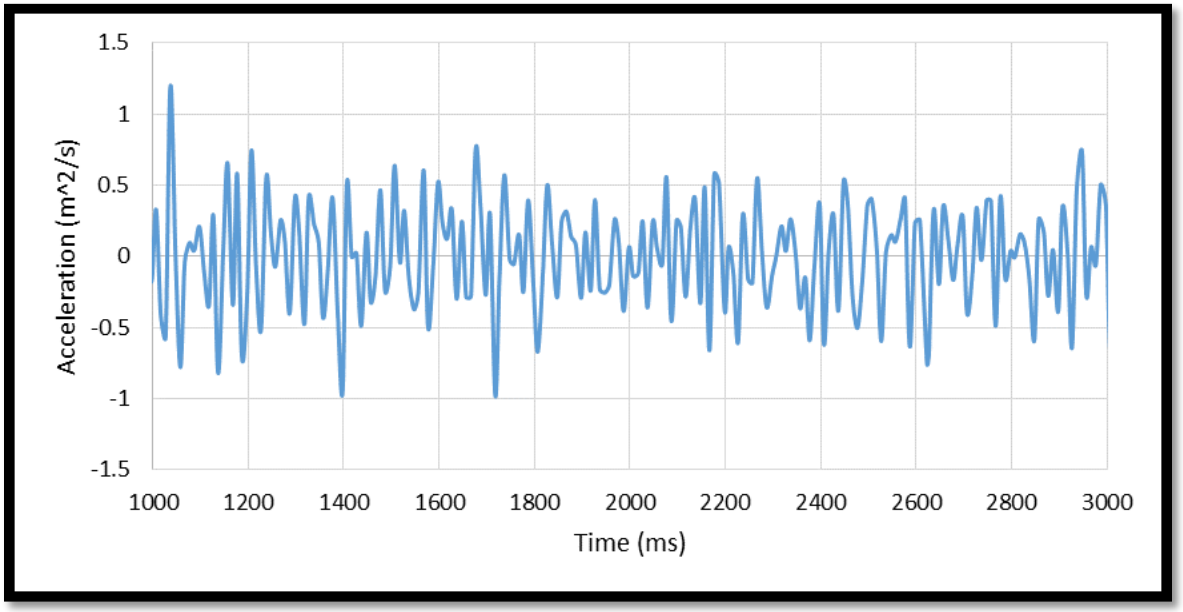

Fig. B42. Model #3e nappe vibration accelerometer data, 0.38 ft^2/s

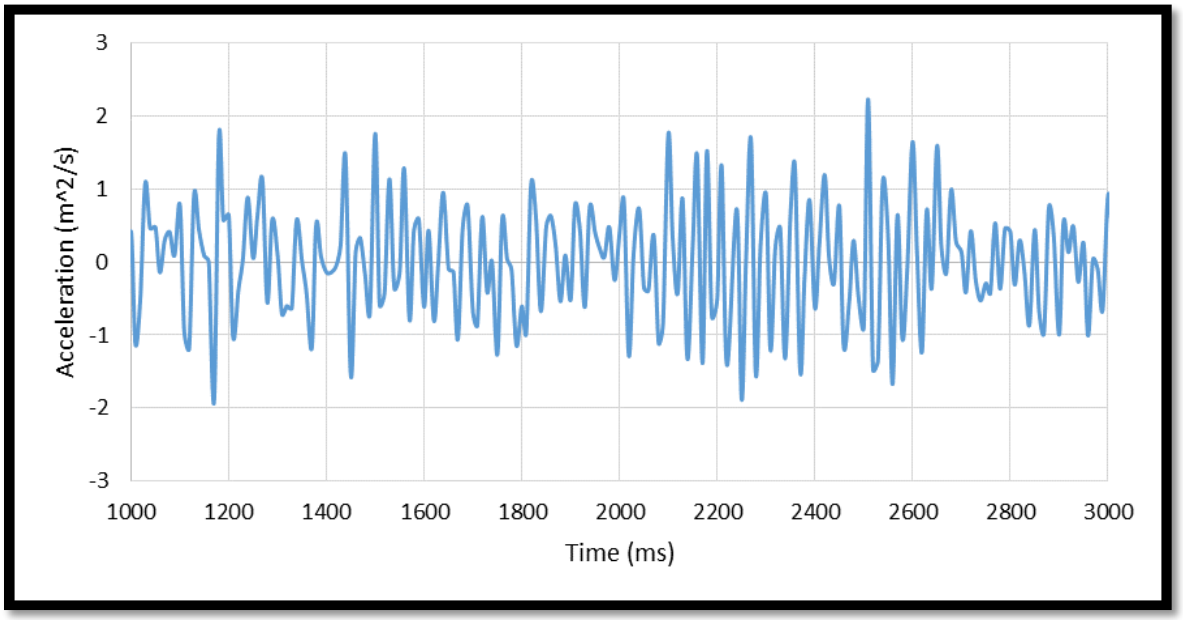

Fig. B43. Model #3e nappe vibration accelerometer data, 0.48 ft^2/s

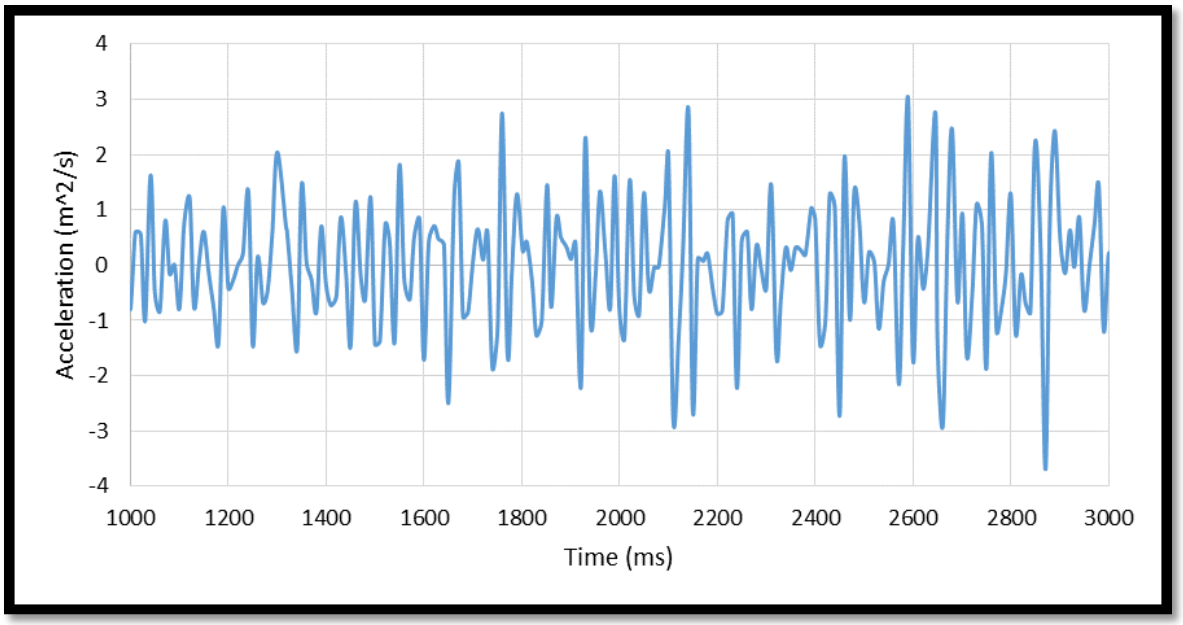

Fig. B44. Model #3e nappe vibration accelerometer data, 0.59 ft^2/s

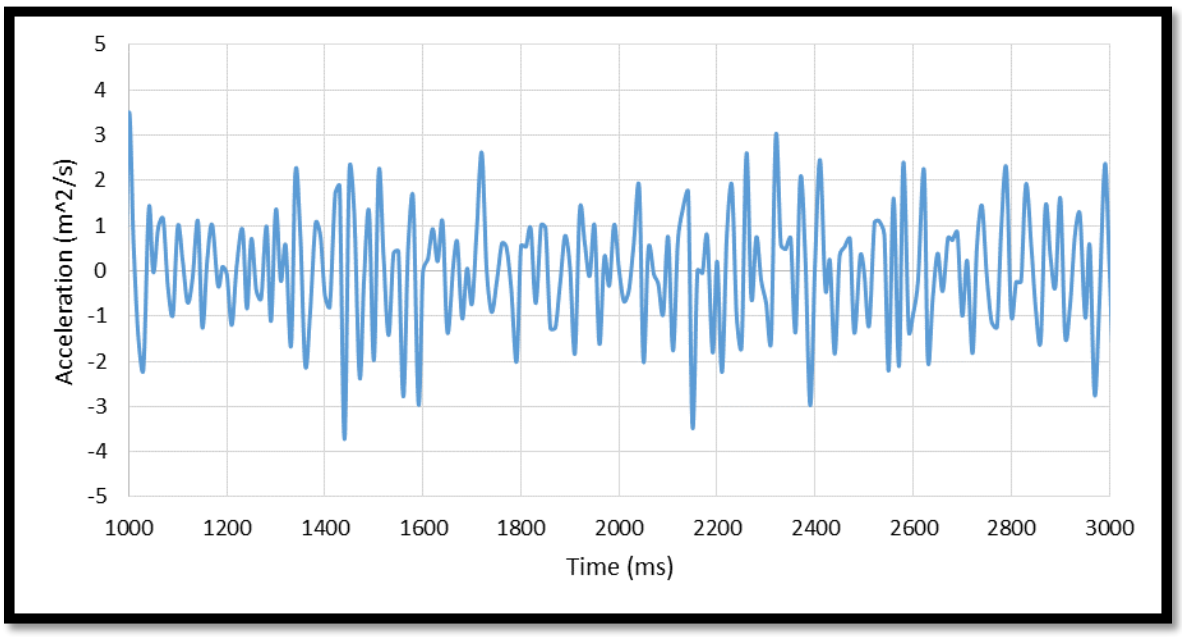

Fig. B45. Model #3e nappe vibration accelerometer data, 0.70 ft^2/s

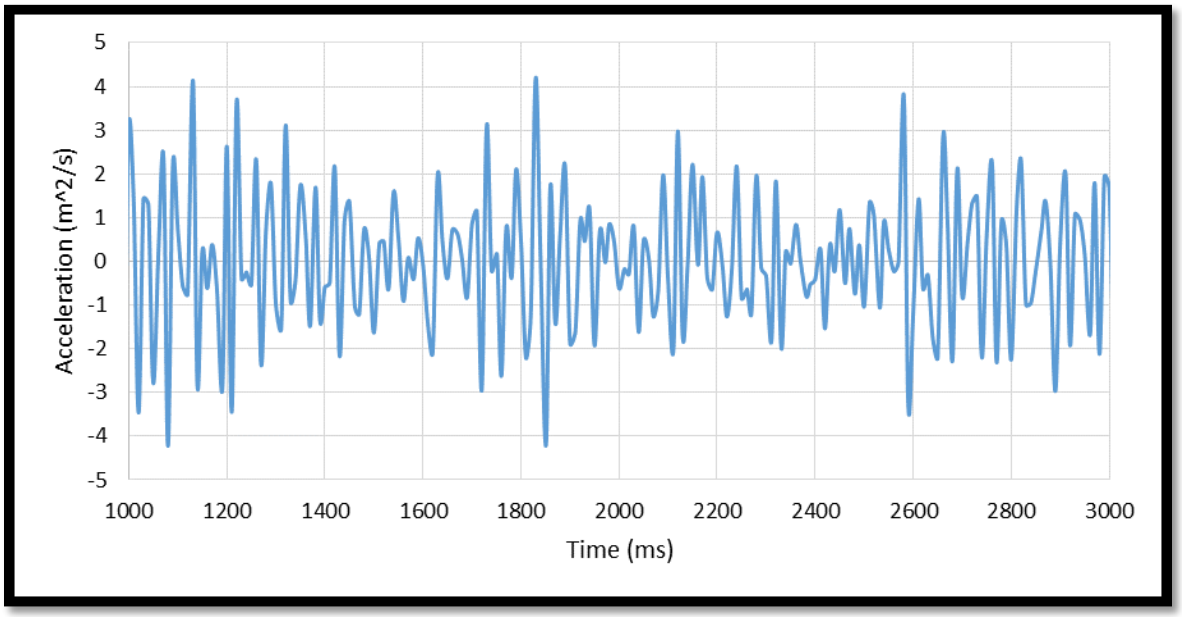

Fig. B46. Model #3e nappe vibration accelerometer data, 0.81 ft^2/s

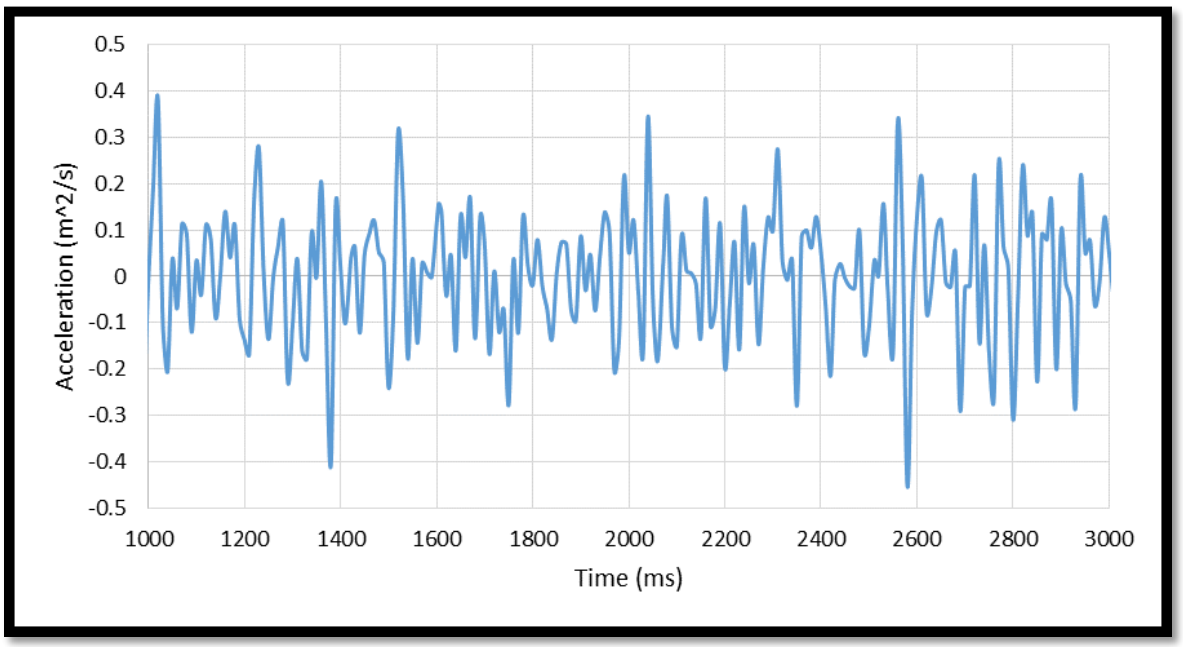

Fig. B47. Model #3f nappe vibration accelerometer data, 0.14 ft^2/s

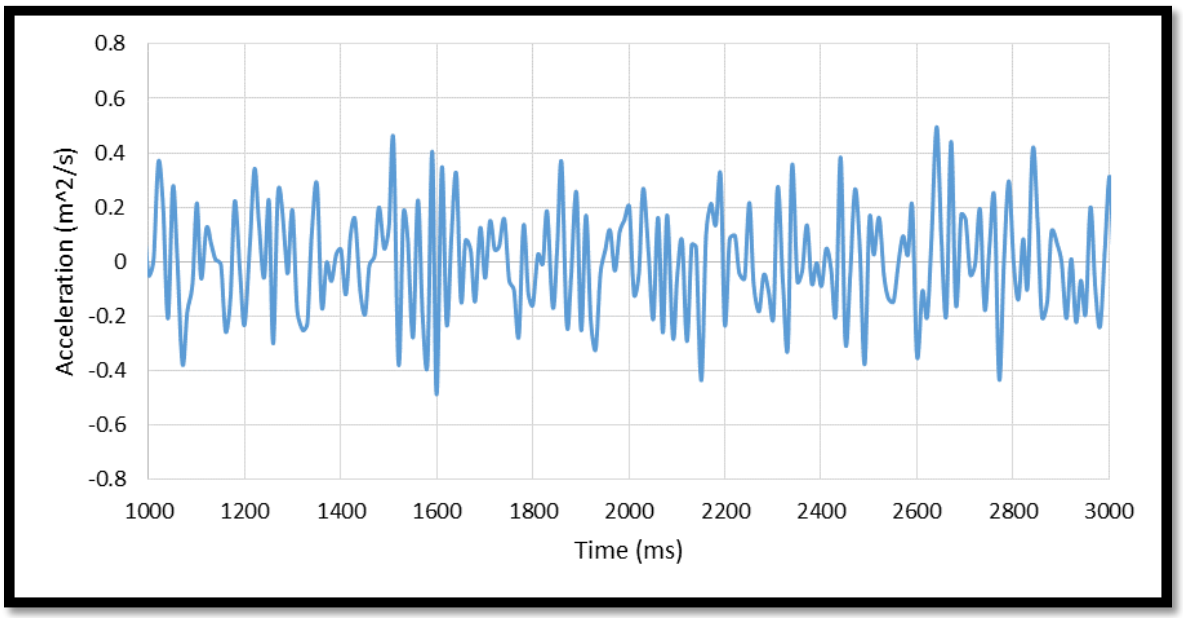

Fig. B48. Model #3f nappe vibration accelerometer data, 0.20 ft^2/s

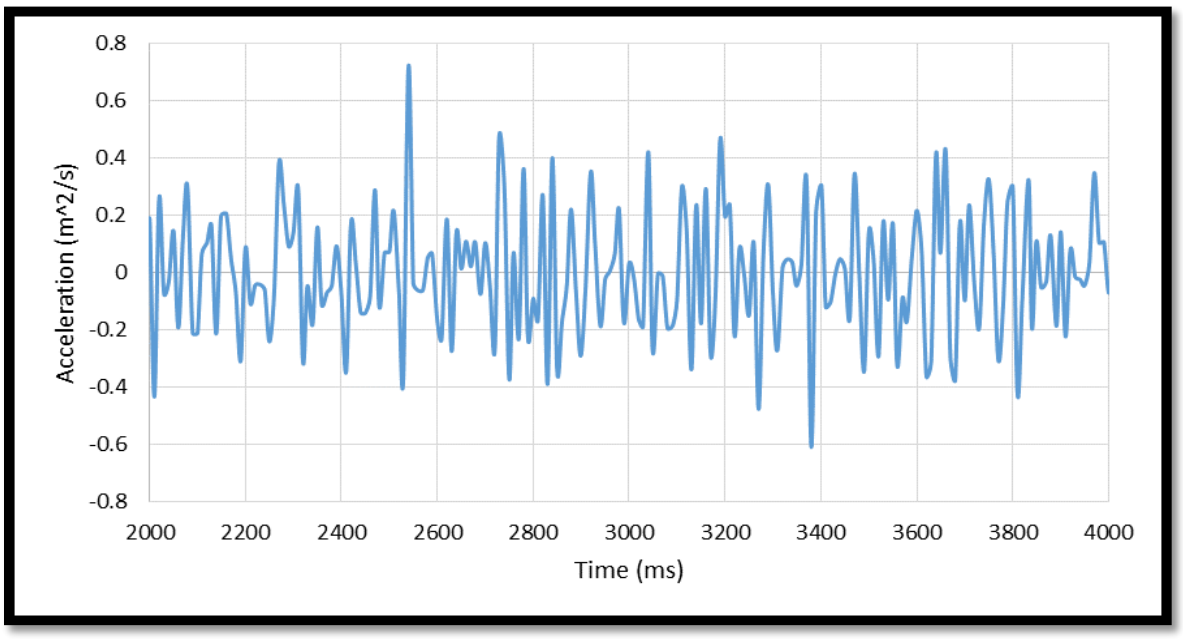

Fig. B49. Model #3f nappe vibration accelerometer data, 0.25 ft^2/s

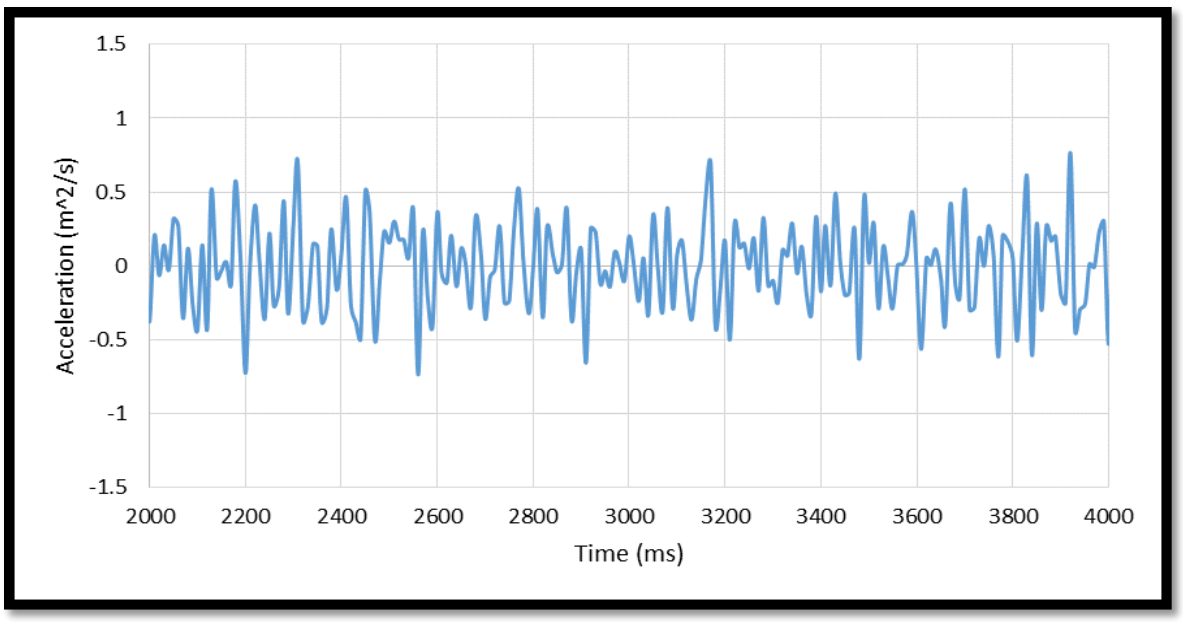

Fig. B50. Model #3f nappe vibration accelerometer data, 0.31 ft^2/s

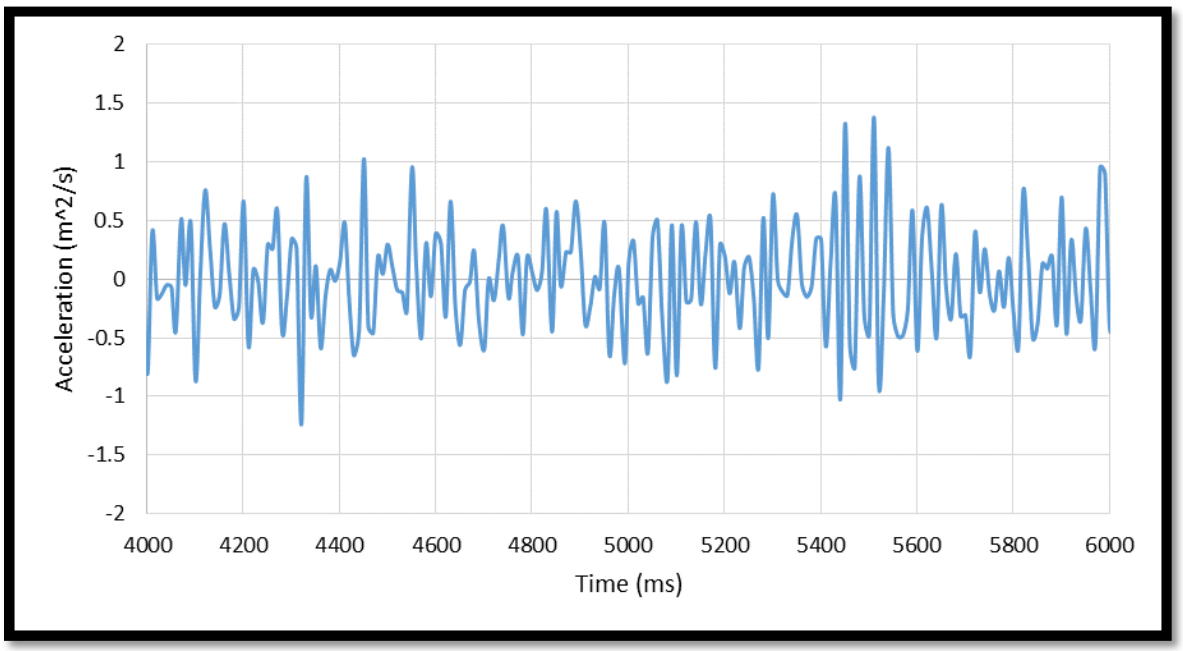

Fig. B51. Model #3f nappe vibration accelerometer data, 0.36 ft^2/s

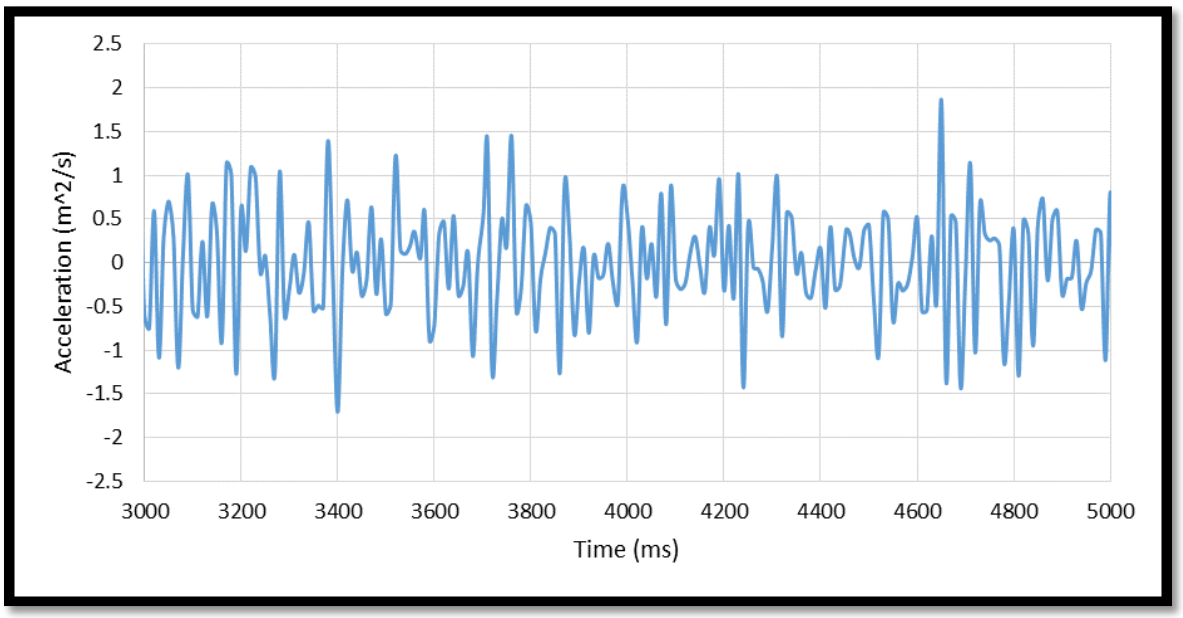

Fig. B52. Model #3f nappe vibration accelerometer data, 0.42 ft^2/s

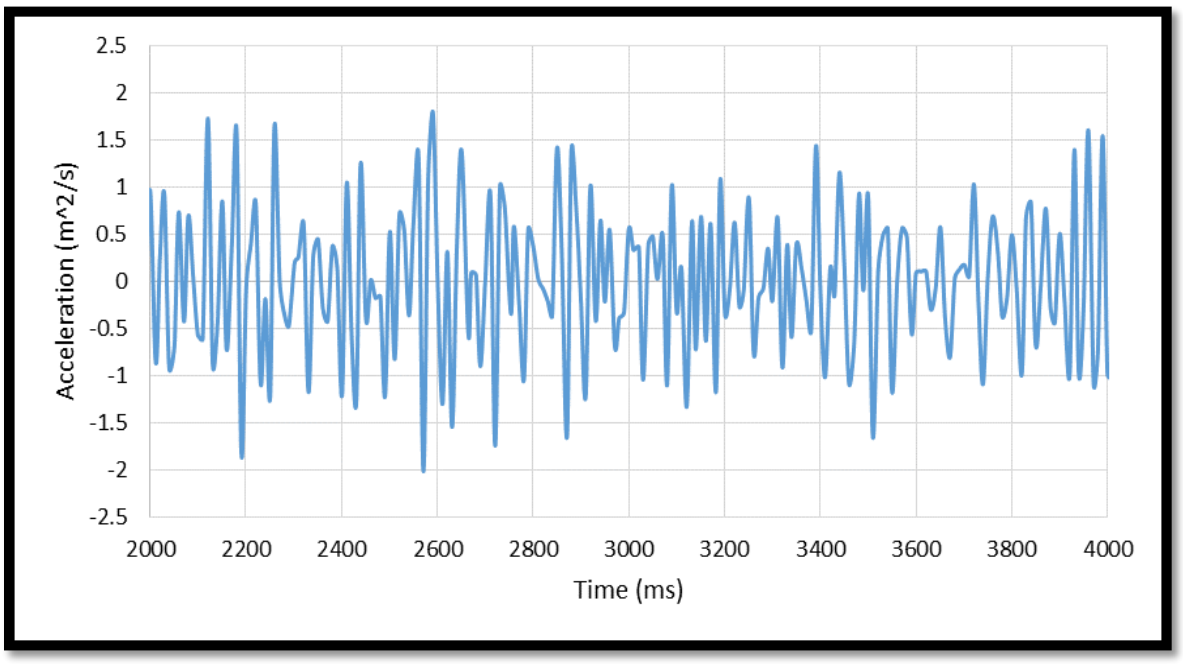

Fig. B53. Model #3f nappe vibration accelerometer data, 0.48 ft^2/s

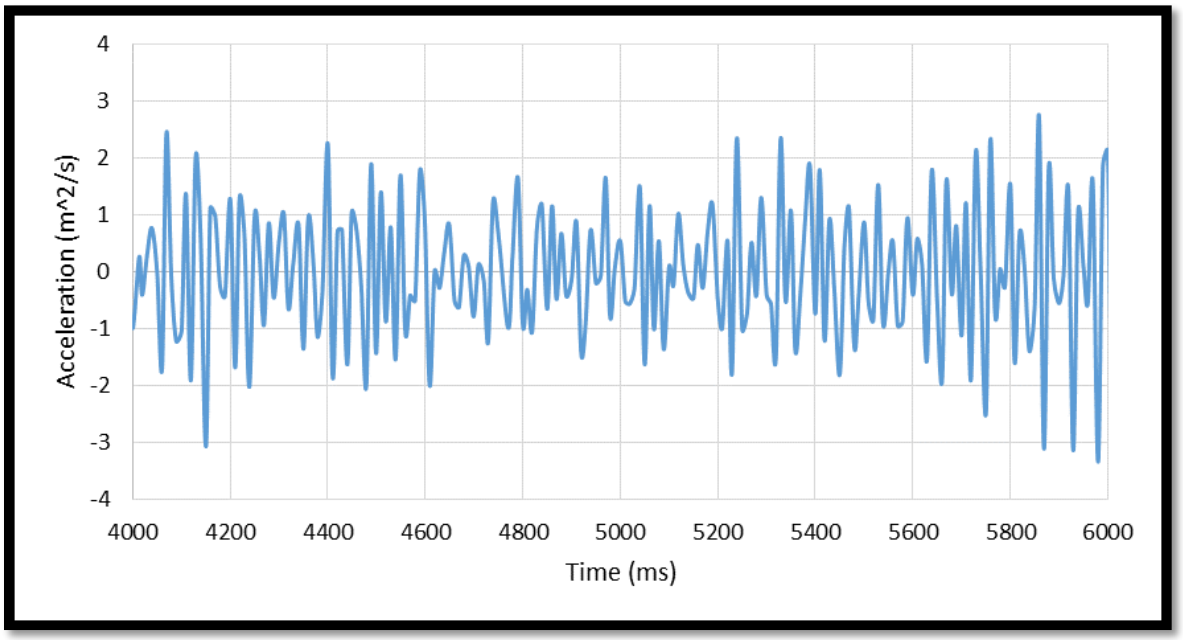

Fig. B54. Model #3f nappe vibration accelerometer data, 0.59 ft^2/s

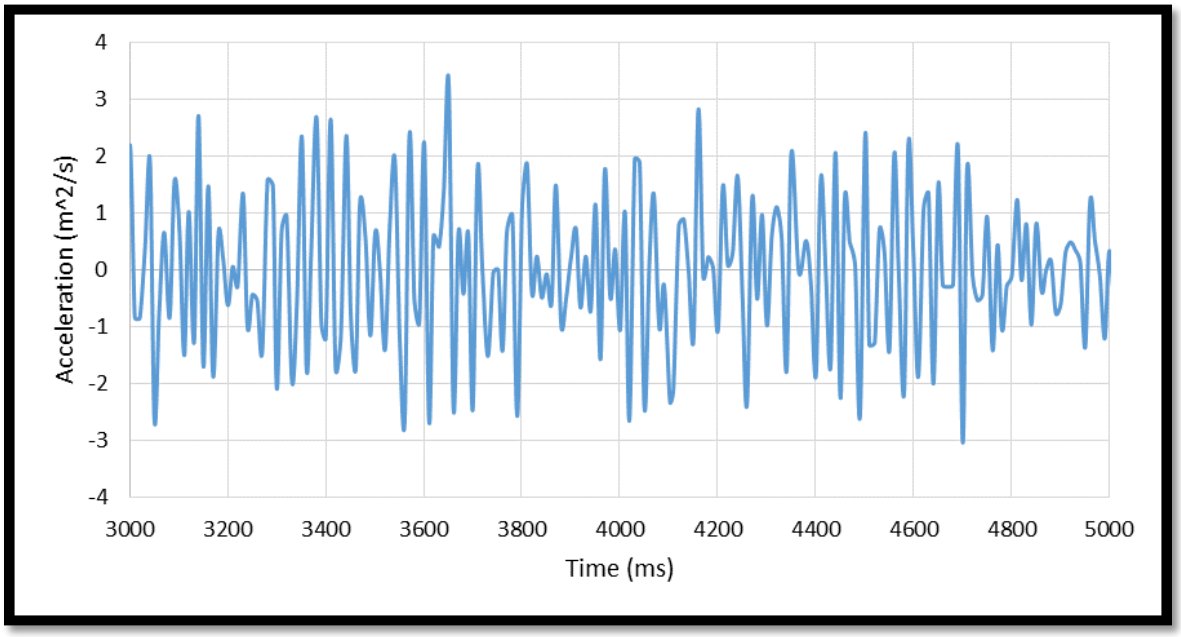

Fig. B55. Model #3f nappe vibration accelerometer data, 0.70 ft^2/s

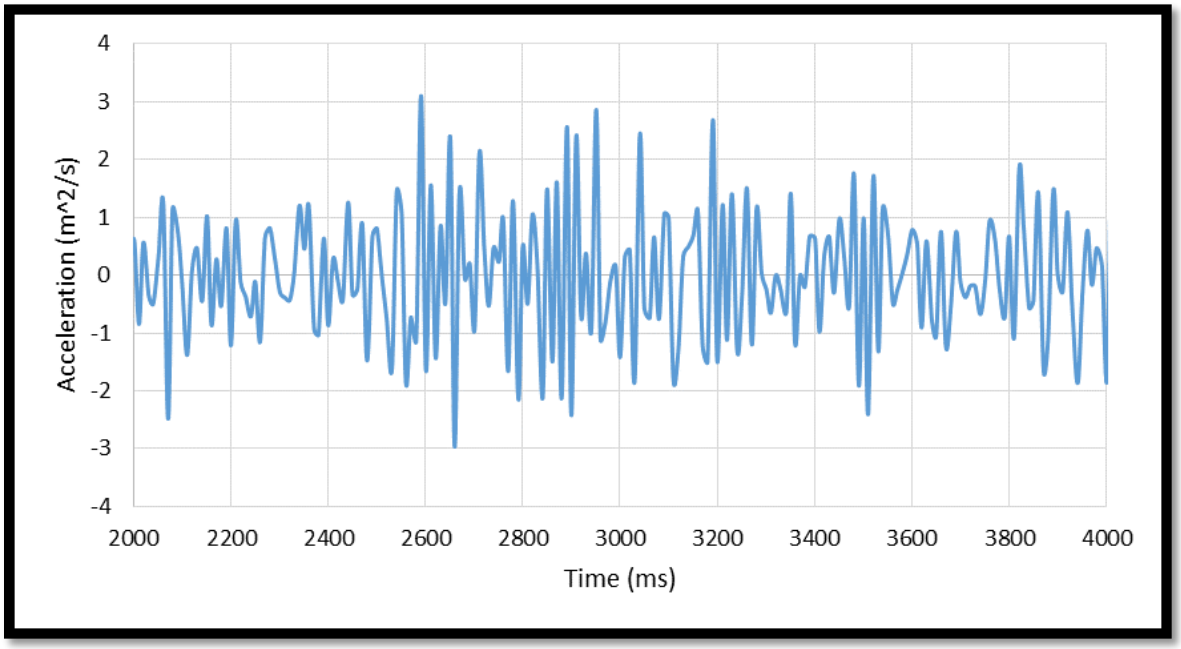

Fig. B56. Model #3f nappe vibration accelerometer data, 0.81 ft^2/s

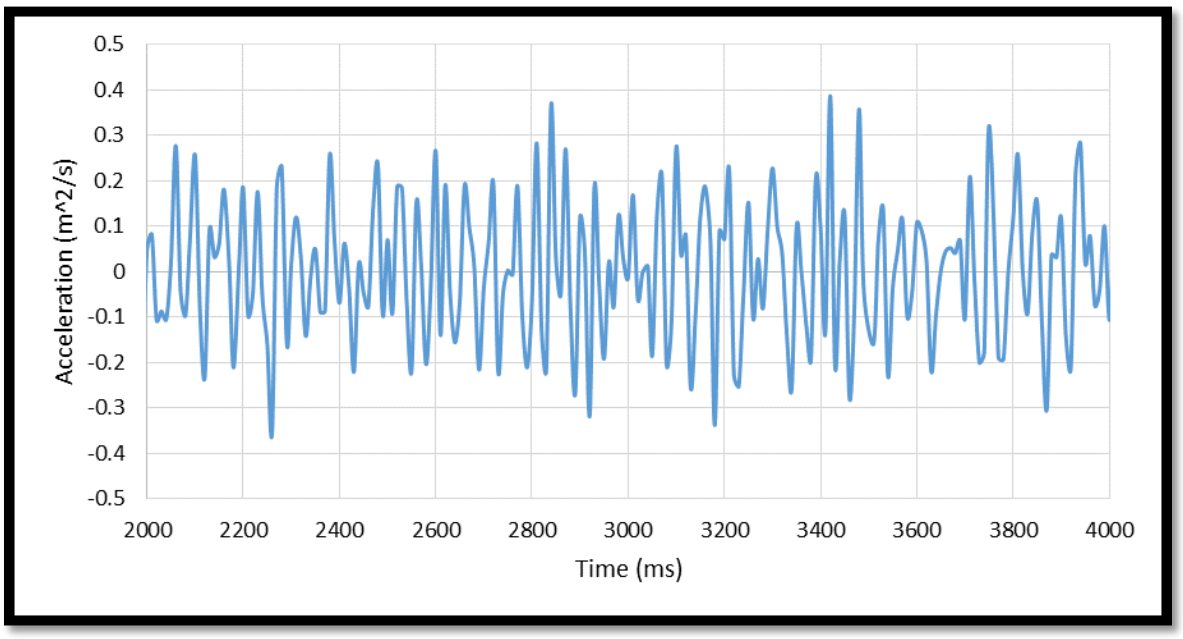

Fig. B57. Model #3g-b nappe vibration accelerometer data, 0.14 ft^2/s

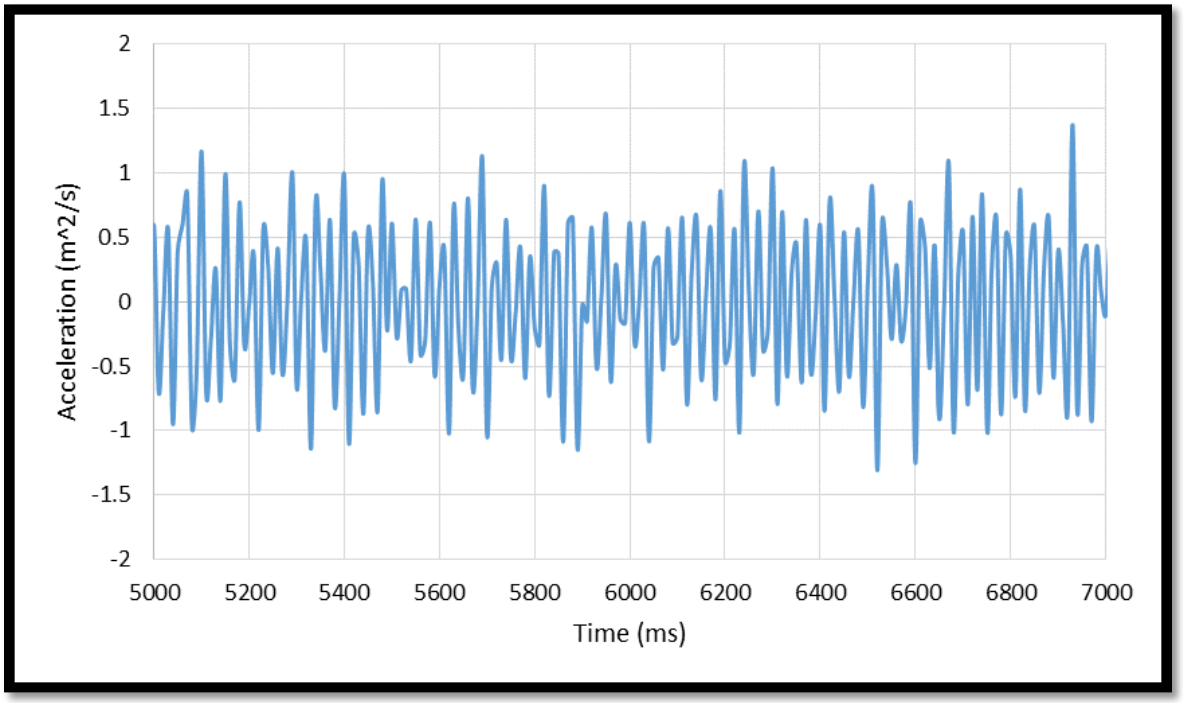

Fig. B58. Model #3g-b nappe vibration accelerometer data, 0.20 ft^2/s

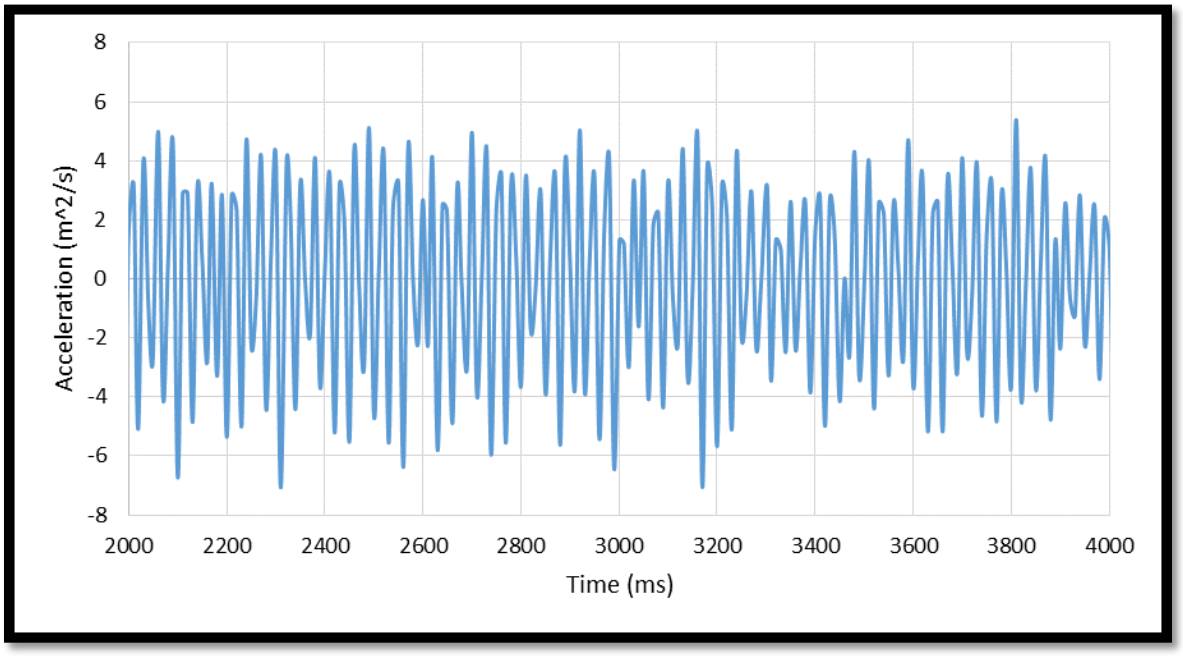

Fig. B59. Model #3g-b nappe vibration accelerometer data, 0.25 ft^2/s

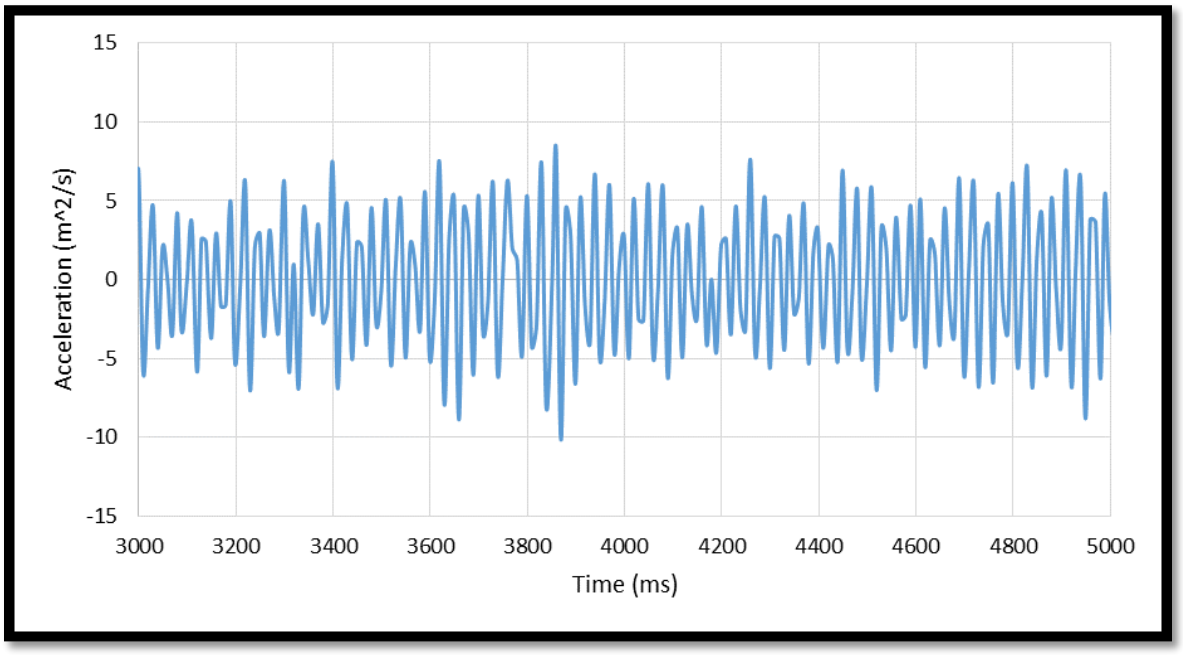

Fig. B60. Model #3g-b nappe vibration accelerometer data, 0.31 ft^2/s

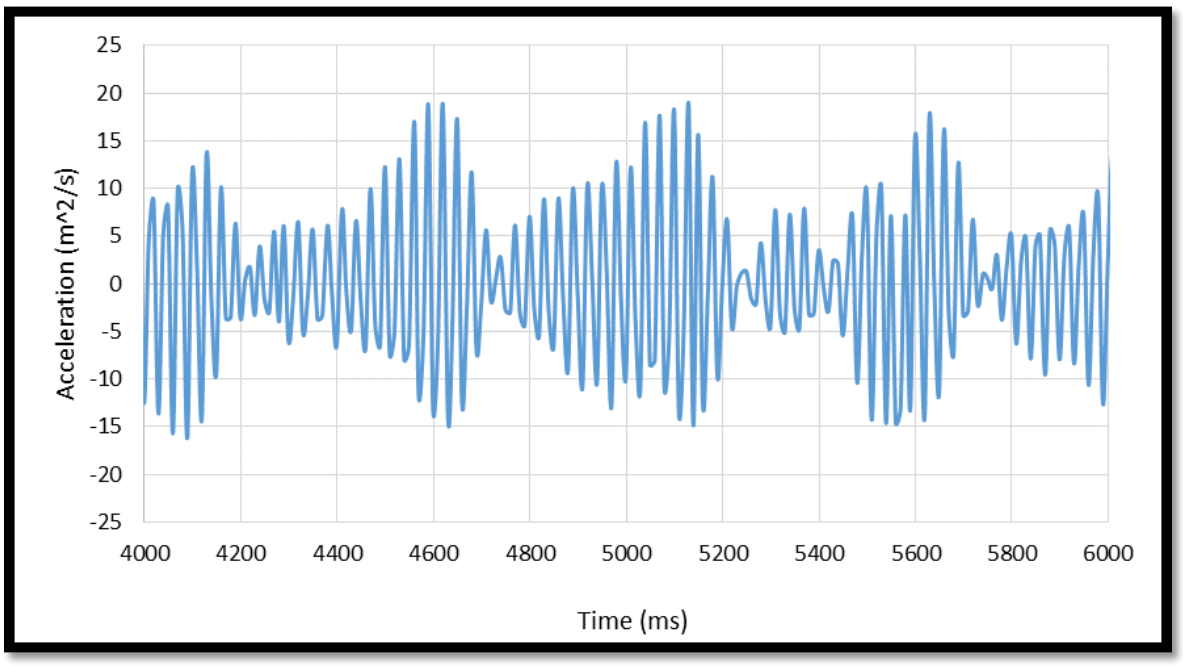

Fig. B61. Model #3g-b nappe vibration accelerometer data, 0.36 ft^2/s

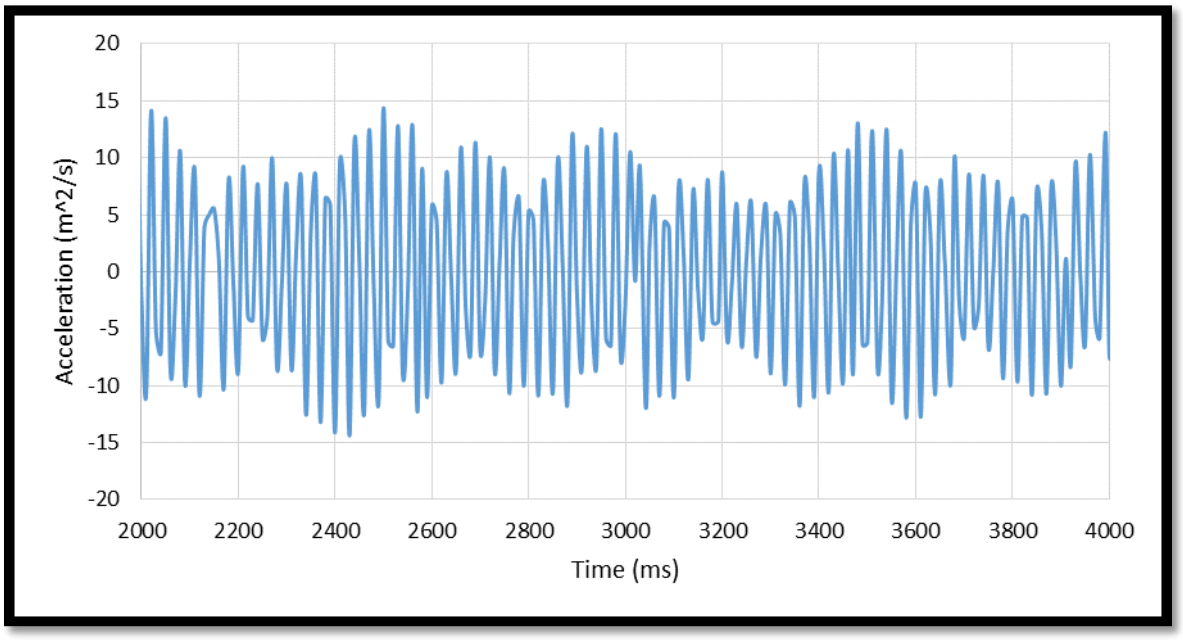

Fig. B62. Model #3g-b nappe vibration accelerometer data, 0.42 ft^2/s

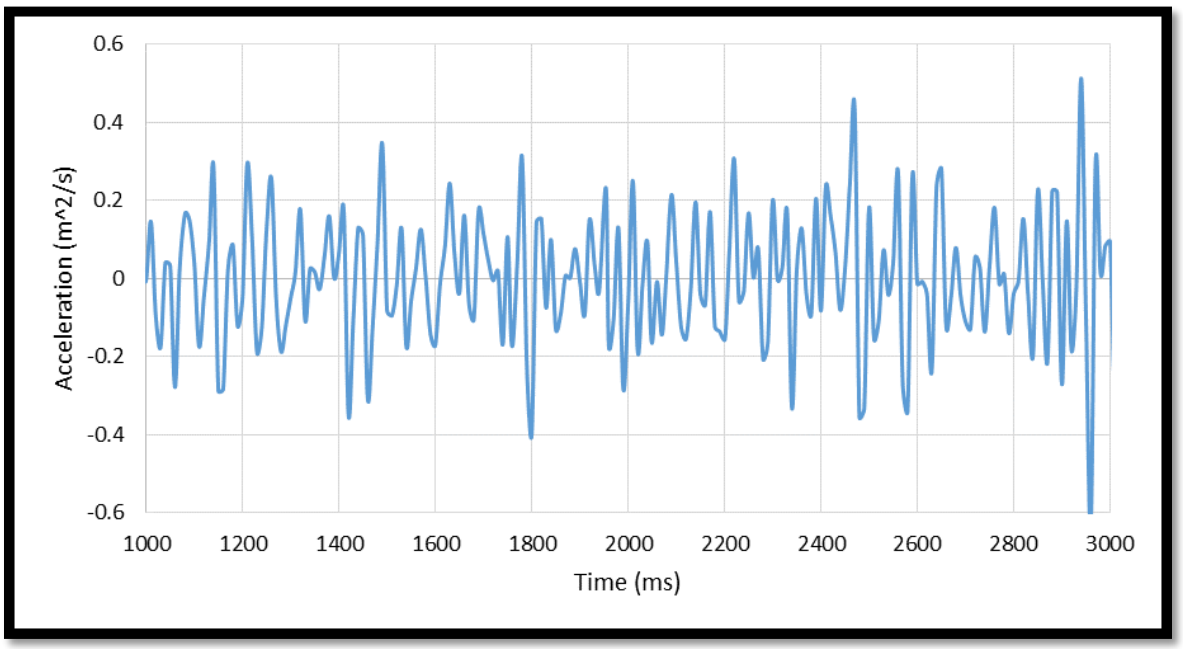

Fig. B63. Model #3h nappe vibration accelerometer data, 0.14 ft^2/s

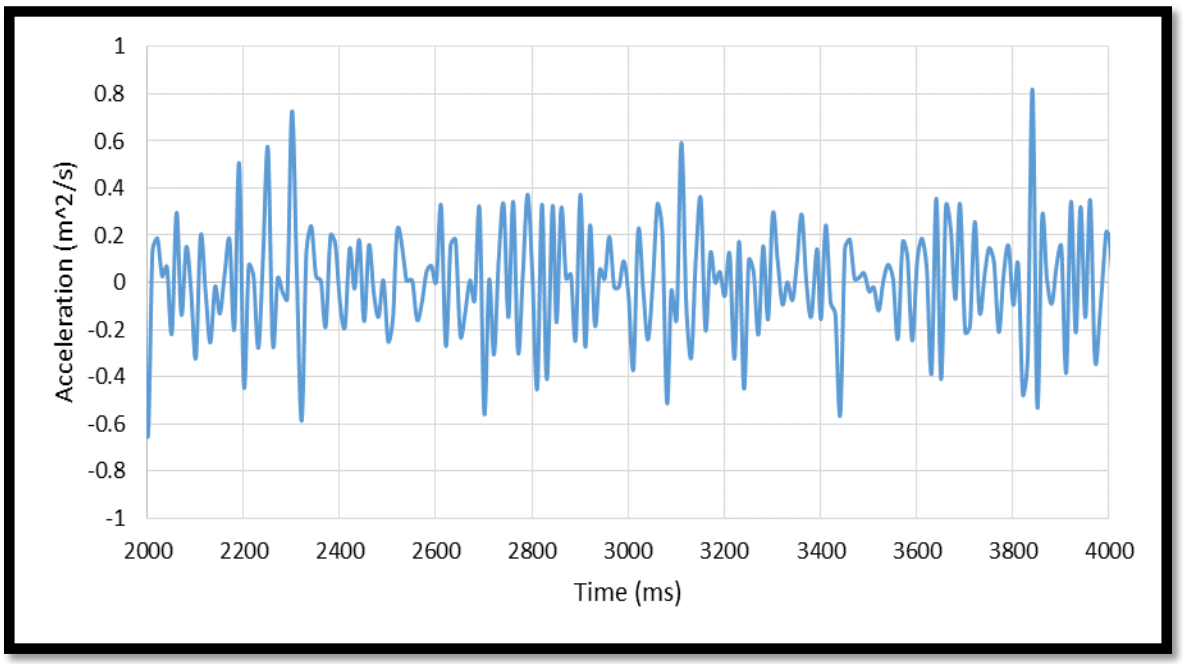

Fig. B64. Model #3h nappe vibration accelerometer data, 0.20 ft^2/s

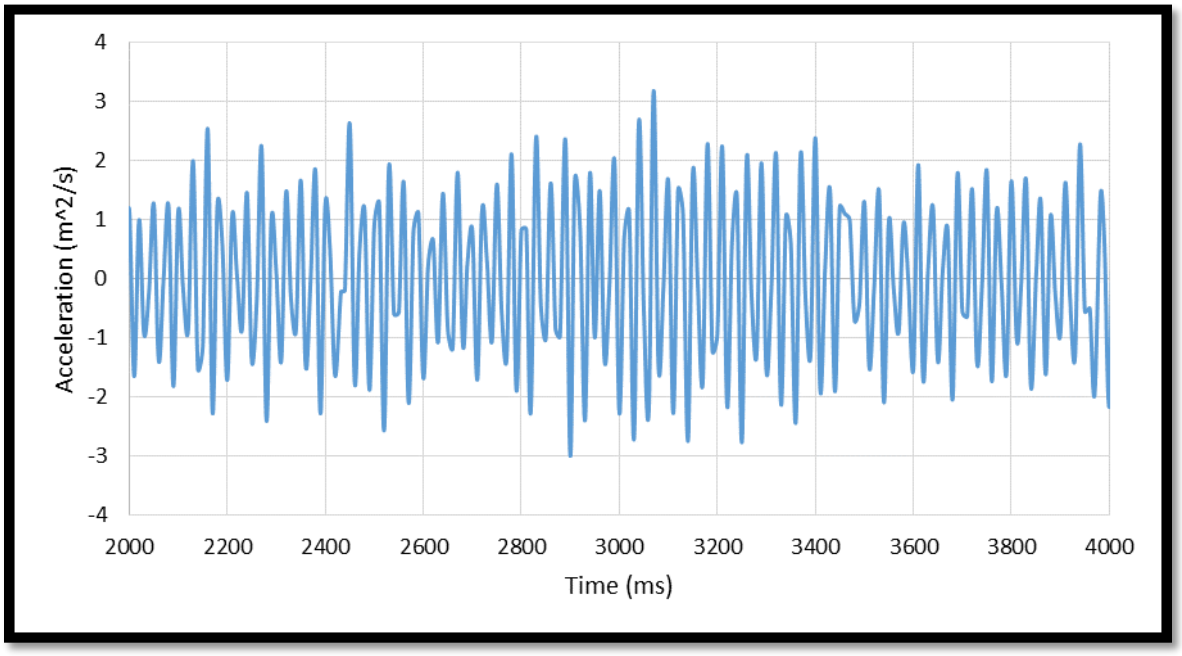

Fig. B65. Model #3h nappe vibration accelerometer data, 0.25 ft^2/s

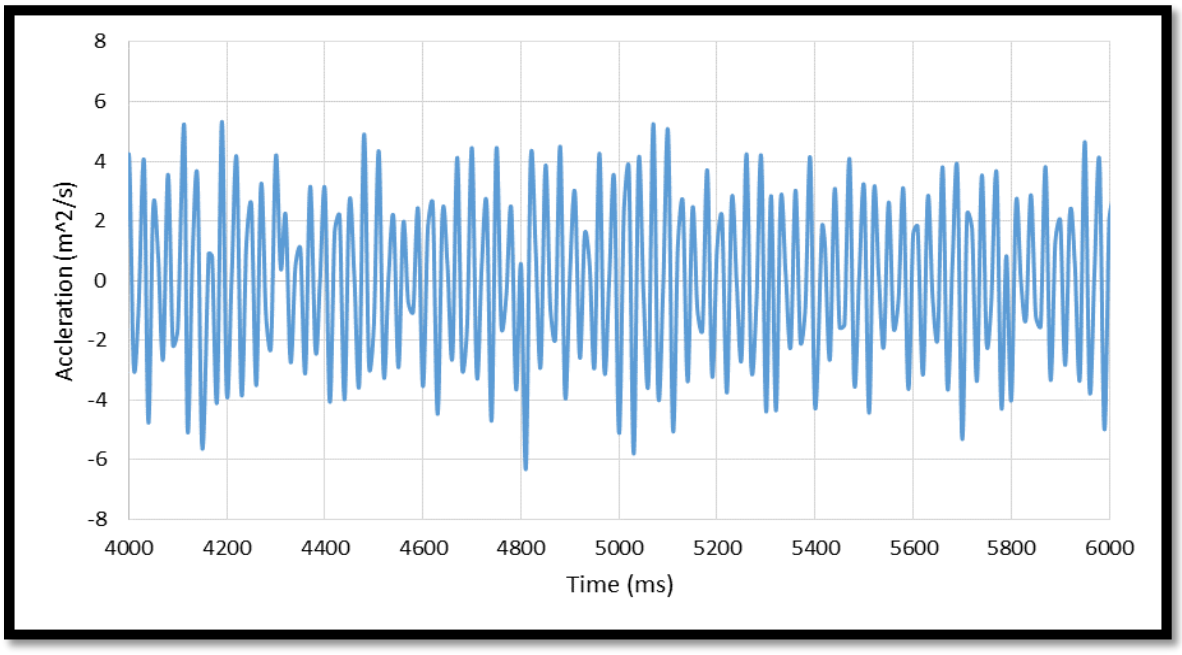

Fig. B66. Model #3h nappe vibration accelerometer data, 0.31 ft^2/s

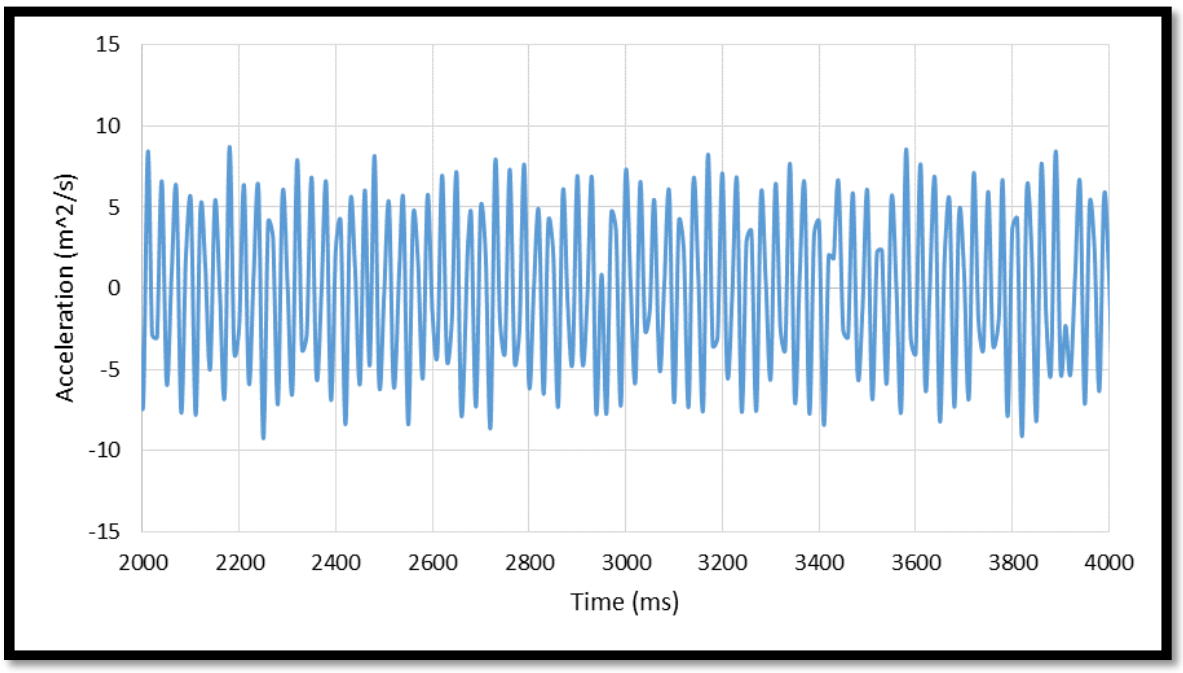

Fig. B67. Model #3h nappe vibration accelerometer data, 0.36 ft^2/s

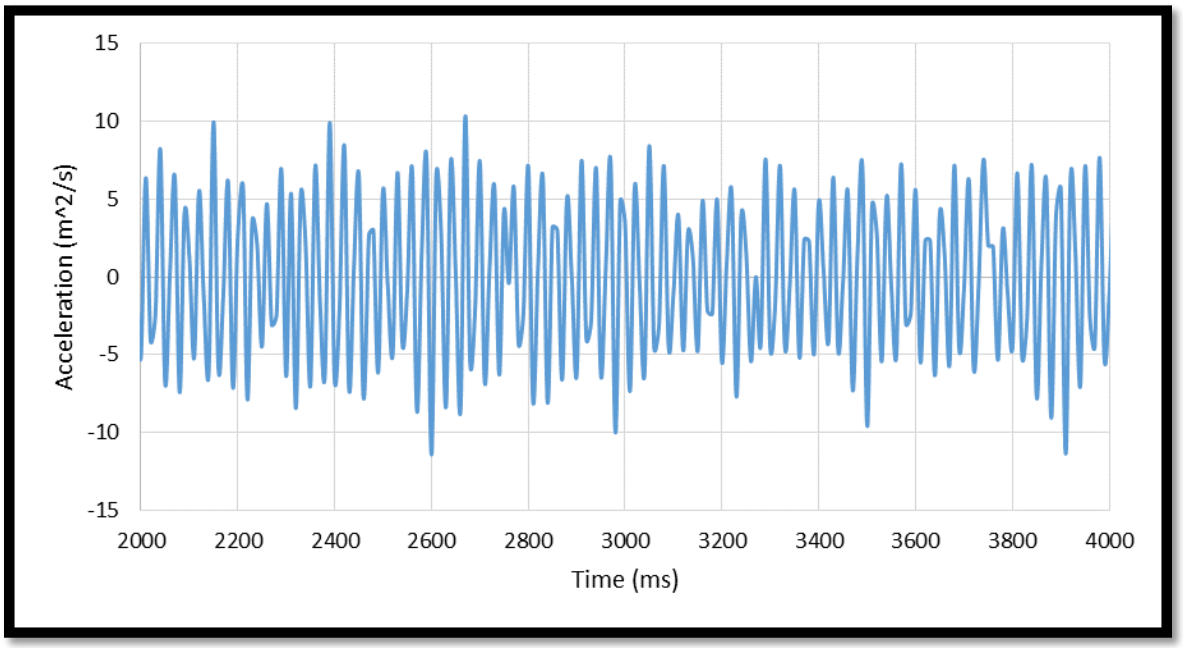

Fig. B68. Model #3h nappe vibration accelerometer data, 0.42 ft^2/s